Single Cells to Spheres: Microfluidic Assays for Characterization of Cancer Stem-like Cells

by

Patrick Neal Ingram

A dissertation submitted in partial fulfillment
of the requirements for the degree of
Doctor of Philosophy
(Biomedical Engineering)
in The University of Michigan
2015

Doctoral Committee:

Professor Euisik Yoon, Chair
Associate Professor Ronald J. Buckanovich
Assistant Professor Somin Lee
Professor Shuichi Takayama
Professor Emeritus Kensall D. Wise

Acknowledgements

Over 5 years ago when I began my work as a graduate student, I could not imagine the experiences that were in store for me in my tenure as a graduate student at the University of Michigan (who knew there were temperatures lower than 0˚F). I have certainly learned a great deal and have had a wonderful experience with my friends and colleagues.

First and foremost, I would like to acknowledge the contributions of my advisor, Professor Euisik Yoon. He has provided me and my research with direction and motivation, and I have learned a great deal from him. They skills I have learned working in his lab will be invaluable in the future, and I hope we will have the opportunity to work together again in the future.

I would like to thank my dissertation committee Professor Shuichi Takayama, Professor Ken Wise, Professor Ronald Buckanovich, and Professor Somin Lee. I greatly appreciate their feedback and encouragement. I would also like to thank Professor Michael Mayer, though he was not able to be a part of my committee his advice was integral to my success. I greatly appreciate my collaborations with Professor Buckanovich and Professor Max Wicha, and the assistance their labs have provided throughout my time at Michigan. Dr. Sean McDermott, Dr. Kun Yang, Mangala Iyengar, Dr. Ebrahim Aziz, and Dr. Michael Brooks, in particular, were critical to my success. I really appreciate all of their research contributions, time, and intellectual input.

For his foundational contribution to the presented work, I would also like to extend my appreciation to Dr. Jaehoon Chung. His single cell capture approach, microwell designs, and preliminary testing served as the foundation upon which these microfluidic assays build.

Dr. Yu-Chih Chen, Dr. Xia Lou, Yu-Heng Cheng, and Zhixiong Zhang each deserve special recognition for their contributions to this research as well. The success of the Yoon lab biogroup is a result of each of their efforts and ability. Each of them has helped me considerably in brainstorming, in research, and through their friendship. I would finally like to thank all current and past lab members of the Yoon lab.

For funding, this work has been supported in part by the Rollin M. Gerstacker Foundation Fellowship, the Microfluidics in Biomedical Sciences Training Grant, and in part by the DoD, the NIH, and Thermo Fisher Scientific under the Center for Chemical Genomics at the Life Sciences Institute at the University of Michigan. We would also like to acknowledge the support of the Lurie Nanofabrication Facility, and in particular the assistance of Dr. Pilar Herrera-Fierro, Thomas Latowski, and Dr. Sandrine Martin.

Table of Contents

List of Tables

List of Figures

Abstract

The cancer stem-like cell (CSC) model proposes that a small subset of stem-like cells are necessary to sustain cancer growth. CSC are resistant to traditional therapy and capable of division to give rise to a heterogeneous population to recapitulate tumors. Therapeutics which target CSC have shown potential to drastically improve patient survival. However, CSC are difficult to study as they are rare, transient, and difficult to culture. Additionally, conventional bulk assays, such as drug screens that measure success through reduction of total cell number, average out the behavior of rare but important sub-populations like CSC. There is a clear need to provide single cell tools to expedite the characterization of CSC and the development of CSC based therapies. As such, we have focused on the development and use of robust, user-friendly high throughput single cell microfluidic assays for the study of CSC. In adherent single cell assays of ovarian cancer, we have examined CSC behavior and biological factors controlling division and differentiation. It was seen that ovarian CSC exist in distinct hierarchies with possible rare de-differentiation events. In separate experiments, it was shown that bone morphogenetic protein 2 and epidermal growth factor-like protein 6 modulate self-renewal and asymmetric division, respectively. With the same approach, we screened novel therapeutics for their CSC targeting potential. Through the development and integration of novel surface coatings, we have also developed suspension based single cell derived sphere devices for marker free identification and characterization of CSC in breast cancer. We have demonstrated the use of this on-chip mammosphere assay for CSC identification, genetic analysis, stromal interactions through the use of conditioned media, and finally marker-free drug screening.

Chapter 1: Introduction

In 2014, it was expected that 585,720 Americans and more than 7 million people worldwide would die of cancer [1]. 1 in 4 Americans and ~15% of all human deaths on earth will be attributable to cancer and cancer metastases. If Michigan's cancer related diagnoses were concentrated to here in Ann Arbor, almost exactly half of the city would be stricken this year alone (Figure 1) [1]. Cancer is certainly omnipresent in modern life, and with our increased longevity

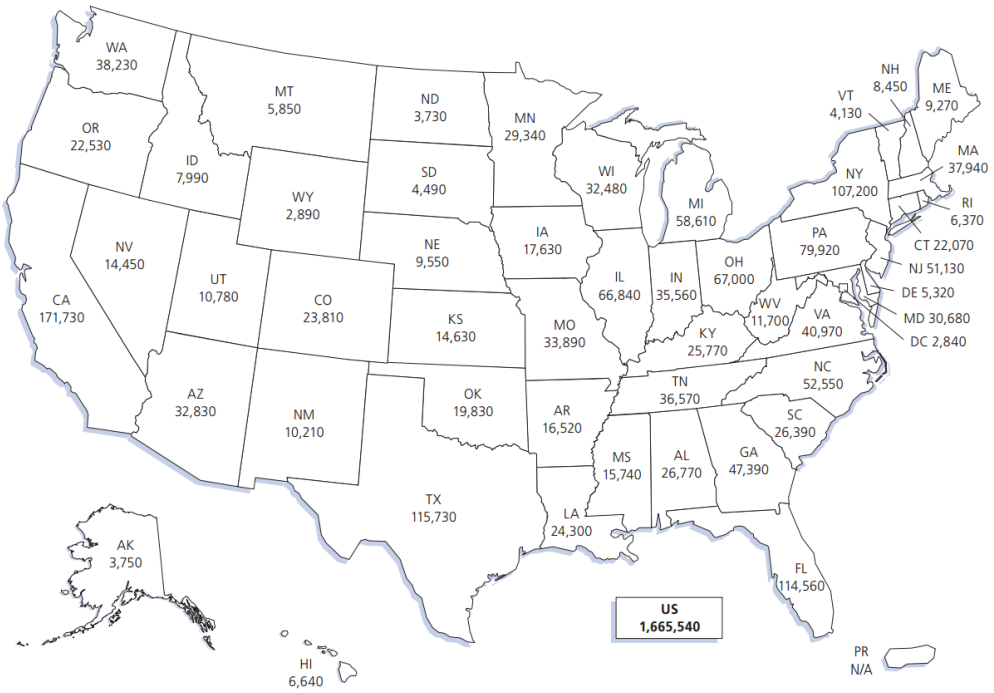

Figure 1: Number of new cancer cases by state (ACS, 2014).

comes increased susceptibility. Sobering statistics indeed. But illness is personal, not just statistics. With certainty, you who will read this will have had personal experience with this disease, but despite this prevalence, cancer is still a mystery the scientific community is trying to unravel.

Though referred to in monolith, cancer is a collection of diseases characterized by uncontrolled and abnormal cell growth [1]. Though there are said to be many external (smoking, viral infections, chemicals, radiation) and internal (heritable factors, hormones, autoimmune disease) "causes" of cancer, the true source is more fundamental, rooted in the ideas of evolution and growth itself. In the normal cells that make up our body, genetic material in the form of DNA carries information that controls the processes of life, including cell growth and division [2]. Normal growth requires a balance between genes that promote cell proliferation and those that

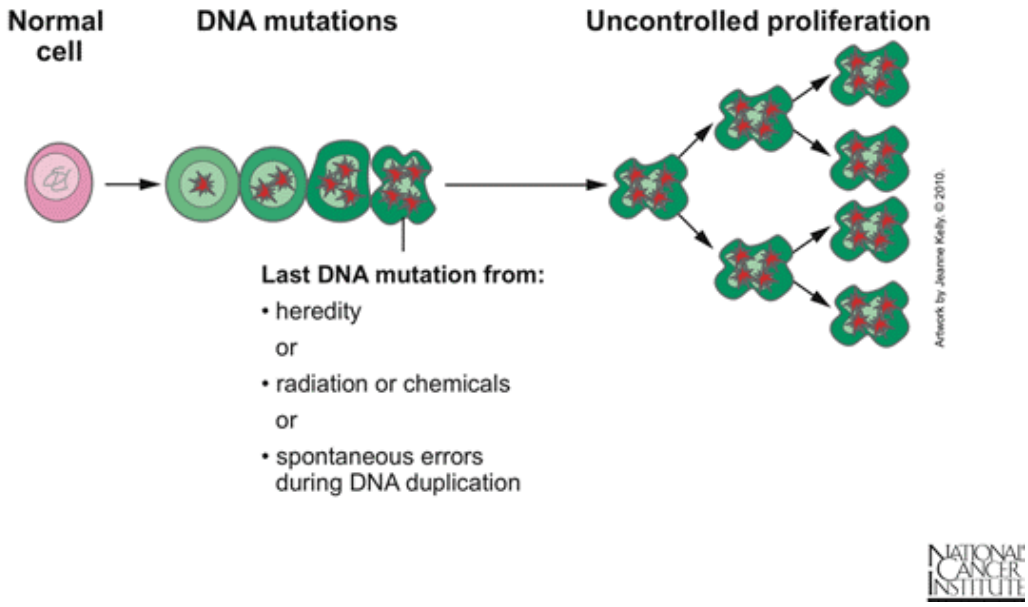

Figure 2: Normal cells acquire mutations from many sources, resulting in uncontrolled cell proliferation (Jeanne Kelly, NCI).

suppress it. When a cell divides, it must make copies of this genetic material so that each cell will have an instruction set of their own. But over time, genes accumulate mutations, changes in the genetic material, through the previously described external and internal sources that are passed on to daughter cells. The process of copying the genetic material itself can even result in mutations (Figure 2). In fact, it has been estimated that an individual cell suffers up to one million DNA changes per day [3]. Though mechanisms exist to correct these changes in the form of

"proofreading enzymes," lasting genetic changes are expected to occur at rates of .0001 to .000001 per cell for a given gene [4]. With nearly 40 trillion cells for the average person, it is guaranteed that we are all filled with mutations. So called "tumor suppressor genes" exist to cause death in those cells that receive too many mutations, but these instruction sets themselves can themselves be mutated and overwhelmed.

According to research findings from the Cancer Genome Project, most cancer cells possess 60 or more mutations [2]. The process is piecemeal, with these mutations accumulating over time as a result of independent events. Mutations will begin affecting genes that promote or suppress cell proliferation, conferring growth advantages on these aberrant cells. Daughters of these cells will outcompete healthy neighbors due to these changes and further mutations will occur giving even greater advantage. This process is in fact natural selection, the driver behind the evolution of all organisms [2]. Thus it seems, if we are lucky to live so long, cancer is unavoidable due to the processes that facilitated the development of life.

Scientific views of cancer have changed considerably throughout history, and for most of the modern era, there has been little progress in cancer treatment. In fact for many, the belief that cancer is incurable has persisted into the 21st century. Yet more and more each day, oncologists and cancer biologists add to our understanding of the origins and behavior of cancer, advancing hope for patients with new treatments. In particular, the discovery of rare tumor cells referred to as cancer stem-like cells (CSC) may provide an exciting new direction for cancer treatment. These cells provide resistance to traditional chemotherapy and other treatments and have the ability to divide and differentiate to recapitulate whole tumors [5]. Understanding the source of CSC and how to target their behavior in the clinic may provide solutions for how to manage, if not cure, cancer when it arises [6]. Conventional cell assay tools do not provide the resolution or abilities

needed to properly assess CSC behavior due to their rarity and complexity. The combined efforts of oncologists, cancer biologists, and engineers working on novel micro- tools and assays are needed to advance cancer treatment into the next millennia.

1.1 Evolving Views of Cancer

Though viewed as a modern disease, possibly due to lifespan requirements, cancer has likely existed as long as multicellular life itself. It is first described in the written record nearly 4,600 years ago, in a scroll called the Edwin Smith papyrus written by the Egyptian polymath Imhotep [7, 8]. Imhotep was an influential engineer, architect, and physician (and to reward him for his foundational contributions to these fields, we remember him most for his depiction as a vengeful undead in 1932's and 1999's *The Mummy*). The medical descriptions held within were remarkable for containing no magical ideas, only anatomical observations. 48 cases were described within including 27 head injuries, 8 injuries to the sternum, 6 neck injuries, 3 arm injuries, 1 abscess, 2 collarbone injuries, 1 spinal injury, 1 to the shoulder, and finally, 1 description of a breast tumor. Though offering treatments for the other cases, when speaking of treatment for the breast tumor, the scroll only states that, "[t]here is none."

In approximately 400 BC, the disease received the name we know, "cancer." The Greek physician Hippocrates used the terms *carcinos* and *carcinoma,* meaning crab to describe the tumors and finger-like spreading projections from it. With no understanding of cells, nor tools to observe and study the disease with precision, ancient Greek and Roman physicians had to view and treat the disease on a macroscale via surgical removal. The Greek historian Herodotus tells of a Persian Queen, Atossa, who had an inflammatory tumor removed from her breast, saving her life at least temporarily [8]. Roman physician Galen would surgically remove tumors, and this

remained the approach to cancer management for centuries. But Galen, like Imhotep, knew this was ineffective describing, "[a]fter excision, even when a scar has formed, none the less the disease has returned."

Following early Greek thought, Galen proposed that the human body was composed for 4 primary fluids: blood, phlegm, yellow bile, and black bile. The Greeks knew hydraulics, so of course, the human body also happened to be a hydraulic system. In healthy individuals, these fluids were kept in balance, but when this balance was lost, illness occurred (heart disease was caused by too much blood, for instance). Cancer was linked to the overabundance of black bile. In Galenic medicine though tumors could be removed, there was still a systemic issues of black bile regulation. Black bile was thought to seep back into the wound and regrow the removed tumor.

Surgical approaches remained the primary approach for cancer treatment well into modern times and increased in popularity with the advent of widespread anesthesia in 1846. The true source of cancers was not discovered until the 19th century invention of the microscope. When examining tumors with these newly developed tools instead of black bile, scientists saw cell upon cell, dividing and invading into other tissues. It has taken over a century to develop our understanding of the genetic regulation at play that causes this uncontrolled proliferation, but at the time with the tools available, only more radical surgical removal was possible. Surgeries to remove the entire tumor along with any region where the cells had seemed to spread were developed. In breast cancers, surgeons such as William Steward Halsted at Johns Hopkins performed radical mastectomies, removing the breast, chest muscles, and lymph nodes [8]. Such procedures were common up until even the 1970s.

With the advent of X-rays in the early 1900s, radiation therapies were also developed. X-rays, capable of disrupting DNA, selectively target rapidly dividing cells, making them effective

for targeting cancers [9]. Like surgery, radiation is effective at treating locally confined tumors, however, once the tumor has spread, no increase in radiation dose results in better treatment [9]. Increased radiation doses had far worse effect, in fact causing cancers by inducing DNA damage.

Non-solid tumors, such a leukemia, were not observed until the late 1800s by German doctor Rudolph Virchow. Especially prevalent in childhood, acute leukemia was effectively a death sentence as no previously developed treatments were effective. These cancers of blood cells had no means of surgical removal and radiation could not be systemically applied. A different way of thinking about cancer treatment was necessary. Could chemical drugs, systemically applied, selectively target cancer cells? The key to the development of such drugs would be the ability to understand the differences between cancer and normal cells. American pathologist Sidney Farber was the first to identify such a difference that could be harnessed for systemic cancer treatment [10]. Using available tools, he found that folic acid stimulated leukaemic cell growth and enhanced disease progression. As such, he hypothesized that folic acid antagonists would disrupt the proliferation of cancer cells. In 1948 with chemicals synthesized by Yellapragada Subbarow, Farber showed for the first time that drug-induced disease remission was possible using aminopterin. These observations led to the development of other drugs for cancer treatment; a systemic cure for a systemic disease was possible.

These chemotherapeutic approaches, however, suffer their own drawbacks. The same genetic mechanisms that provide cancer cells with increased proliferative potential also facilitate the ability to evolve over time. Each new cancer cell contains additional mutations that can increase its fitness. Chemotherapeutic agents apply a selective pressure, and though this may kill most cells, it selects for drug resistance. Like antibiotics create resistant bacteria, drugs may produce resistant cancer cells, explaining the prevalence of cancer remission even with systemic treatment.

Strangely, cancer relapse is not a certainty, nor is its timing and therapeutic resistance consistent. In fact, there is a deeper explanation for cancer persistence and resistance. Recent advances in cancer biology have shown significant cell heterogeneity among tumor cells that were previously treated as a single population of cells [11, 12, 13, 6, 14, 15], and treatments with the ability to target particularly important subpopulations will provide the next advancement in patient care.

1.2 Cancer Stem-Like Cells (CSC)

In a landmark 1994 paper, Professor John Dick and his team at the University of Toronto experimentally demonstrated differential cancer initiation potential among leukemia tumors cell subpopulations [16]. This was a controversial finding, because in traditional stocastic models of cancer, any cell is expected to reform the entirety of a tumor (Figure 3), though not necessarily with high probability. Trained as a stem cell biologist, Professor Dick was very familiar with the hierarchical organization of blood, and believed there might be evidence for such a hierarchy in hematological cancer as well [17]. All blood cells (white, red, platelets, etc.) arise from a population of blood stem cells [18]. Stems cells are defined by two key behaviors: 1) the ability to self-renew nearly indefinitely (normal cells have limited replication potential) and 2) the ability to

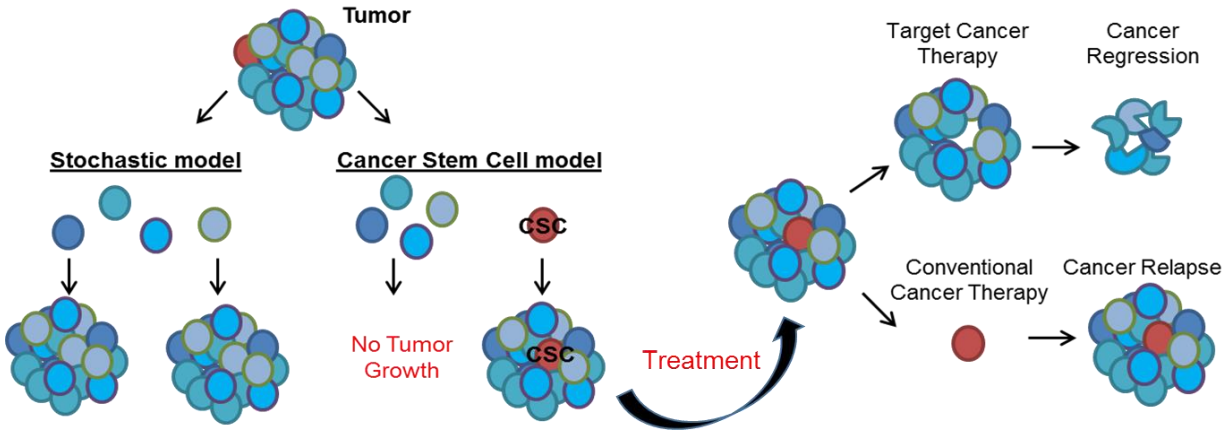

Figure 3: Stochastic and cancer stem cell models for tumor initiation and drug response in cancer. Cancer stem cells resist conventional therapy and must be targeted to cause cancer regression.

differentiate into other cells. This creates a hierarchy of potency with stem cells at the top, generating all other cell types and renewing itself, and progenitor cells serving as intermediate proliferation amplifiers for the final differentiated cells (red blood cells, B-cells, T-cells, etc.) (Figure 4) [19]. If a large number of blood cells are depleted, say by chemotherapeutic drugs, stem cells proliferate and produce replacement cells while self-renewing their own population. Due to the long term self-renewal potential of the stem cells, this process can occur any number of times. If the pool of hematological stem cells is depleted, the system gradually collapses.

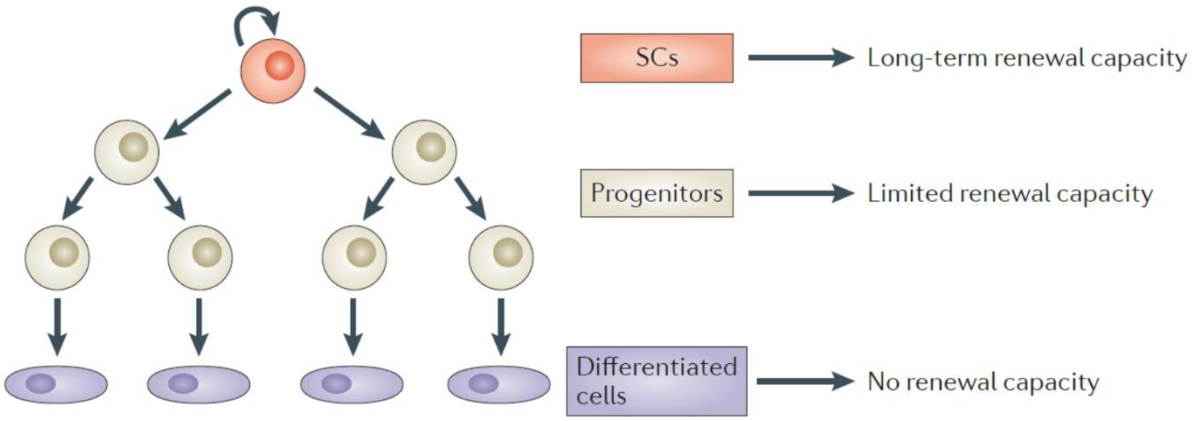

Figure 4: Stem cell hierarchies consisting of stem cells, progenitors, and fully differentiated cells (Blanpain and Beck, 2013).

If such a hierarchical model is applied to cancer, it would still explain key pathological features such as overactive proliferation, invasion, and mutation, but it would also help explain contradictions involved in relapse and therapy [17]. To investigate this possibility, Dick et al. implanted leukemia cells in varying concentration in severe combined immune deficient (SCID) mice and observed the rate at which tumors formed [16]. Implantation of nearly one million cells was needed to be sure that at least one cell could generate a new leukemia. When examining this one-in-a-million cell, it was found that it expressed surface markers similar to those found on healthy blood stem cells. When cells were sorted for these markers and then used for serial

leukemia initiation, the numbers required for leukemias to form were orders of magnitude less than bulk, implying potential for indefinite self-renewal and the ability to recreate the whole cancer population (Figure 3). Noting the parallels, these cells were termed ***cancer stem cells*** (CSCs or cancer stem-like cells).

This finding generated considerable interest in cancer biology. In 2003, researchers here at the University of Michigan (Morrison, Clake, Wicha) identified CSCs in solid tumors (breast) as well [20]. To date, potential CSC populations have been identified in brain [21], colon [22], breast [20], ovarian [23], pancreatic [24], prostate [25], melanoma [26] and myeloma cancers [27], but the CSC model need to be applicable to all cancer types in order to be clinically impactful. Most traditional chemotherapies act against rapidly diving cells, thus having a slight specificity for cancer cells over healthy cells. CSCs, on the other hand, have shown radiation and chemotherapy resistance and have overall lower division rates, allowing them to survive therapy [5, 6, 28, 29] and eventually cause relapse. Targeted therapeutics that destroy the CSC pool sustaining a cancer have the potential to cause cancer regression.

Finding agents capable of targeting CSCs, though, is no simple task. Screening large chemical libraries against CSCs or identifying chemical or behavioral targets exclusive to CSCs are both complicated by the nature of the cells themselves. First, CSCs are rare, representing typically <5% of cells in cell lines and <1% of cells in tumors. Second, CSCs are a "moving target," undergoing symmetric and asymmetric division, such that pure CSC populations are transient and difficult to study over time. Finally, primary human CSCs are surprisingly difficult to grow in vitro and in vivo. Large scale screens for therapeutics capable of specifically targeting CSCs are challenging since traditional methods typically focus on reduction of overall tumor cell numbers to evaluate success of cancer treatment. Thus, therapies eliminating the rare, but critical, CSCs

would be missed in traditional screen. Likewise, conventional assays that study cell characteristics require large numbers of cells. In these cases, the behaviors of CSC would be averaged out or overwhelmed. Experiments using macroscale methods to handle these rare microscopic cells have led to incorrect or at least imprecise and harder to replicate results. Attempts to tease out rare cell behavior are labor intensive, low-throughput, often impure, less physiologically accurate, and difficult to integrate with other assays. To identify possible anti-CSC drugs, we should not only develop new chemicals, but also need to develop new assays and culture technologies to study CSC characteristics in a more in-depth way.

1.3 Advances in Cell Culture Methodology

Conventional culture petri dishes and plates have a long history, starting with their invention in 1877 by German physician Julius Richard Petri for applications with bacterial culture. Despite their simplicity, they have remained the standard for tissue and cell culture since the advent of cell lines. Culture dishes, in essence, are nothing more that shallow cylindrical glass or plastic lidded containers; no active functionality is present. Cells are simply loaded with growth media and/or chemicals and the resulting behavior is observed. These traditional culture tools create data that are averages over large numbers of cells, with an assumption of similar cell behavior, where in actuality cells may be a mixture of different cell subtypes, such as with bulk tumor and CSC. In many biological labs, brute force adaptation of conventional protocols is widespread. Serial dilution methods, where samples are diluted in multiple steps to a concentration where only a few cells exist in a hundreds of microliters for loading in multiwell plates, are commonly employed for single cell analysis. Though researchers have shown it is possible to study single cells and their

heterogeneity with these macroscopic methods, it is labor intensive, low-throughput, often impure, less physiologically accurate and difficult to integrate with other assays [30].

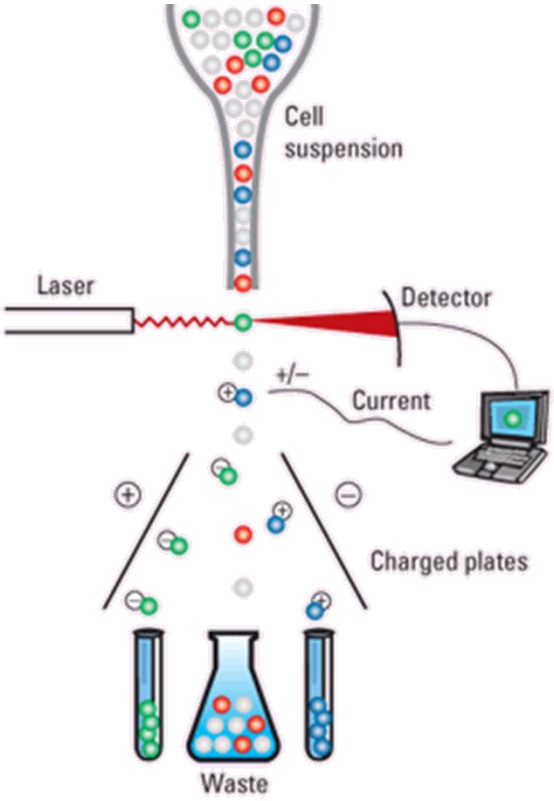

Figure 5: A schematic of fluorescence-activated cell sorting where single cell fluorescent states are measured and charge plates deploy single cells into separate containers (Willis, 2004).

Fluorescent Activated Cell Sorting (FACS) has offered an alternative way to look at single cell behavior. This method is capable of sorting heterogeneous mixtures of cells into separate containers, one cell at a time. For FACS-based sorting (Figure 5) [31], cells are fluorescently labelled with targets of interest and loaded into the machine as a suspension. The cells are concentrated into a thin stream and passed through a vibrating nozzle to produce droplets with individual cells. As each droplet passes through a detector, FACS hardware measures the fluorescent properties. If the proper fluorescent markers are seen, the droplet is given an electrical charge. The droplets then pass through charged plates and are directed to various collection tubes based on the sorting markers. The FACS process, though, has a number of drawbacks and

limitations: 1) FACS machines are expensive, 2) the process can actually be damaging to the cells, lowering overall cell viability after sort, and 3) FACS is known to have a small but significant contamination rate of unwanted cells. This contamination rate may in fact contribute to the current contentious nature of the CSC model [32]. FACS machines have been used to facilitate single cell seeding into multiwall plates, but anywhere between 1-20 cells can actually be loaded. On its own, FACS can only provide relative population distributions and is regularly used with conventional culture systems to perform phenotypic assays, though rarely (and unreliably) with single cell resolution.

Microfluidic technology offers the opportunity to create tools that overcome the limitations of culture plates and FACS machines. Microfluidics refers to fabricated microsystems capable of manipulating small fluid volumes (μL, nL, pL). In the 1960's, development of photolithography enabled the miniaturization and microfabrication of electronics and integration of thousands of transistors on semiconductor wafers. The use of microfabrication expanded over the following decade, and new material etching and deposition processes were developed. This facilitated the creation of devices containing movable micro-elements in addition to the electronics. These devices, called micro-electro-mechanical-systems (MEMS), saw widespread adoption as integrated sensors. As more MEMS based systems were applied in biology, chemistry and biomedical fields, fluidic channels and control were necessary. With integrated fluidic control, these novel microfluidic MEMS devices were used for integrated on-chip laboratories and clinical operations. To reduce cost and fabrication times, polydimethylsiloxane (PDMS) based soft lithographic methods were developed enabling a large number of laboratories to conduct researches in microfluidics [33].

Microfluidic technologies use small quantities of samples and reagents, are low in cost, and are simple to fabricate. These devices also occupy a small three dimensional space, making them ideal for applications as analytical devices for both basic cell biological studies and clinical use. Laminar fluidic control, additionally, facilitates the development of novel processes not possible on a macro-scale [34]. More recently, cell-based microfluidic devices have created new opportunities for the control of cell growth and stimulation through microfluidic channels that regulate the transport of fluids and soluble factors. To date, microfluidic cell-culture assays have been applied for a variety of cells including bacteria, human carcinoma cells, and stem cells for example [35, 36, 37, 38, 39].

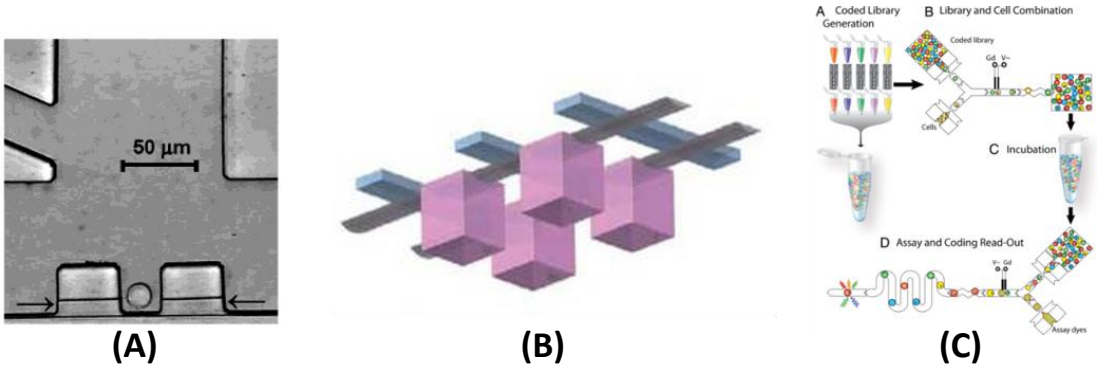

***Figure 6: State-of-the-art single cell resolution microfluidic devices for (A) viability and Ca^{+} measurements** [41], **(B) hematopoietic single cell division tracking** [39], **and (C) high throughput drug screening and readout** [42].*

More recently microfluidics has become an important tool in enabling analysis of single cells [39]. Breakthrough single cell systems, such as those presented by Lecault *et al* in Nature Methods [39], offer huge advantages over traditional methodologies in capture, culture, and analysis of single cells. In this case, researchers were able to systematically track hemopoetic stem cell division. Applied to the study of CSC behavior, such platforms would facilitate direct observation of the rare population. This and other single cell microfluidic systems provide unique opportunities, but several disadvantages hinder their use [40, 41, 42] (Figure 6 and Table 1). In the device from Lecault [39], the probabilistic capture mechanism results in low capture efficiency

(~10-30%). Droplet based approaches, such as those used by Brouzes et al [42], have high capture efficiency and extremely high throughput, but require external pumps and connections, multiple fluidic ports, and can only perform short term assays. Flow based methods allow moderate to high throughput, but offer no ability to actually culture cells. Extremely high capture efficiency was demonstrated by Wheeler et al [41], but again, external equipment was required and assay

Table 1: Advantages and disadvantages of single cell microfluidic systems

Single Cell Capture System	Capture Efficiency	Throughput	External Systems	Assay Capability	Operation
Brouzes et al [42]	High	1000s	Yes	Limited	Complex
Yu et al [40]	Moderate	100s	Yes	Limited	Complex
Wheeler et al [41]	High	1-10s	Yes	Limited	Complex
Lecault et al [39]	Low	1000s	Yes	Various	Moderate

capability was limited to non-culture applications. Several devices that actively manipulate cells, through electrically [43, 44, 45] or optically [46] driven dielectrophoresis, provide selective cell capture and more precise control. These approaches require special conductive media and complex external equipment for operation, however, limiting their overall utility in biological laboratories.

As such, these tools remain used only in the labs that develop them, due to required external systems, expertise in operation, and complications with translating them into current laboratory practices. More importantly, these systems cannot work with small initial suspension (10-100 cells) such as those received from primary CSC samples. Alternative passive hydrodynamic capture schemes are more attractive due to their simple operation and user-independent cell capture [48, 49, 50]. A passive capture structures with improved efficiency has been reported [47], but it is unable to culture cells for a long enough period of time. More recently, A. C. Rowat *et al.* demonstrated a microfluidic chip capable of tracking lineages of single cells [48]. While their line-

shaped microchamber is appropriate for non-adherent cell expansion, it poses spatial constraints that may restrict growth and introduce phenotypic changes in adherent cells. But high efficiency capture, the capability for long term culture, and simple integration are all required to study CSC.

As one can see, researchers are devoting considerable effort to the development of single cell based biological assays and approaches, but as these tools seldom leave the labs in which they were developed, brute force adaptation of conventional bulk protocols for single cells is widespread in biological labs. Serial dilution methods, where samples are diluted in multiple steps to a concentration where only a few cells exist in hundreds of microliters for loading in multiwell plates, are commonly employed for single cell analysis. These methods, however, are labor intensive, have low throughput, and are often difficult to repeat, leading to poor reproducibility in the generated data. Fortunately, a single cell hydrodynamic capture scheme and microwell design previously developed by Dr. Jaehoon Chung in the lab of Professor Euisik Yoon [49] provides ideal characteristics for the creation of assay technology for widespread use to advance our understanding of cancer and CSCs in particular.

1.4 Hydrodynamic Single Cell Capture

To address the shortcomings in many current approaches, Dr. Jaehoon Chung in the Yoon lab developed a passive microfluidic scheme for efficient cell capturing using hydrodynamic guiding structures [49]. The simple microwell structure utilizes changes in hydrodynamic resistance to facilitate cell capture from simple gravity flow (3-5 μL/hour). No external components or equipment (save a micropipette) are needed to operate the device. A schematic representation of the original microwell design and method of operation is show in Figure 7 [49].

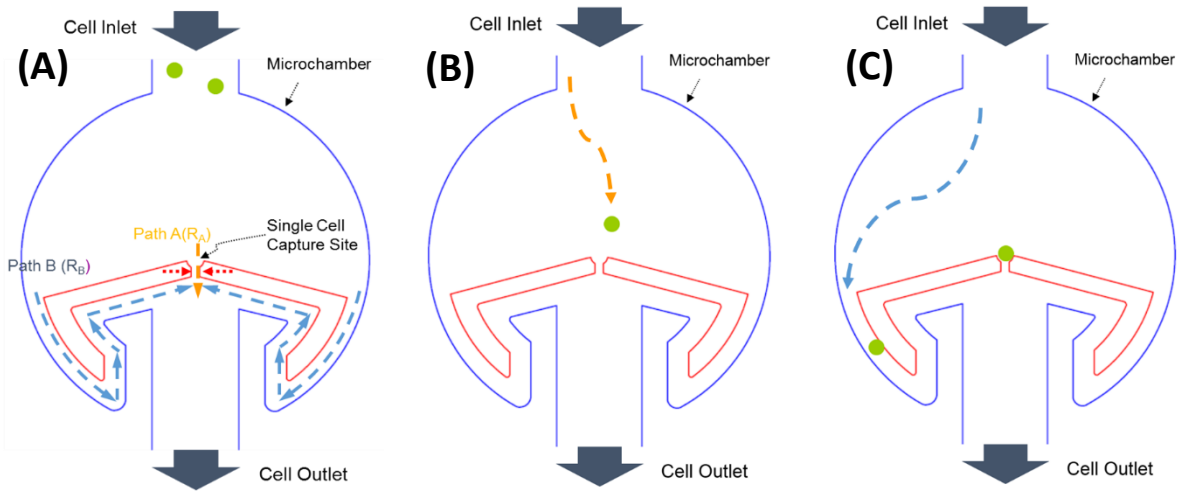

Figure 7: (A) In the passive hydrodynamic capture scheme, Path A has a low hydrodynamic resistance but small size compared to bypass Path B. (B) Single cells are sterically captured in the Path A, increasing its hydrodynamic resistance. (C) This diverters following cells to downstream microwells *[49]*.

In each unit well, a hydrodynamic guiding structure is present to divide the injected flow into two streams: path A through the center and path B along the border of the microwell (path B consists of two symmetric paths on either side). Path A has a shorter length than path B, and thus, a smaller flow resistance. Due to the flow resistance difference, most of the incoming flow and cells in the suspension will take path A rather than path B. This facilitates capture as path A has a width that is smaller than the cell diameter, creating a steric capture site. Once capture occurs, the resistance of the flow path greatly increase, diverting cells towards path B and other capture sites that have been array in serial and parallel. This hydrodynamic passive capture scheme significantly increases the cell capturing efficiency and accurately positions cells at the capture sites [49].

The capture efficiency of the scheme can be predicted by assuming a well uniformly dispersed cell solution and calculating the flow volume balance ratio between the two paths. The flow volume that passes through path A represents captured cells, while the flow volume though path B represents lost cells. The volumetric flow ratio between path A and path B can be simply

modeled based on the geometric parameters of the microwell that define the hydrodynamic resistance, given by:

$$\frac{Qb}{Qa} = \left(\frac{La}{Lb}\right)\left(\frac{Wa + Ha}{Wb + Hb}\right)^2 \left(\frac{WbHb}{WaHa}\right)^3$$

where Q is a volumetric flow rate, L is the channel length, W is the channel width, and H is the channel height. The capture probability can then be calculated as the ratio of the volumetric flow stream passing through path A to the total injected flow, which is given by:

$$Pa\left(\frac{Qb}{Qa}\right) = \left(\frac{1}{1 + \frac{Qb}{Qa}}\right)$$

From these equations, $\left(\frac{Lb}{La}\right)$ and $\left(\frac{Wb}{Wa}\right)$ can be identified as important design parameters dictating well geometry and cell capture efficiency. Using these factors to guide his design, Dr. Chung modeled, fabricated, and testing various geometries of this capture scheme (Figure 8) in 8 by 8 arrays [49]. Fabrication was performed using standard soft lithographic techniques with one layer of polydimethylsiloxane. The 25 μm-thick mold was patterned on a bare silicon substrate using epoxy-based negative photoresist, SU8-10 (Microchem, MA). Liquid PDMS was cast on it and solidified at 90 °C on a hotplate for 3 h. Then, the cured PDMS was cut into pieces and detached, and holes for the inlet and outlet were punched. Channels were bonded to a glass slide with oxygen plasma. Fabricated microwells were 400μm in diamters with flow channels of 150μm width and

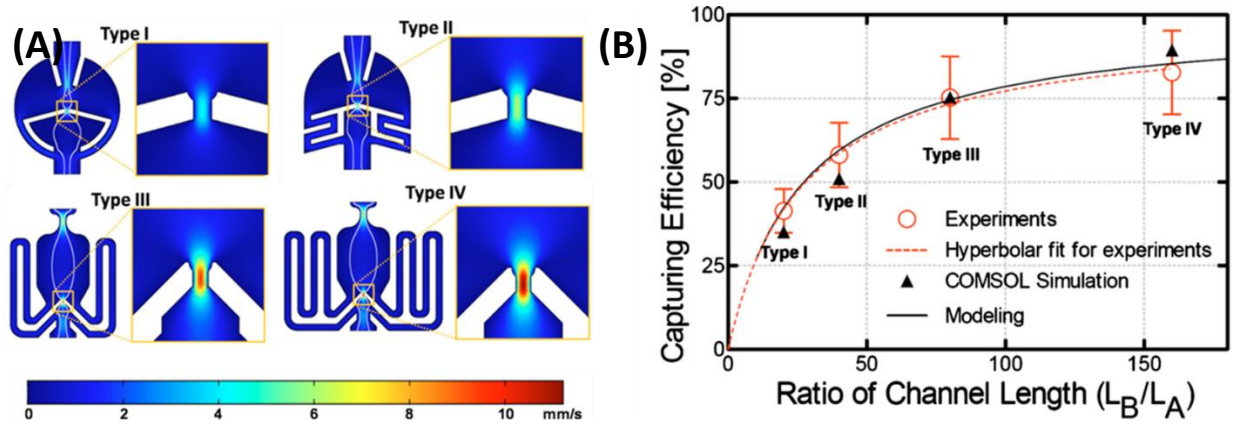

Figure 8: (A) Simulations of microwell flow rates and (B) simulations/experimental performance of high efficiency single cell capture schemes, Type I through Type IV *[49]*.

25μm height. Simulations performed using Comsol Multiphysics support improved capture with increased path B to path A hydrodynamic resistance ratios. The computation results also match very well with observed experimental results. For quantitative analysis, the devices were first tested using microbeads (15 μm in diameter, micromer-M, Micromod, Germany). Capture efficiency values were obtained by counting all microbeads that passed through one column of microwells until all capture sites were occupied. Multiple design architectures were tested when modifying the path parameters to minimize well size. This helps maintain maximum well packing density, while improving single cell capture.

Capture experiments were also performed with PC3 prostate cancer cells, and matched well with microbead data (Figure 8). PC3 cells were loaded into the device (~$5x10^4$ cells/ml) by pipetting a cell suspension into the inlet well. After only a few minutes, over 80% of wells have captured single PC3 cells. On chip culture was performed for 3 days in RPMI media +10% fetal bovine serum (FBS), and good cell viability and proliferation were observed, confirming that the hydrodynamic guiding structure does not affect cell viability. This single cell capture scheme developed by Dr. Chung can be easily expanded to a larger array size for high throughput single cell assays and drug screening application [50]. Devices operating on this approach meet biological

user needs for single cell approaches: high single cell capture rates and efficiency and simple, equipment free operation that allow these devices to be deployed in a variety of lab settings. This scheme serves as the fundamental design approach for all assays and devices presented herein.

While Type IV devices (Figure 8), showed the highest capture efficiency in the smaller array sizes used in this study, this does not take into account performance as array size is increased. The high overall fluidic resistance of Type IV can affect device performance. When arrayed into hundreds and thousands of wells, Type IV architectures experience diminished capture due to lower flow rates. For this reason, Type III- based microwells were used for increasing array sizes and throughout our experimentation in this dissertation. In this work, we have applied the capture scheme to investigate CSC division, differentiation, and drug response, and to create robust single cell mammosphere assays for marker-free CSC characterization.

Chapter 2: Adherent Assays of Single CSC Behavior

In order to study important cancer cell subpopulations such as CSC, we must develop single cell approaches capable of capturing and culture heterogeneous populations for long term analysis. Two key characteristics of CSC are their reported resistance to traditional chemotherapy and treatment and their ability to divide and differentiation to recapitulate whole tumor heterogeneity. In this chapter we will examine the development of a high efficiency highly scalable single cell capture scheme and how it has been applied in applications that investigate these key CSC characteristics, namely 1) drug screening in heterogeneous and target cell populations and 2) monitoring of CSC division and factors that control this process. The assays will be performed in high throughput, user friendly single cell adherent culture devices.

2.1 Drug Screening in Heterogeneous Cancer Cell Populations

Cancer heterogeneity has received considerable attention for its role in tumor initiation and progression, and its implication for diagnostics and therapeutics in the clinic. Even within purified cancer cell lines, recent studies have shown that cells are not identical but heterogeneous in metabolic, proliferative, and differentiation potentials, and in response to drug treatment [51, 52, 53, 13, 54]. For example, PC3 prostate carcinoma cells, used to characterize device performance in Chapter 2.1, give rise to a mixture of three clonal phenotypes: holoclones, meroclones, and paraclones [53, 13, 54]. The cellular differences are often identifiable through changes in progeny, differentiation potential, subtle but repeatable differences in proliferation, and morphology or physiological response to various treatments. As conventional approaches were used in these

studies, special care had to be taken to observe these subtle differences in bulk culture. As such, confirming these results and performing heterogenous drug screening on-chip was an ideal first application for Dr. Chung's scheme. The single cell capture array was optimized to promote clonal proliferation, and he designed a selective surface patterning (hydrophobic SU8 coated with pluronic) to prevent cell migration out of the well to ensure clonal uniformity within the microwell. This thereby enables traceable lineage expansion and subsequent on-chip characterization of clonal phenotype and drug response. As with previous iterations, the devices used here were designed to operate utilizing no external power or equipment (save a pipette) by employing gravity-driven flow. To investigate the potential of the system, we captured and cultured single PC3 prostate cancer cells in microwells, identified the three different sub-phenotypes in the cancer model, performed chemotherapeutic treatment, and correlated their clonal drug responsiveness to cell phenotype.

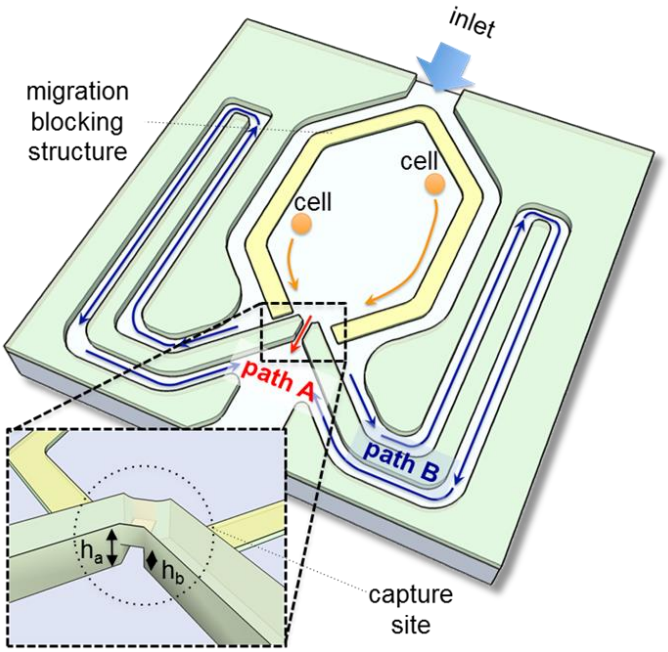

Figure 9: Schematic representation of final microwell design with improved capture site for single cell characterization *[50]*.

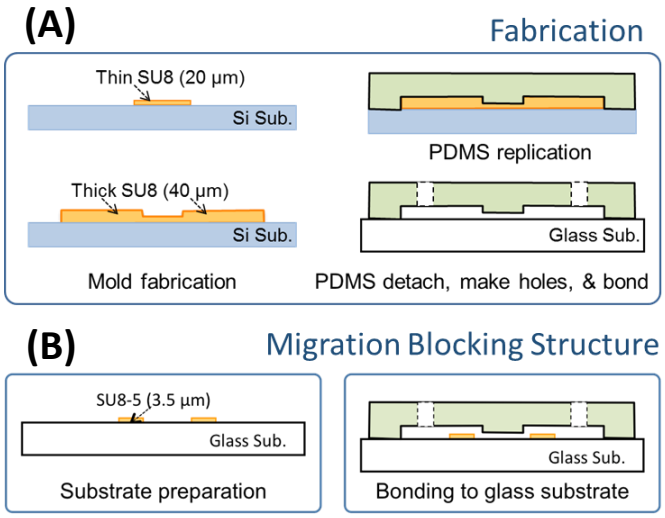

Figure 10: Fabrication of (A) single cell capture array and (B) substrate for migration blocking structures *[50]*.

Figure 9 shows the schematic view for a unit microwell of the array chip, illustrating the hydrodynamic guiding structure including a capture site and the developed migration blocking structure. For optimal capture, the capture site was modified to have a smaller channel height (h_b) as compared to the rest of the features (h_a). This reduced height ensure that captured cells completely block path A, diverting any following cells through path B. The other dimensions were chosen to increase the resistance difference while maintaining unobstructed cell flow (width, length, and height as 10 µm, 10 µm, and 20 µm for path A, and 20 µm, 800 µm, and 40 µm for path B, respectively).

The fabrication procedure uses a single PDMS layer and a glass substrate (Figure 10). A mold for the microchannels and microwells was made on a silicon wafer using negative photoresists, SU8-10 and SU8-25 (Microchem). To generate two different heights (20 µm and 40 µm), we performed photolithography twice to produce different thicknesses. The first layer was patterned with SU8-10 (20 µm) to generate the gap in the single cell capture sites and the second layer was done with SU8-25 (40 µm) to define all microchannels and microwells. After fabricating

the mold, PDMS (Dow Corning) was cast and cured to replicate it. Subsequently, two reservoirs were generated by punching through the PDMS using a 5mm diameter biopsy punch (Miltex).

To control growth and migration inside each microwell, Dr. Chung embedded migration-blocking patterns around the microwells; these patterns restrict cell movement in the microwells during proliferation. Without the blocking pattern some cells can migrate to adjacent microwells during long term culture. There are several reported techniques for blocking cellular migration, namely physical trenches/walls and chemical surface modification [55, 56, 57, 58, 59]. Using PC3 cells it was found that surface modification with pluronic copolymer (F108), a coating material with known anti-fouling properties to repel cells and other proteins [60, 61, 62], was most effective. F108 was selectively deposited by patterning a hydrophobic surface with 5 µm thick photoresist (SU8-5, Microchem) on a hydrophilic glass substrate. Inner surfaces were coated by flowing F108 and collagen successively conferring antifouling to only the SU8-coated-area. After glass slides were patterned, the PDMS replica was aligned and bonded to the separately prepared glass substrate.

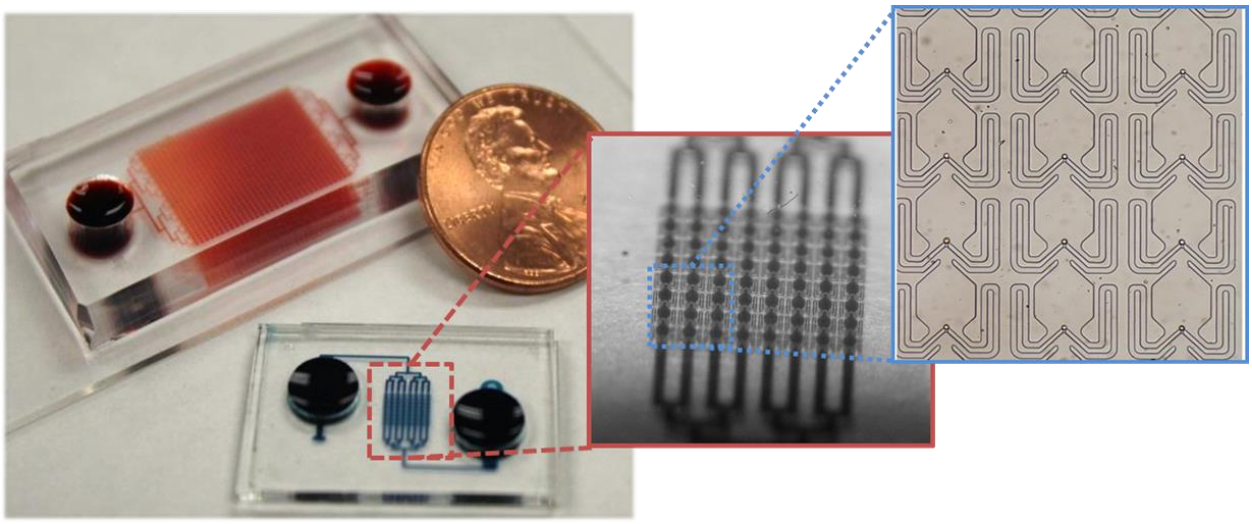

Figure 11: Fabricated example single cell capture arrays containing 64 and 1,024 microwells with inserts showing magnification of individual microwell structures.

We fabricated and tested chips featuring arrays of 64, 256, 320, and 1024 of these microwells (Figure 11) in order to demonstrate the scalability of this approach; however as previously discussed when array size increases, fluidic resistance changes may affect capture rates. As flow is generated through a passive gravity mechanism, increasing array size can decrease flow rates. The passive flow mechanism acts as a pressure source as gravity pushes the fluid down in the inlet, thus as the channel resistance increases, flow rates will decrease. In the design of the 1,024 well devices, two factors were modified to optimize the capture. First, the size of the culture area was reduced to a width of 115 µm. If the microwell is large, the flow velocity in this area may slow (reduced fluidic resistance leads to slower flow with constant pressure), reducing overall capture rates and efficiency. The second geometry optimized was the capture gap size. Capture gap size, must remain small to facilitate cell capture, but this has a negative effect of increasing the hydrodynamic resistance. As the capture site *length* does not contribute to cell capture, we minimized it to reduce the central path resistance without affecting cell capture. The final geometry in 1,024 of the central path is 5.6 µm by 15 µm, with a length of 6.2µm. The fabricated 1,024 well devices was fabricated using the same process as used for smaller arrays and has shown similar capture rates (80%) for all tested cell types. These larger arrays can facilitate considerably higher throughput data collection, which is especially important for rare cell subtypes such as cancer stem-like cells. In the course of this experiment, however, we completed testing with 64-well designs for both ease of data collection and analysis and because throughput was not an issue.

To validate his devices, testing was performed with fluorescent prostate carcinoma (PC3) cells. Cell loading was performed by simply adding cell suspension to the inlet reservoir. Gravity flow (3-5 µL/hour) and the hydrodynamic guiding structures automatically and efficiently load single cells into the microwell array. Then, the captured cells were cultured in the microwell array

over several days, with a continuous supply of culture medium in a 37˚C incubator. During culture the average doubling time was 1.7 days in the microfluidic chip which was comparable to the 1.5 days from conventional Petri-dish culture, demonstrating minimal effect on viability. For a proof of concept study of cellular heterogeneity, Dr. Chung replicated the experiment of Zhang et al. using the platform to show our capability to perform these experiments in a simple and repeatable manner.

After 4 days of culture on-chip, three different sub-phenotypic clones, namely holo, mero, and paraclones, could be identified and sorted from the heterogeneous parental PC3 cell line (Figure 12) based on their morphology and proliferation rates. Cells in the holoclones were relatively small and proliferated fast. Much like a cancer stem-like cell population, these cells should have considerable self-renewal potential and have been shown to be capable of recapitulating each of the three observed phenotypes given significant time [53]. Cells in the paraclones were large, proliferated much slower, and have a short replicative life-span. Cells in the merclones showed medium size and growth rate. As expected, holoclones are observed much

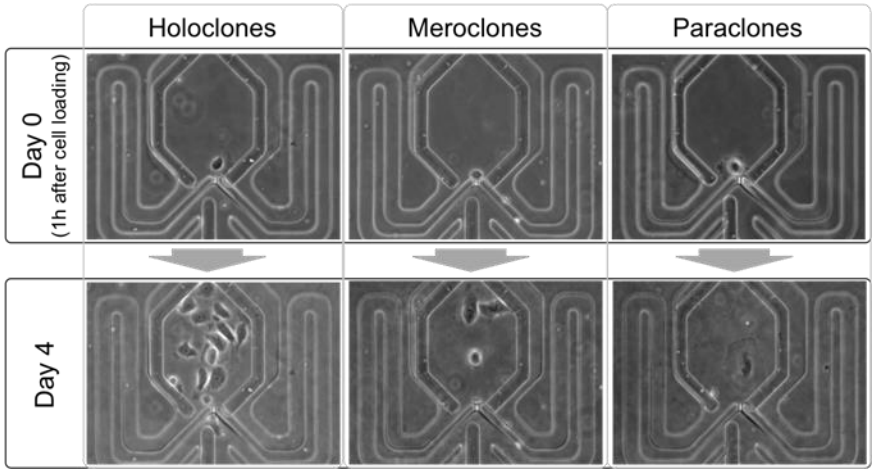

Figure 12: Heterogeneous clones (holoclones, meroclones, and paraclones) identified within the microfluidic platform *[50]*.

less frequently than either paraclones or meroclones. These results match well those obtained with the conventional dilution assay.

After validating culture functionality, Dr Chung used the the clonal culture chips to investigate the effectiveness of chemotherapeutic agents on different clones with the PC3 population. The ability to screen targeted or agents that are selective to cell subtypes is a key feature we desire for tools for the study of heterogeneous single cell populations. As before, PC3 cells were captured as single cells into the microwell array and cultured to identify subclones. Chemotherapeutic agents were introduced to all cells and drug effectiveness was verified by

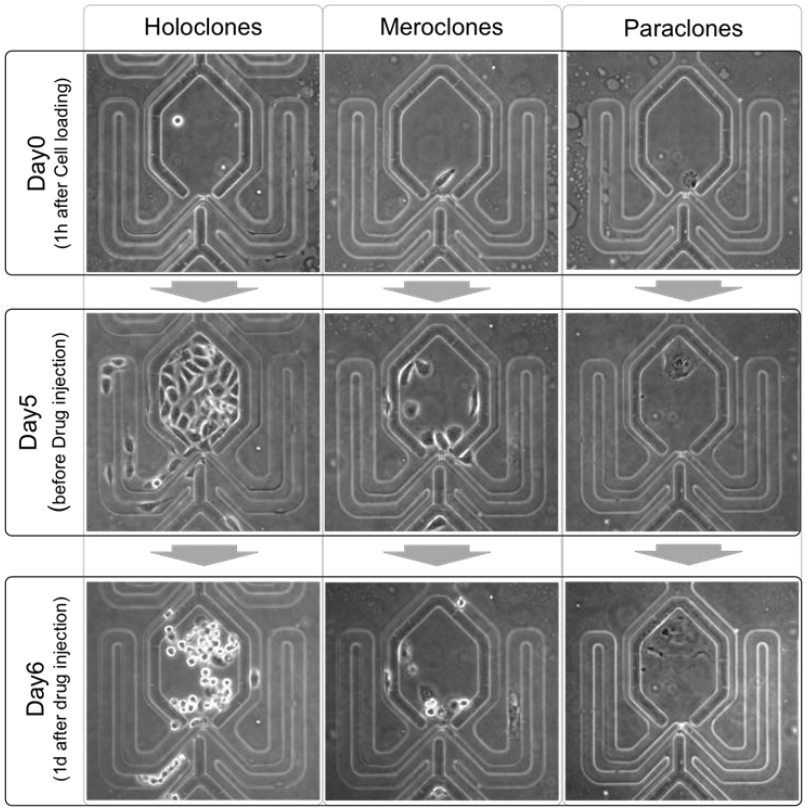

Figure 13: PC3 holoclone, meroclone, and paraclone response to 40nM/mL Docetaxel treatment on-chip after 5 days of culture and 1 day of drug treatment *[50]*.

calculating percentage of cell death in each sub-phenotype. Well-defined cell and colony location facilitates easy identification, tracking, and analysis of drug effectiveness in the heterogeneous PC3 population (Figure 13). 1 day after introducing 40 nM/mL of Docetaxel, a clinically relevant

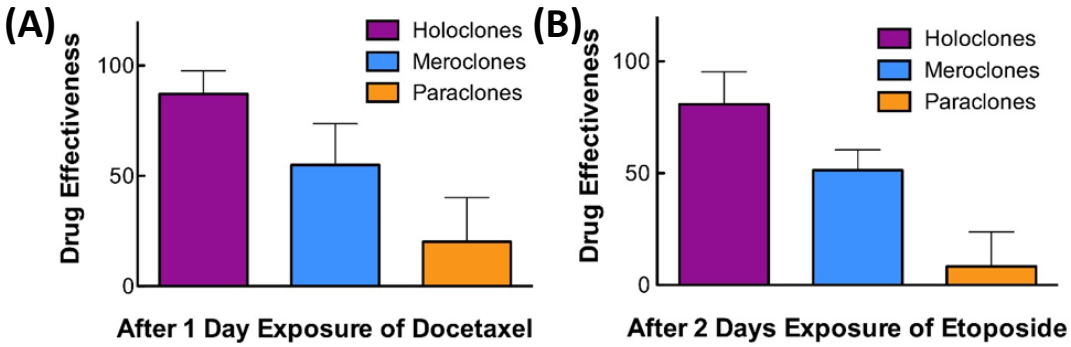

Figure 14: Quantification of PC3 subpopulation viability after treatment with either (A) Docetaxel or (B) Etoposide chemotherapy *[50]*.

anti-mitotic chemotherapeutic agent for prostate cancer, it was observed that the drug killed most of the progeny cells from the highly proliferative holoclones (>80%). In contrast, Docetaxel was less effective in eradicating paraclones and meroclones, with less than 30% and 50% cell death respectively (Figure 14). With Etoposide, a topoisomerase inhibitor, similar results were observed (Figure 14). These results can be attributed to both Docetaxel and Etoposide's mode of action: Docetaxel disrupts microtubule function while Etoposide disrupt DNA ligation. Both mechanisms are critically important during cell division and proliferation, and thus these agents have selective high potency against actively dividing cells. In a traditional assay, the subtle differences in the PC3 heterogeneous response would not have been as easily observed or quantified. In rarer populations, such as holoclones or CSCs, single cell methods must be used. This microfluidic approach sorts single cells into individual microwells in a parallel, high-throughput, and user independent manner utilizing only a pipette, facilitating their use in any laboratory or testing environment. As such, these experiments demonstrate the potential applications of the microfluidic clonal chip for on-chip characterization of clonal phenotype and *in vitro* drug screening assays. The presented results are proof that we can utilize our microfluidic single cell platform to study how heterogeneity manifests for future use with CSC drug response.

2.2 Targeted Drug Screening of CSCs

After validation of Dr. Chung's approach for use with heterogeneous populations and drug screening in general, we applied the device for CSC targeted therapeutic screens and assays using an ovarian cancer cell lines. Once CSCs and tumor initiating cells, which exist at the top of the differentiation hierarchy have been identified within a cell type or cancer of interest, we can perform targeted drug screening on single CSC rather than bulk heterogeneous populations (as was done with PC3 cell lines). CSCs are resistant to many traditional chemotherapeutic agents [28, 13, 63], so single cell drug screening is needed in order to observe their response independent of overall population cytotoxicity. In ovarian cancers for both primary human patient samples and lines, it has been recently demonstrated that aldehyde dehydrogenase (ALDH) is an excellent marker of CSCs [64, 63]. ALDH expression is typically present in <5% of ovarian cancer cells, so our high efficiency capture is ideal for this application. Ovarian CSCs are moving targets, often rapidly dividing and diluting sorted populations, so another advantage of the microfluidic culture device is our ability to perform live cell staining and imaging on-chip to confirm cellular identity prior to drug screening. Using the previously developed approach, we confirmed cisplatin resistance of ALDH+ SKOV3 cells and identified several compounds that specifically target ALDH+ versus ALDH- cells on-chip.

First, we evaluated our ability to culture ovarian cancer cell lines in our device, namely SKOV3 and A2780 (Figure 15). The SKOV3 cell line is an ascetic derived ovarian tumor line that is resistant to both tumor necrosis factor and several cytotoxic drugs, including cisplatin and Adriamycin. A2780 cells were establishes from tumor tissue, and both lines contain populations

of CSC [64]. As such while either line could serve as a useful model for performing drug screening, SKOV3 were select for our initial screening.

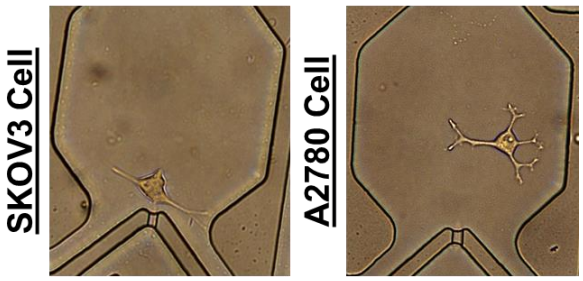

Figure 15: Successful culture of SKOV3 and A2780 ovarian cancer lines at a single cell level.

Prior to cell loading, chips required preparation for cell culture. As the first step, chips were sterilized by treating them with UV light for 5 min in a biobench. The chips were placed in a desiccator for 30 min to depressurize and remove the air trapped in the PDMS channels. Immediately after desiccation, we added 100 µl of 1 wt. % F108 (Pluronic copolymer for migration blocking) in deionized water to the inlet. Due to the depressurization in the device, the solution can easily fill the microchannels without forming air bubbles and flow from gravity pressure. After allowing the F108 solution to flow through the device for 10 minutes, devices were washed by flowing deionized water for 5 min. The bottom glass surface in microchannels was coated with 0.01% collagen to promote cell adhesion by adding 100 µl of a collagen solution into the inlet. Collagen can selectively coat only the glass substrate due to the antifouling properties of F108 that has already been used to coat the PDMS. After coating the collagen in a 37ºC incubator, it was washed out and replaced with cell culture media (RPMI+10% FBS) and placed the chip in the same incubator overnight, allowing the cell culture media to condition the devices.

Prior to loading, cells were culture in standard tissue culture plates in RPMI + 10% FBS. For loading, cell are trypsinized (with 0.05% Trypsin/EDTA) to release them from the surface and form cell suspensions. The cell concentration from the suspension was checked using a

hemocytometer and was adjusted to around $5x10^4$ cells/mL via diluting the culture media volume. For loading, this cell suspension is pipetted into the inlet and the gravity flow and hydrodynamic capture scheme does the rest. After capture, inlets are emptied and refilled with fresh culture media so as to prohibit additional cells from flowing as well as provide nutrients and remove waste continuously.

We loaded FACS isolated ALDH+ and ALDH- SKOV3 ovarian cells within the microfluidic device and then, after allowing cells to recover overnight, repeated our assessment of ALDH activity. The ALDH activity of the cells was assess by performing an ALDEFLUOR assay (StemCell Technologies) in situ and visualizing enzyme expression via fluorescent imaging. Aldefluor assays access the enzymatic activity of aldehyde dehydrogenase within the cell, rather than through a cell surface marker phenotype and can detect stem and progenitor cells in multiple cell types including ematopoietic, mammary, mesenchymal, endothelial, and neural in addition to ovarian lines [65, 66]. Using this assay we could clearly confirm the loading of ALDH+ and ALDH- cells. After 48 hours, cells were re-evaluated with the ALDEFLUOR assay. Consistent with their potential as stem cells, ALDH+ cells were observed to yield both ALDH+ and ALDH- daughter cells. In contrast ALDH- cell only produced ALDH- cells.

To further investigate the ALDH subpopulation, approximately multiple device (with a subset of loaded cells shown in Figure 17) were quickly and efficiently loaded with bulk SKOV3 cells using gravity flow in our device. Of the 896 wells loaded, 24 wells contained single ALDH+ CSC. This ~2.6% ALDH+ population is consistent with values reported in the literature [64, 67, 68] and demonstrates our ability to work with bulk populations in high throughput to obtain statistically significant samples of rare cells.

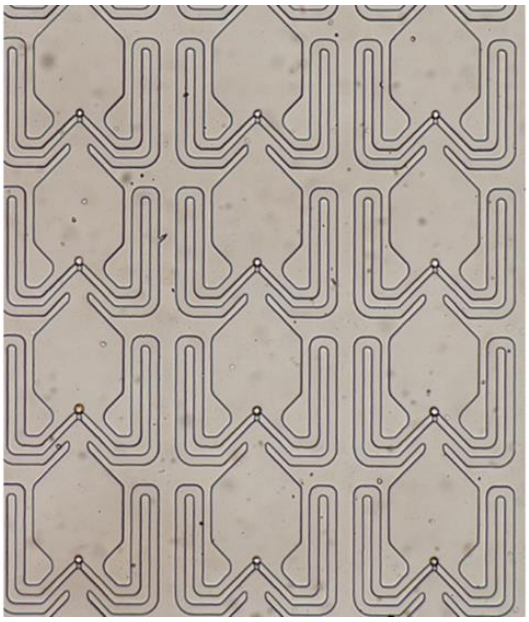

Figure 17: Single cell microwell subset with capture SKOV3 single cells.

In order to increase the percentage of ALDH+ cells for use with targeted drug screening without first FACS isolating, we pre-treated SKOV3 cells with the chemotherapeutic Cisplatin at 1 µg/mL for 3 days followed by a 24 washout period. This allows the selection of chemoresistant cells. Viable chemoresistant cells were then loaded within the microfluidic device and then stained with ALDEFLUOR. ALDH+ cells now represented over 50% of the captured cells. After 1 day

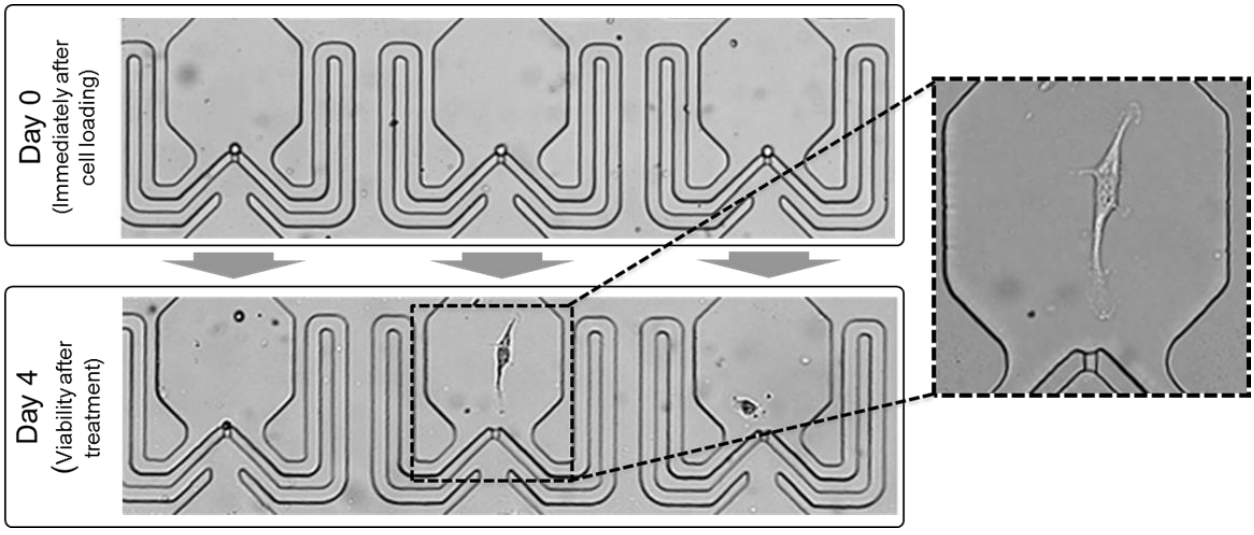

Figure 16: Loading and evaluation of single SKOV3 cell drug response on-chip.

cells were then treated with either (1) cisplatin at 0.25 µg/mL, (2) the ALDH inhibitor disulfuram at 50 µM, or (3) one of two novel ALDH inhibitors at 25µM. After 3 days cells were re-stained with Aldefluor and evaluated by microscopy (Figure 16). Consistent with our expectation, we observed that cisplatin killed more than 80% of the ALDH- tumor cells, however as expected, ~80% of the ALDH+ population were resistant to cisplatin therapy (Figure 18). In contrast, disulfiram and the two novel targeting compounds were essentially non-toxic to ALDH- cells but were 2-3 fold more effective at targeting ALDH+ cells ($p<0.01$) (Figure 18).

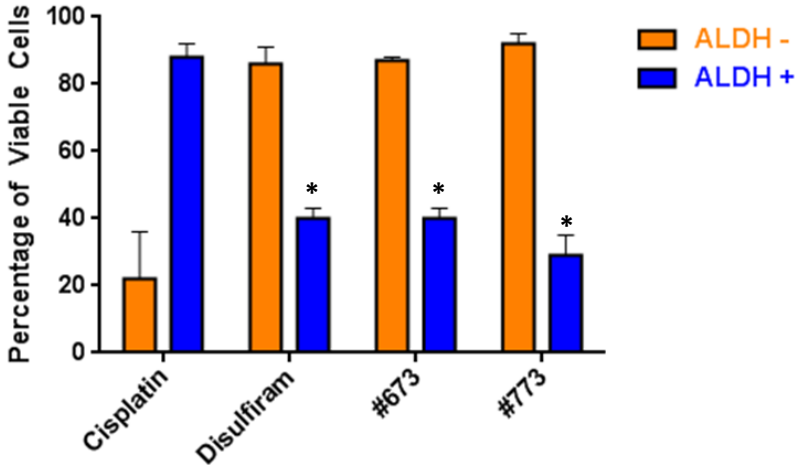

Figure 18: Cytotoxic efficacy of targeted and non-targeted agents versus ALDH+ and ALDH- SKOV single cells (* is p<0.01).

Due to the well-defined single cell isolation within our device, we were able to continue the culture of the treated cells for 6 additional days after initial evaluation. Due to the more limited proliferation and migration of these lines, migration blocking structures were not needed for this experiment. 10 total days after initial loading, ALDH+ populations of SKOV3 treated with cisplatin and disulfiram (controls) had increased in viability and total cell numbers (Figure 20). In contrast, ALDH+ cells treated with a single dose of the two novel ALDH inhibitors continued to show a decline in ALDH+ cell viability. Treated ALDH- populations showed little re-growth.

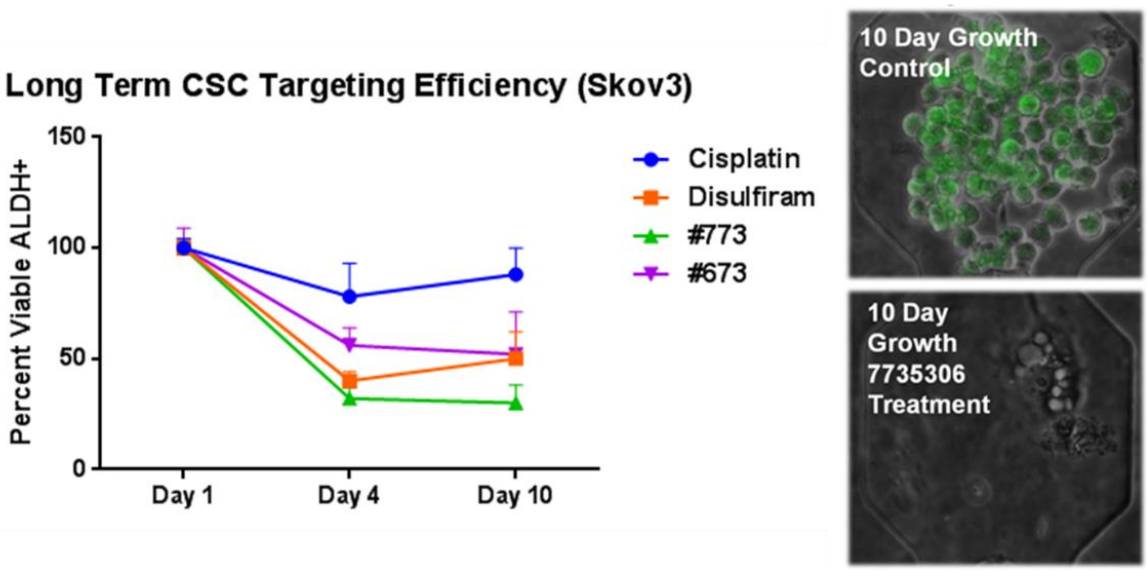

Figure 20: Long term post-treatment evaluation of CSC targeting and recovery in SKOV3

Due to the success of the two novel targeted compounds, they were further investigated by our collaborators and screened against additional cell lines including those like A2780 who's CSC populations are defined by multiple markers (ALDH and CD133) [64, 67]. Interestingly, #673 treatment with A2780 caused a reduction in the ALDH+ CD133+ populations without any evidence of apoptosis. It was hypothesized that #673 might be acting as a differentiation therapy, forcing asymmetric division or differentiation in the double positive CSC population, so we repeated the experiment with our single cell assay in order to directly observe single CSC behavior.

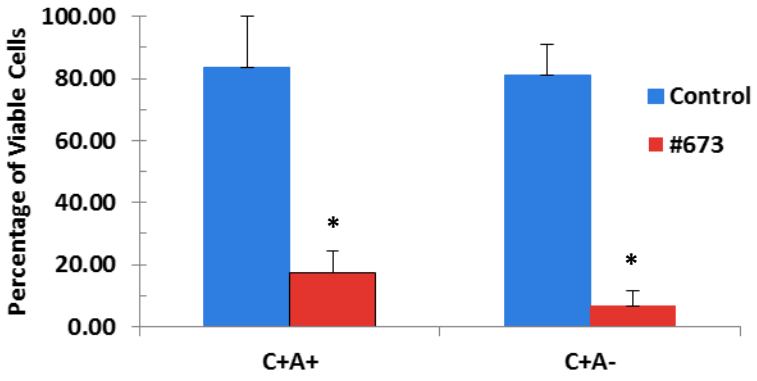

Figure 19: Viability effects of #673 on A2780 ALDH+ CD133+ and ALDH- CD133+ CSC populations (* is p<0.01).

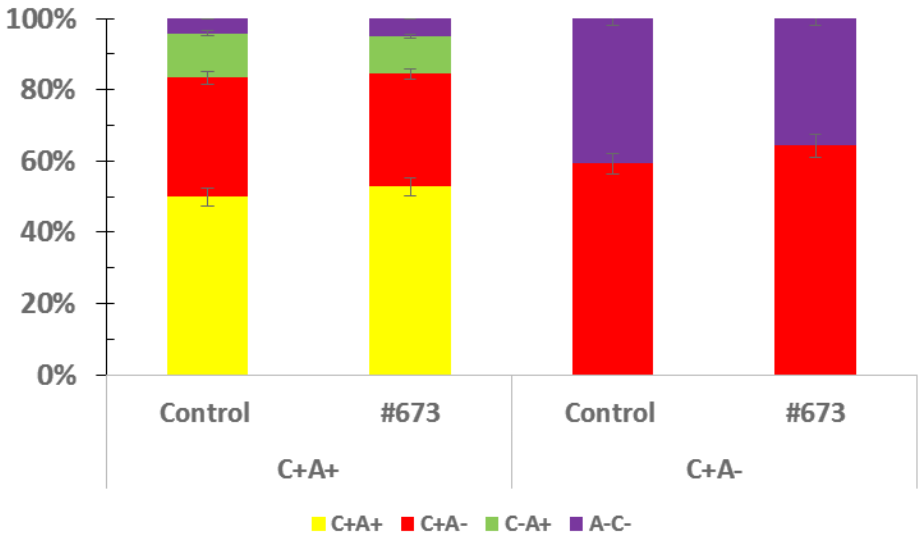

Figure 21: Effects of #673 treatment on CD133+ALDH+ and CD133+ALDH- CSC differentiation.

A2780 ovarian cancer cells were trypsinized, loaded into the device, had their ALDH and CD133 activity assessed, and cultured with RPMI +10% FBS. After 1 day of recovery on-chip, #673 was added at at 25µM and cells were cultured for 3 days. At day 4, CD133 and ALDH activity, as well as, viability were accessed. A significant loss in ALDH+ CD133+ and ALDH- CD133+ cell viability was observed in the treated group compared to the control (Figure 19). When the population distribution (ALDH+/-CD133+/-) of the cells that remained viable was examine after 3 days of treatment at 25µM, there was no significant differentiation observed (Figure 21). This combined with the overall loss of viability rules out the possibility that #673 is acting via differentiation effects. However, direct microscopic observation of single cell morphology led us to believe that cells were undergoing karyorrhexis as a result of necrosis (Figure 22). This finding is very interesting and consistent with bulk screening results not seeing evidence of apoptosis. In contrast to programmed cell death in apoptosis, necrosis is caused by factors that are external to the cell such as trauma and results in unregulated digestion of cell components. While apoptosis

can have beneficial effects, necrosis is normally detrimental, as such, #673 may not be an ideal targeted therapy. Further investigation will be required.

The presented data shows that our platform is capable of long and short term drug studies for evaluating the drug response of specific cancer cell subpopulations. In the future, the simple microfluidic architecture and fabrication makes the addition of parallel inlets (for multidrug screening) or chemo-mixers (for dose response analysis) as easy as changing one

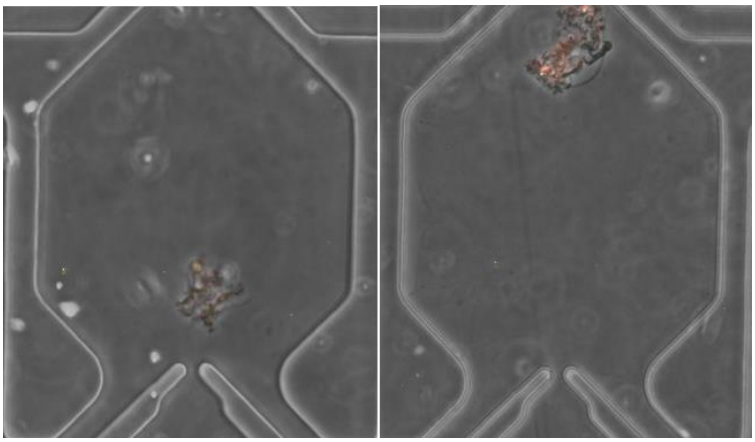

Figure 22: Karyorrhexis and necrosis in #673 treated A2780 ovarian cancer cells.

photolithographic mask. From the long term CSC drug studies performed, we clearly demonstrated that assessing the possible effects of the drug even after many cell divisions and cycles will be critical for understanding treatment consequences. This platform is, thus, ideal for this application in its ability to capture, geometrically confine, and culture single cells in the long term. These same characteristics facilitate observation of symmetric and asymmetric division of differentiating CSC populations as preliminarily observed while confirmed the effects of agent #673 on CD133+ CSC populations (Chapters 2.5 and 2.6).

2.2 Alternative Materials for Microfluidic Fabrication

Though well founded [69, 70], whether human cancer cells follow a hierarchical or stochastic model of differentiation is controversial, so facilitating direct observation is quite impactful. For these studies to be truly impactful, however, we will need to use both cell lines and primary patient samples. Few microfluidic platforms report the use of primary cells, due to sensitive viability, so confirming our ability to culture primary cells on-chip is an important step.

PDMS has become the go-to material for microfluidic fabrication for many applications in cell biology and chemistry. PDMS is cheap, and numerous devices can be fabricated from a single patterned master in a matter of hours. It also facilitates simple closed channel fabrication as it can be covalently bonded to glass and other PDMS surfaces via oxygen plasma treatment. Importantly, PDMS is also gas permeable, allowing adequate oxygen and circulation for cell culture applications [71, 72]. These advantages cause many to overlook the numerous drawbacks that are also associated with PDMS based microfluidic devices. A major issue in cell culture applications is that PDMS absorbs small hydrophobic molecules (e.g. biomolecules, media components, drugs) [73]. As a result, PDMS devices can bias the results of experiments examining cell signaling or drug dose responses. Hydrophobic growth factors or lipid energy sources from the culture media also adsorb into the PDMS, affecting cell behavior. Even more problematic are the PDMS effects on cell viability in long term culture. Complete crosslinking of PDMS polymers is difficult to guarantee, and uncrosslinked low molecular weight monomers can leech from the PDMS into the cell culture media. Here, they may interact and disrupt the hydrophobic cell membrane affecting viability and growth. In cases where media is not provided by continuous perfusion, the same permeability that facilitates oxygen circulation also facilitates water vapor evaporation. This effect can lead to device drying or changes in media osmolarity. Overall when comparing results in

PDMS devices and traditional in vitro cultures, there are significant differences in proliferation, metabolism, gene expression, and mitosis [73]. Although thorough PDMS device cleaning (solvent and thermal aging processes) can be performed in order to minimize viability effects, it is also important to investigate alternative microfluidic device fabrication methods and materials.

To this end, we have investigated solid UV cross-linked Poly(ethylene)-glycol-diacrylate (PEGDA) as a material for microfluidic device fabrication for biological applications. We have evaluated biocompatibility of PEGDA through two separate means: 1) by examining cell viability and attachment on cross-linked PEGDA surfaces for cell culture applications, and 2) by determining if cross-linked PEGDA inhibits the polymerase chain reaction (PCR) processes for on-chip PCR. Through these studies a correlation has been found between degree of curing and cell viability, attachment, as well as on PCR outcome.

Poly(ethylene)-glycol-diacrylate (PEGDA) is a liquid polymer that can be cross-linked into a solid form by exposure to UV light in the presence of a photoinitiator. Recently, solid UV cross-linked PEGDA has been reported as a material for microfluidic fabrication [74, 75, 76, 77]. It offers advantages over traditional polydimethylsiloxane (PDMS) techniques, including greater stiffness, permability control, and importantly, lower nonspecific adsorption of bio-molecules [74]. The method of fabrication (UV crosslinking) also facilitates the high aspect ratio structure fabrication [78] and lithographic patterning [76]. In previous work, our collaborators in the Fould's lab at Kaust (now at Simon Fraser University in Canada) have demonstrated a fabrication process capable of producing an enclosed microfluidic channel and high aspect ratio structures using PDMS soft molds [77]. As UV cross-linked PEGDA has a lower non-specific adsorption than PDMS, it is a promising material for fabrication of microfluidic devices for biological applications.

One of the more common uses of PEGDA is in the form of hydrogels as biocompatible tissue engineering scaffolds because of their similarity in structure to natural tissue [79, 80]. A PEGDA hydrogel is obtained when the liquid polymer is dispersed in an aqueous medium prior to cross-linking. Its use as a tissue scaffold material implies high biocompatibility, and studies of cell viability encapsulated in PEGDA hydrogels with different photoinitiators have been previously reported [81, 82]. However, the differences between PEGDA as a hydrogel and as a solid material, in both fabrication methodology and application require further characterization, which cannot be inferred directly from hydrogel studies alone. For example cell encapsulation in hydrogel involves the radiation of UV light on both cells and polymer simultaneously, limiting the total exposure dose that can be acceptable to avoid cell damage. Another difference is the effect of oxygen as an inhibitor of the cross-linking reaction of PEGDA [83], which is less significant in the case of hydrogels since the reaction naturally occurs in a low oxygen environment, and more significant in the case of solid UV cross-linked PEGDA. The importance of having minimal amounts of prepolymer to ensure good biocompatibility has been previously reported for solid UV cross-linked PEGDA; however, results have been only qualitative [75]. As such, we investigated, quantitatively, the biocompatibility of solid PEGDA in microfluidic devices applications.

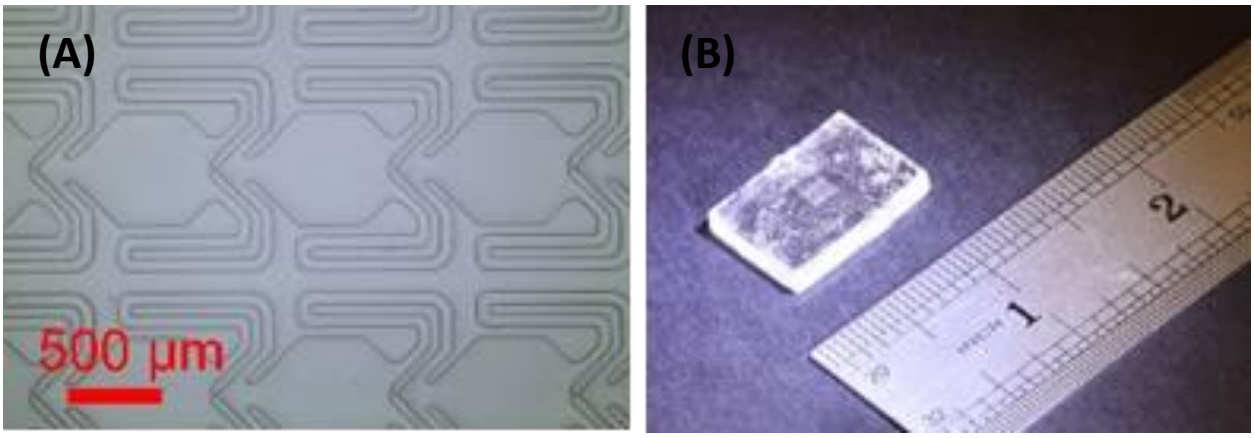

Figure 23: (A) Microscope and (B) photographic image of single cell devices fabricated in UV-cross-linked PEGDA instead of PDMS.

Test samples were fabricated following a process previously published by the Foulds' group [77]. This process enables the fabrication of microfluidic devices for biological applications, such as our single cell capture platform [49] (Figure 23), using solid UV cross-linked PEGDA. The fabrication process is relatively simple. Liquid 258 PEGDA, mixed with a photoinitiator, is poured into a polydimethylsiloxane (PDMS) soft mold of the device. The mold is covered with glass slides, compressed between two clamps and cured using a UV light box (7mW/cm2). Samples are then demolded by peeling off the PDMS soft mold and rinsed with isopropyl alcohol (IPA) and DI water. A variety of photoinitiators and fabrication parameters were tested to examine various conditions. Samples of 1 inch x 3 inch size were fabricated under different fabrication conditions shown in Table 2.

Table 2: List of tested polyPEGDA samples.

Material	Fabrication Parameters		
	Photoinitiator, Concentration w/w %	Atmosphere	Curing Time (min)
PEGDA	DMPA, 0.1%	Air	30
PEGDA	DMPA, 0.1%	Air	5
PEGDA	DMPA, 0.1%	Air	1.5
PEGDA	DMPA, 1.0%	Air	5
PEGDA	Irgacure 2959, 1.0%	Air	45
PEGDA	Irgacure 2959, 1.0%	Air	30
PDMS	Sylgard curing agent, 10%	Air	1440 (at 65 C)
PEGDA	DMPA, 0.1%	N_2	120
PEGDA	DMPA, 0.1%	N_2	360
PEGDA	DMPA, 0.1%	N_2	720
PEGDA	DMPA, 0.1%	N_2	1440

When performing initial cell viability testing with the fabricated polyPEGDA, a correlation between curing time and cell viability was clearly observed. As oxygen inhibits the cross-linking of PEGDA [83], curing the samples in an air atmosphere showed adverse effects on biocompatibility. This effect can be easily visualized in looking at the 3-day cell viability (Figure 24). SUM159 cells were cultured on two different types of PEGDA surfaces: 1) those cast from PDMS molds and 2) those cast off flat glass surfaces.

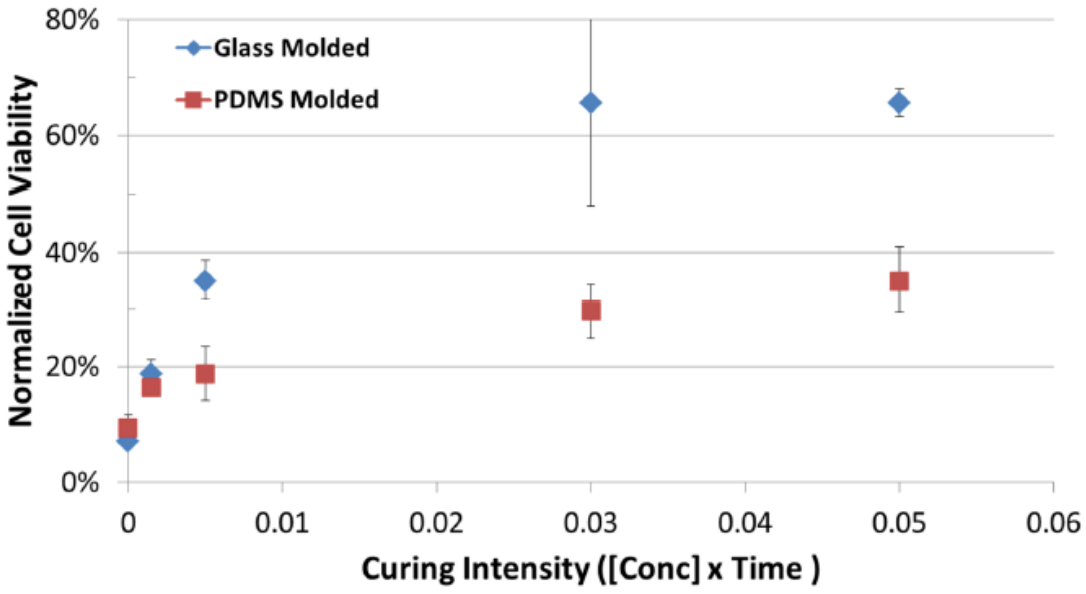

Figure 24: 3-day cell viability cell vs. curing intensity of in air UV-cured PEGDA samples.

During fabrication, the top surface of the PEGDA sample is in contact with a glass slide, while the bottom surface is in contact with the PDMS mold. As PDMS is more gas permeable than glass, the adjacent liquid PEGDA is exposed to a greater oxygen concentration, which results in a lower curing intensity and therefore reduced cell viability. With the same curing intensity (quantified as curing agent concentration multiplied by curing time), surfaces from the glass surface showed significantly higher viability. As such, we included in our testing samples fabricated in “low” oxygen environments (Table 2).

Curing in an oxygen free atmosphere, for example carbon dioxide or nitrogen [83], has in fact previously been shown to minimize the effects of oxygen inhibition, so its inclusion here to improve cell viability is important. An additional 30 minute vacuum step was added before covering the mold with a glass slide, to minimize the oxygen present in the liquid PEGDA and PDMS mold. Additionally, a nitrogen chamber that could fit on top of the samples during UV exposure was fabricated. Prior to exposure, the chamber was filled with nitrogen and run for 30 minutes to ensure all oxygen was displaced. Flow of nitrogen was maintained throughout the entire procedure.

To assess cross-linked PEGDA as a cell culture material, cells (SUM159 breast cancer cells) were seeded onto the sample surfaces and evaluated for their surface attachment and viability. Prior to loading, cells were cultured on tissue culture treated petri dishes in DMEM + 10% FBS (Invitrogen) culture media. Cells were trypsinized and re-suspended at $5x10^6$ cells/mL for loading onto samples. PEGDA surfaces were fabricated with the various parameters described

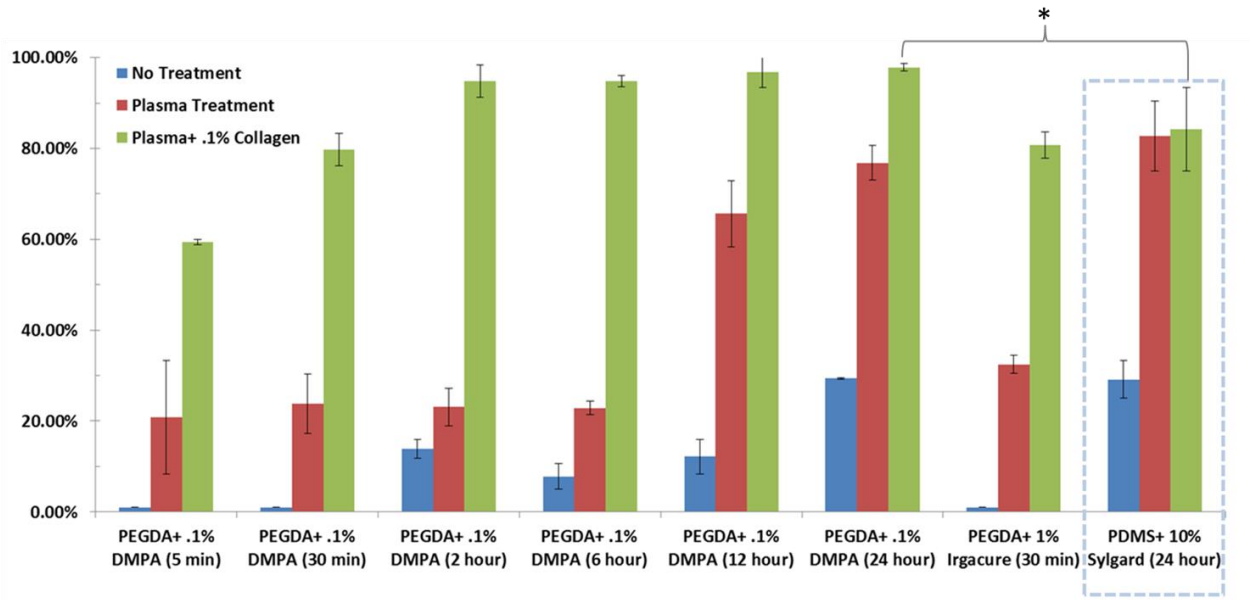

Figure 25: Increased normalized cell attachment on polyPEGDA with plasma and ECM surfaces treatments as compared to PDMS surfaces.

above. PEGDA surfaces were then left untreated, treated with oxygen plasma (80W for 60 sec), or treated with plasma and submerged in D-PBS or .1% collagen solution (to create an ECM coating). The resulting cell attachment and viability was observed and compared to untreated PEGDA surfaces as well as to polystyrene (PS) and PDMS surfaces.

Cell surface attachment percentage was analyzed by assessing cellular morphology, 4 hours after initial loading. Figure 25 shows the marked increased in cell attachment after surface treatment with both plasma and ECM coatings as expected (cell attachment normalized to attachment rates on polystyrene plate at same seeding density in graph). Increased PEGDA curing time also lead to more effective cell attachment. PEGDA, slightly but significantly, outperformed PDMS surfaces in enabling cell attachment when subjected to increased curing, plasma treatment,

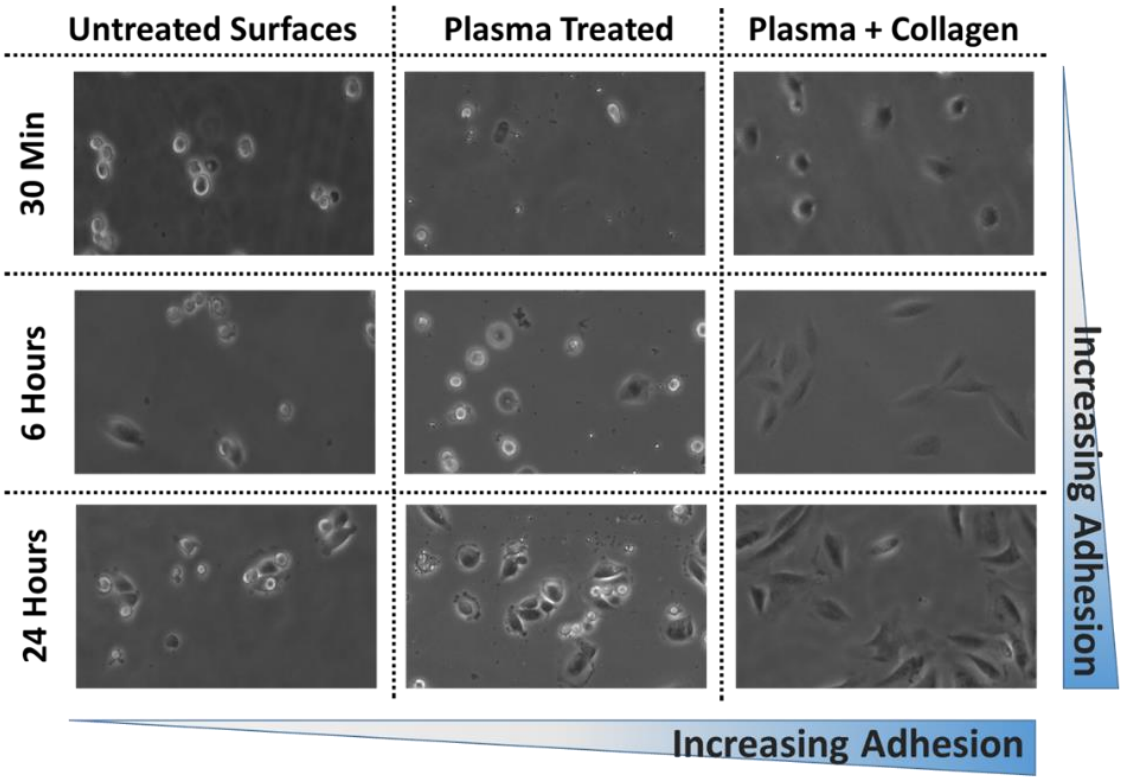

Figure 26: SUM159 breast cancer cells attaching to PEGDA surfaces with different exposure times and surface treatments.

and coated with ECM. However, without increased curing times, plasma treatment, or ECM coating, PEGDA significantly underperforms when compared to PDMS samples. Example cell images can be seen in Figure 26, and they show the very different cell morphologies obtained depending on curing time and surface treatment. The rounded morphology shown in the top left images is indicative on an un-attached cell. However, as the cells adhere, their morphology becomes more elongated and spread as seen in the bottom right.

Stable cell viability must be maintained over long time periods for reliable cell assays, and is precisely where PDMS devices can be problematic for cell culture applications. As such, cellular viability was assessed over an 8 day time period. Traditional cell Live/Dead stains (Invitrogen) were used to visualize cellular viability, and PEGDA surfaces were compared to PDMS and PS, as a control. The resulting 8 day viability (Figure 27) was shown to be lower than that presented in PS but comparable to PDMS when cured for at least 24 hours. Again, we observe a clear correlation between curing degree and cell health. While PEGDA surfaces still underperform PS,

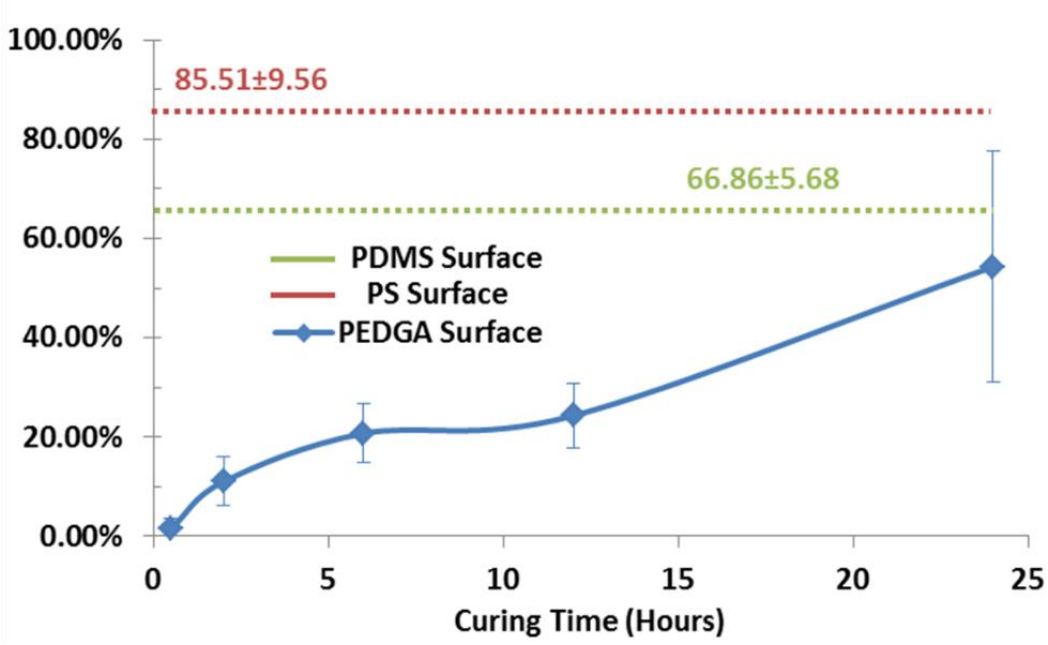

Figure 27: 8-day cell viability vs. curing time of nitrogen atmosphere UV-cured PEGDA samples as compared to baseline viability in polystyrene and PDMS.

we believe further steps can be taken to improve long term viability, including further optimization of curing time and better selection of a biocompatible photoinitiator.

Another major drawback of PDMS is its adsorption of biomolecules. This causes interference with many biological assays including PCR. In order to quantitatively assess improved polyPEGDA performance, PCR was performed with PMDS, with PEGDA, or without either in conventional PCR assay wells. The PCR compatibility was performed following a previously developed methodology [84]. A PCR master mix was prepared, using male saliva genomic DNA as a template. The primers were used to amplify a gene fragment from the Sex-determining region Y (SRY), with an expected amplification product size of 93 base pairs. Presence of amplified product indicates male saliva; no amplification indicates saliva of female origin.

The material samples to be investigated were cut with a blade into pieces of approximately 1.4 mm x 1.4 mm x 1 mm and introduced into individual PCR microteter plate wells. This was done to be able to have comparable results among the different tubes, given the fact that the inhibitory effect on PCR is surface area related. 30 µl of the master mix was pipetted into each of

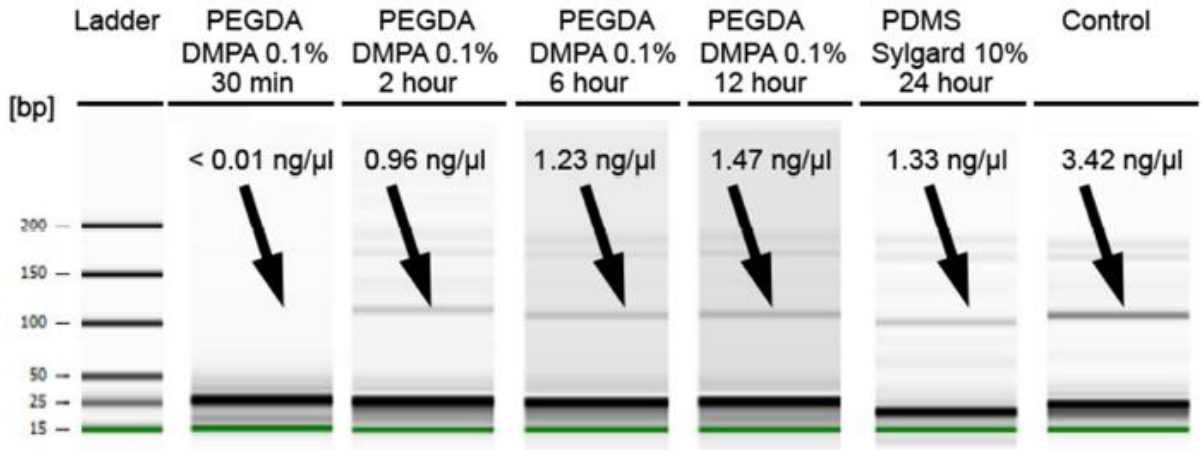

Figure 28: Gel-like Bioanalizer image of PCR performed with different materials.

the wells containing material samples, and additionally two positive controls that did not contain

any material were included. The tubes were incubated in ice for 30 minutes prior to the thermocycling process. The PCR outcome was quantified using an Agilent 2100 Bioanalyzer, running DNA 1000 assays, which can produce a gel-like image for quick result assessment, as shown in Figure 28. Quantitative concentration results for the band of interest were also calculated and presented in Figure 29. A more successful PCR reaction produces a greater quantity of DNA, and the intensity of the fluorescent band on the gel-like image will stronger. Because of the length (measured in base pairs) of the DNA being amplified in this experiment, the presence of band at 100 base pairs (bp) range indicates successful DNA amplification and higher concentration. We observed that sufficient curing of PEGDA shows improved performance over PDMS.

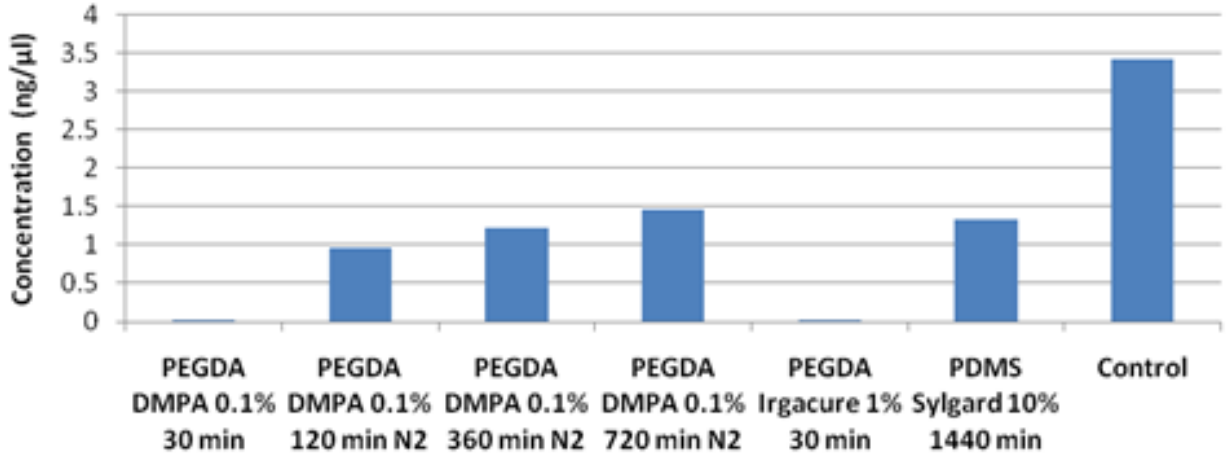

Figure 29: Concentration of amplified DNA at 100 bp band for different materials tested.

When measuring and quantifying the values of concentration at the 100 bp band, virtually no signal (<0.01 ng/µl) was detected for the PEGDA samples cured for less than 30 minutes. Increased exposure times and the addition of the nitrogen atmosphere during fabrication show a decrease in PCR inhibition as compared to thus without. Cured PEGDA shows comparable inhibitory effects to PDMS at 6 hours curing time, but better performance for 12 hours. It is

important to note, however, that all conditions with PDMS and PEGDA performed at least 2x worse than controls.

The testing presented here assess cell viability in PEGDA device with conditions that closely resemble microfluidic culture conditions. From this testing, we have established a quantitative correlation between degree of curing and cell viability, cell attachment and PCR inhibition. Solid UV cross-linked PEGDA shows improved performance over PDMS as long as exposure time and surface chemistry are adequately controlled. Interestingly in the cytocompatibility study for cells encapsulated in PEGDA hydrogels reported by Bryant et al. [81], it was reported that DMPA photoinitiator at 0.1% concentration is one of the least cytocompatible. Despite of this, our work, which uses DMPA at 0.1%, has demonstrated good 8-day cell viability. We expect to be able to greatly improve performance if DMPA is replaced with a more cytocompatible photoinitiator.

For high exposure times, PEGDA shows a statistically significant, but slight, improvement over PDMS for cell attachment when both are treated with oxygen plasma and 0.1% collagen solution. Cell viability is found to be equivalent to PDMS for high curing times. Inhibition on PCR outcome is reduced with higher exposure times, outperforming PDMS when cured for times longer than 12 hours. Disappointingly compared to polystyrene control, PDMS and polyPEGDA both underperform in producing cell culture and PCR outcomes. Although thoroughly cured PEGDA has slightly improved absorptive and long term culture characteristics as compared to PDMS, its native surface chemistry, like PDMS, is not conducive to cell adhesion and survival. With no extracellular binding domains, cells cannot adhere to unmodified PEGDA surfaces. While the UV fabrication procedure may enable unique device architectures and structures, it seems the slight

biological improvements alone are not enough to justify adapting our microfluidic procedures from PDMS to polyPEGDA devices.

2.3 Primary Cell Culture in PDMS Devices

Thus, our PDMS devices must be conditioned for use with sensitive patient samples. First, we added a thorough PDMS cleaning procedure to our fabrication protocol to remove any unbound and uncured monomer chains from the material that can affect cell viability. Any PDMS samples are cured for an additional 24 hours period at 80ºC after removing from SU8 molds to thermally age the sample. The samples are then soaked in 1% tween solutions for 24 hours, washed, and then soaked in 100% ethanol for another 24 hour period. After autoclaving (1-3 times), the samples are dried at 65ºC overnight. These processes help to eliminate low molecular weight chains that might diffuse out from the material during long term culture [85]. Second, laminin (Corning, 1mg) is added to the ECM coatings used on the device glass surface to improve cell adhesion, growth, and differentiation. Patient primary sample viability was then assess in our microfluidic device.

Informed consent was obtained from all patients before tissue procurement. All studies were performed with the approval of the Institutional Review Board of the University of Michigan. Tumors were stage III or IV epithelial ovarian or primary peritoneal cancer. For these studies cells were harvested in the laboratory of our collaborator, Dr. Ronald Buckanovich, from ascites. Cell pellets were collected by centrifugation, and red cells were lysed using ACK buffer (Lonza), washed, passed through a 40-μm filter, and then passed 4 times through a Standard Hub Pipetting needle to isolate single cells.

Primary samples were then loaded into our platform as previously described. Primary cells were then culture on chip in supplemented MEBM media. At 5 days, total viability leveled off to ~80% and significant proliferation was observed (Figure 31). Compared to cell lines however,

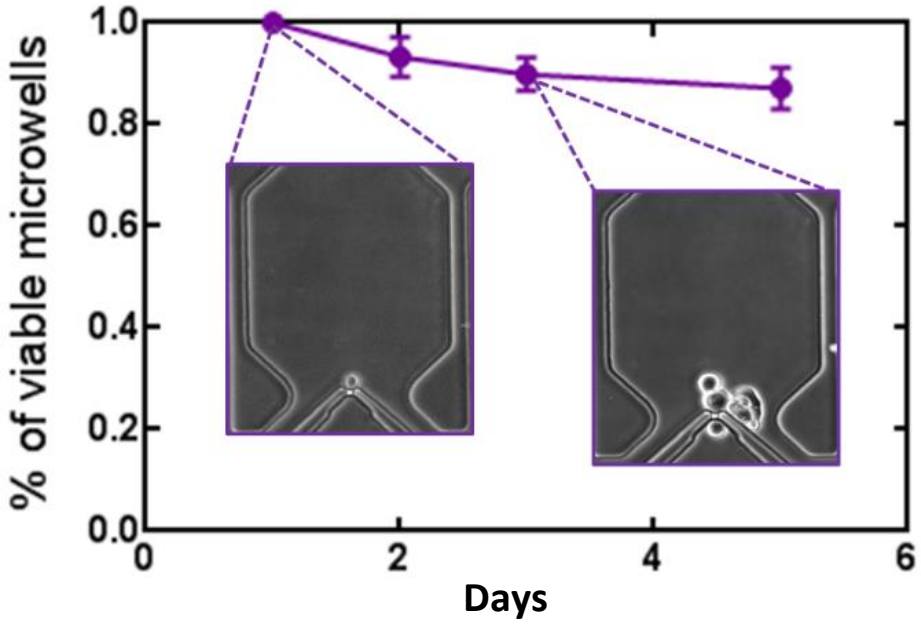

Figure 31: On-chip viability of primary ovarian tumor cells FACS sorted from acities.

primary samples had a large pool of quiescent cells. In order to evaluate quiescence, these non-dividing cells were stained with LIVE/DEAD (Life Technologies) at 12 days and found to be still viable on chip (Figure 30). Only these quiescent cells survive to this 12 day time point, with

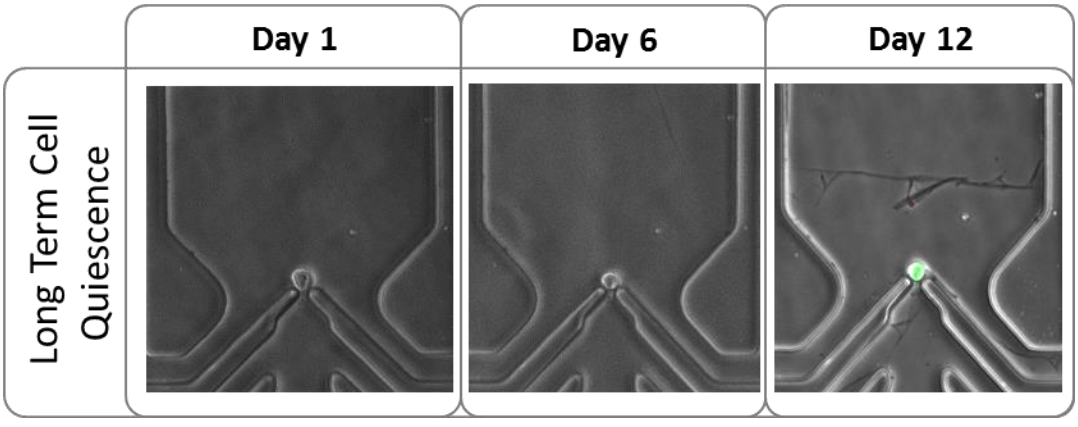

Figure 30: Long term tracking of quiescent primary cell viability on chip assessed with Live/Dead staining.

proliferating primary cell viability dropping sharply after 7-10 days (~20%). Thus, we have successful demonstrated our ability to culture primary ovarian cancer cells on chip for a time period (5 days) appropriate for assessing possible CSC behavior (differentiation, division, drug response, etc.) in future studies.

2.4 BMP2 and CSC Self-Renewal

Our ability to track single cells accurately over a long time period, as demonstrated by our in situ drug screening, is useful in investigating contentious claims related to CSC division behavior. As we can capture and confined single cells, stain them on chip to confirm their identity, and follow them over days and weeks to monitor division, we can directly assess CSC differentiation potential. Furthermore as the factors which regulate CSC self-renewal vs. asymmetric division are largely unknown, we can introduce biological factors of interest and monitor their effect.

In addition to ALDH activity, stem cell marker CD133 has been identified by our collaborators as a marker stemness in cancer [64, 67]. Together, ALDH and CD133 can define a heterogeneous population of ovarian cancer cells. The presence of ALDH+CD133+ cells in primary tumors is associated with poor outcomes for patients. Only ALDH, CD133, and CD44 are enriched after chemotherapy, implying drug resistance in these populations. Additionally, ALDH and CD133 can be identified in normal ovarian stem cells. When performing tumor initiating studies, the gold standard for identification of CSCs, only ALDH+CD133+ and ALDH+CD133- tumor cells initiated new tumors in mice. ALDH+CD133+ cells, however, showed greater initiation potential and generated aggressive, poorly differentiated tumors [64]. ALDH+CD133- tumors required longer growth periods. Based on this data, it was hypothesized that ALDH and CD133 can be used to define a hierarchy of Ovarian CSC differentiation; highly tumorigenic

ALDH+CD133+ CSCs give rise to somewhat less tumorigenic ALDH+CD133- CSCs/progenitors which in turn give rise to differentiated ALDH-CD133- cells. Using our device, we can directly examine this hierarchy and observe possible "de-differentiation" as well, if there are any.

Our collaborators had also previously reported that cancer-associated mesenchymal stem cells promote tumor growth and 'stemness' via the production of BMP proteins [86], but the role of BMP proteins in cancer remains controversial as several studies have suggested BMP proteins are tumor suppressors as well [87]. With direct interrogation by our microfluidic device, we observed that BMP2 promotes self-renewal of the ALDH+CD133+ CSC and inhibits the proliferation of progenitors.

We sought to test the differentiation capacity of each of the four ALDH+/-CD133+/- (ALDH+CD133+, ALDH-CD133+, ALDH+CD133- and ALDH-CD133-) cell populations in ovarian cell lines and primary samples. The four ALDH+/-CD133+/- cell populations from three primary patient specimens and 3 cell lines (PEO1, A2780, and OVCAR8) were FACS isolated and loaded as single cells into separate devices. Once loaded, the identity of each cell was confirmed using in situ ALDEFLUOR and CD133 immunofluorescent microscopy within the microfluidics

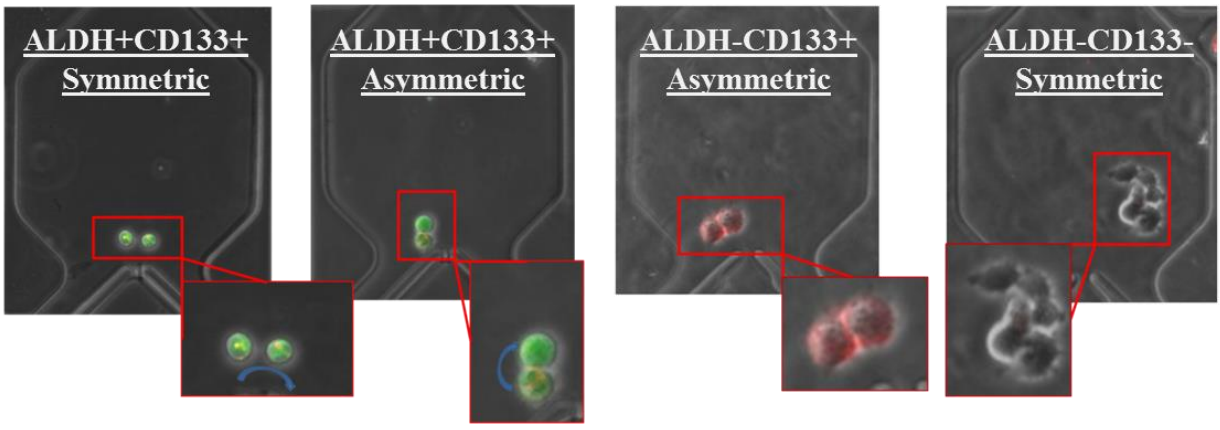

Figure 32: Example cell divisions from A2780 ovarian cancer cell lines with Aldefluor activity in green and CD133+ surface markers in red.

chamber. Cell divisions were then tracked over 2-5 days, depending on cell proliferation rates for each sample. Endpoint staining was then performed to assess cell division state (Figure 32). Overall, primary cells had lower viability (~60%) and proliferation rates with a large number of non-dividing cells.

For most divisions, only ALDH+CD133+ cells were capable of giving rise to all four ALDH+/-CD133+/- cell populations: ALDH+CD133+ cells demonstrated symmetric divisions resulting in two ALDH+CD133+ cells, an asymmetric division resulting in an ALDH+CD133+ cell and an ALDH+CD133- cell, or an asymmetric division resulting in an ALDH+CD133+ cell and an ALDH-CD133+ (Figure 33). ALDH-CD133- cell progenitors were observed in wells initially seeded by ALDH+CD133+ cells, however, we never observed a direct division of an ALDH+CD133+ cell into a ALDH-CD133- cell, suggesting these cells were the result of an asymmetric division of either ALDH+CD133- or ALDH-CD133+ progenitor cells. Isolated ALDH-CD133+ cells could symmetrically divide or asymmetrically divide to produce ALDH-CD133+ and ALDH-CD133- cells. We never observed the ability of an ALDH-CD133+ cell to produce ALDH+ cells. Similarly, ALDH+CD133- cells generally underwent symmetric division or asymmetric division to produce ALDH+CD133- cells and ALDH-CD133- cells. Finally,

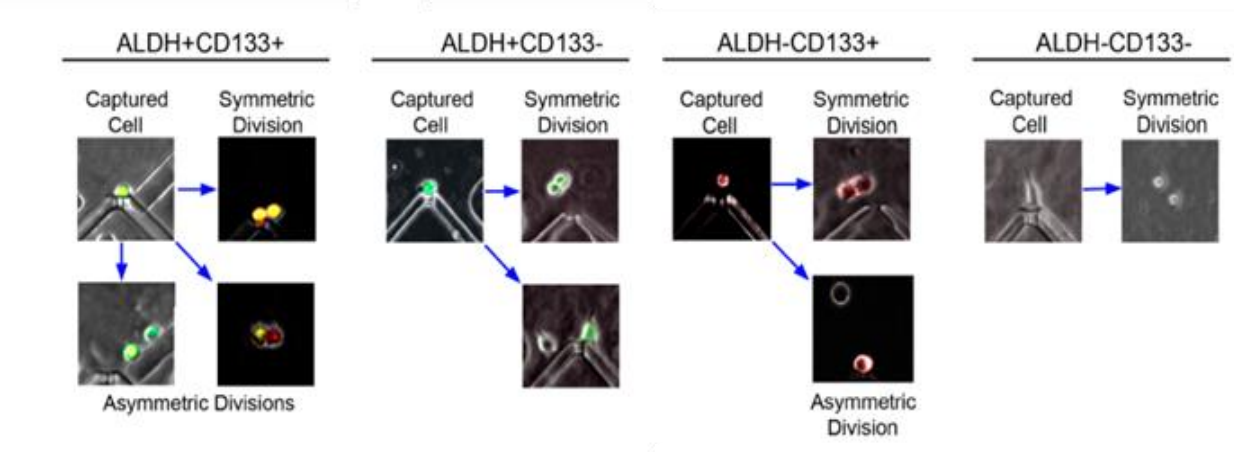

Figure 33: Differentiation potential of ALDH+/-CD133+/- ovarian CSC.

ALDH-CD133- cells were only observed to divide symmetrically. Quantification of aggregated data can be seen in Figure 35 and Figure 34 (patient and lines, respectively). Non-dividing cells

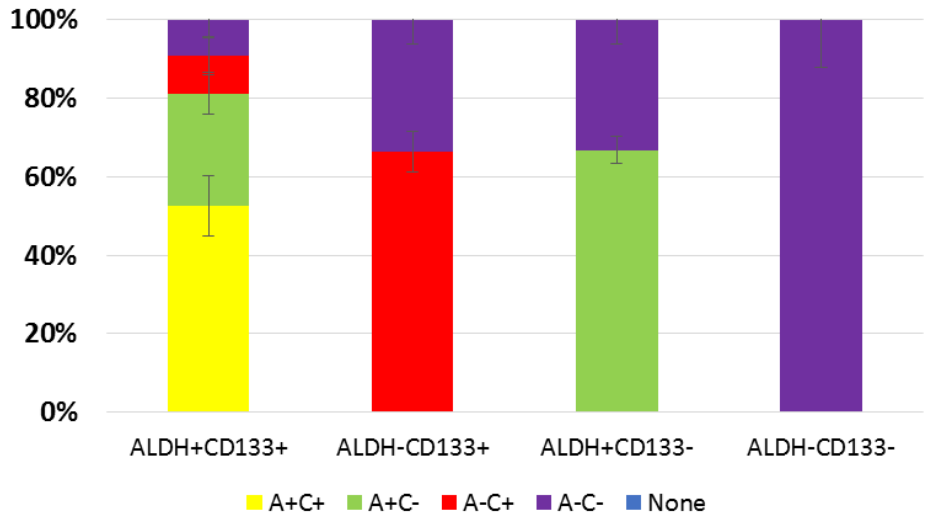

Figure 35: Differentiation potential of ALDH+/- CD133+/- cells ovarian cancer cell lines (A2780, PEO1, and OVCAR8).

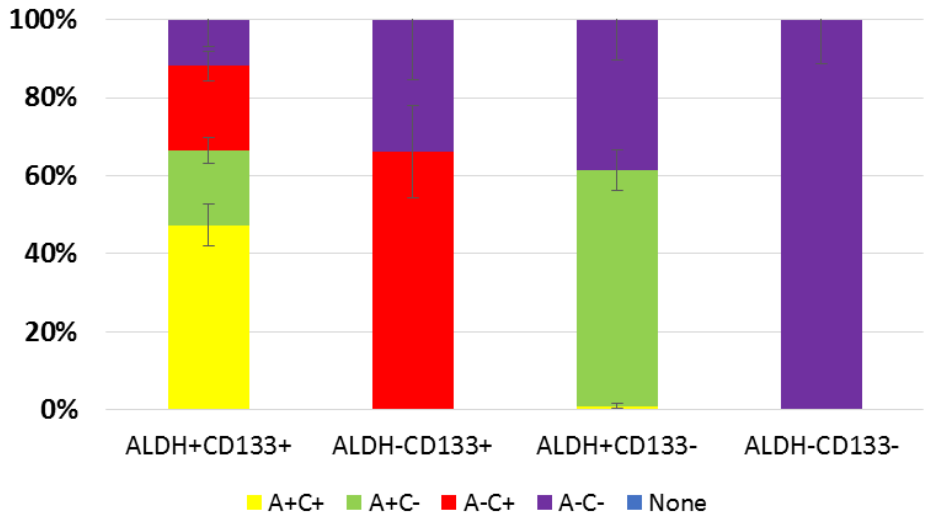

Figure 34: Differentiation potential of ALDH+/- CD133+/- cells in ovarian cancer patient ascites samples.

are excluded from this quantification. From a single primary sample however, we observed one ALDH+CD133- cell which produced an ALDH+CD133+ cell and an ALDH+CD133- cell (small yellow A+C+ population in Figure 34), suggesting the potential for dedifferentiation (Figure 36).

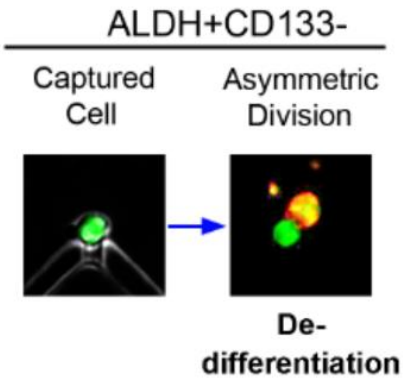

Figure 36: De-differentiation even in ALDH+CD133- patient sample.

To further assess the potential for de-differentiation, our collaborators FACS analyzed xenograft tumors initiated from 1000-5000 ALDH+CD133- primary cells from 4 patients. While all initial xenografts were CD133-, upon subsequent passaging, one of the four patients developed a population of CD133+ cells (Figure 37) suggesting a rare de-differentiation event. Together with or single cell data, this indicates an ovarian CSC differentiation hierarchy with ALDH+CD133+ cells at the top and with potential rare dedifferentiation events. Alternatively, there may be rare

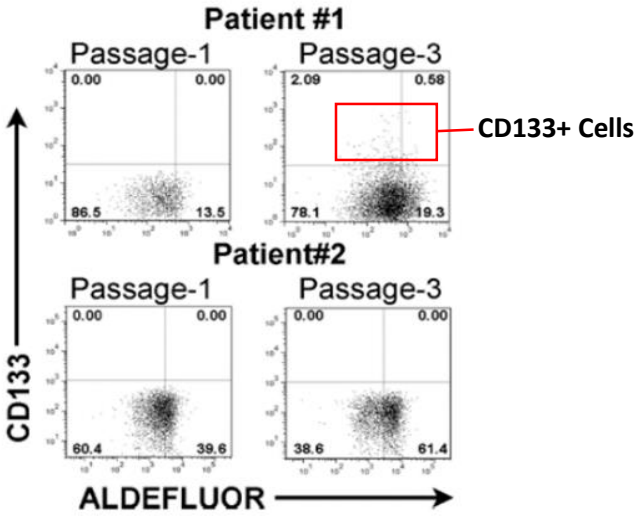

Figure 37: One patient sample in four (Patient #1 vs. Patient #2-4) shows potential for de-differentiation as over multiple passages a CD133+ population emerges from originally FACS sorted ALHD+CD133- sample.

ALDH+CD133- cells that are distinct from the bulk of the ALDH+CD133- cells and differentiate into ALDH+CD133+ cells.

With the hierarchy established, we next investigated the effects of BMP2 on CSC division and differentiation in order to clarify BMP2's clinical relevance. BMP2, or bone morphogenetic protein 2, is in the TGFβ super family of proteins and has been shown to play a role in bone development, EMT, and differentiation. In fact, BMP2 has been shown to be expressed in both ovarian cancer cells and mesenchymal cells [86, 88]. As a first step to investigate exactly how BMP2 impacts stemness, we acquired FACS-isolated ALDH+CD133+, ALDH+CD133-, ALDH-CD133+ and ALDH-CD133- cells from cell lines (A2780, PEO1) and 2 patient samples (Pt179,

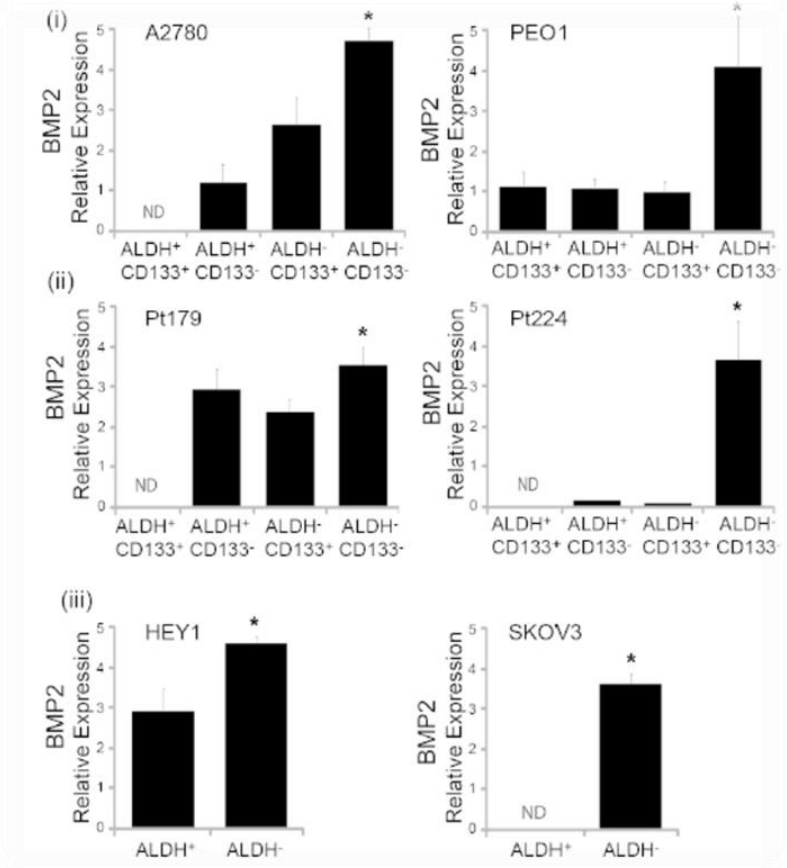

Figure 38: BMP2 is more highly expressed in bulk CD133-ALDH- and ALDH- populations than ALDH+ and CD133+ CSC populations across cell lines (i) A2780, PEO1, (iii) HEY1 and SKOV3 and patient samples (ii) Pt179, Pt224.

Pt224) in the Buanovich lab and performed qRTPCR to characterize BMP2 mRNA expression in the different populations of ovarian cancer cells. BMP2 mRNA was undetectable or expressed at low levels in the ALDH+CD133+ cells and more highly expressed in ALDH+CD133-, ALDH-C133+ and ALDH-CD133- cells (Figure 38). Differential expression of BMP2 was also observed between ALDH- and ALDH+ cells from cell lines (HEY1 and SKOV3) in which CD133 expression is not detectable. Together this data suggest BMP2 is differentially expressed in the distinct populations of ovarian cancer cells with low expression in CSCs and increased expression in progenitor cells. Co-immunofluorescence with ALDH or CD133 in primary tumor biopsies demonstrated BMP2 protein was generally expressed in ALDH- and CD133- tumor cells in human tumor samples (Figure 39). This can be seen as there is minimal overlap of the green (CD133 or ALDH) and red (BMP2) areas in the histology.

Collaborators in Dr. Buckanovich's lab also evaluated the expression of BMP receptors/co-receptors in these same cellular populations. qRT-PCR confirmed the expression of several

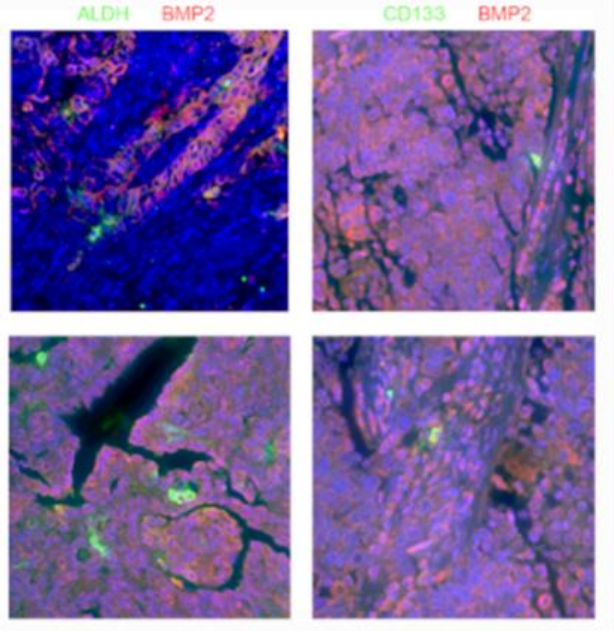

Figure 39: Co-immunofluorescence of ALDH, CD133, and BMP2 in primary tumor biopsies, showing minimal overlap in areas expressing ALDH/CD133 (green) and BMP2 (red).

members of the BMP/Activin Receptor family (Figure 40). Most receptor mRNAs were broadly expressed in all ALDH+/-CD133+/- sub-populations. In A2780 cells and in 2 of 4 patient samples BMPRII was preferentially expressed in ALDH+CD133+ and ALDH-CD133+ cells (Figure 40) suggesting that BMP2 acts on these populations. In non CD133 expressing samples (SKOV3 lines and Pt118), receptors were preferentially expressed in ALDH+ cells versus ALDH-.

Given the differential expression of BMP2 in the different ovarian cancer cell populations, bulk primary patient cells, A2780 cells and SKOV3 cells were treated with BMP2 or Noggin (BMP2/4 inhibitor). Surprisingly, both BMP2 and Noggin treatment restricted proliferation

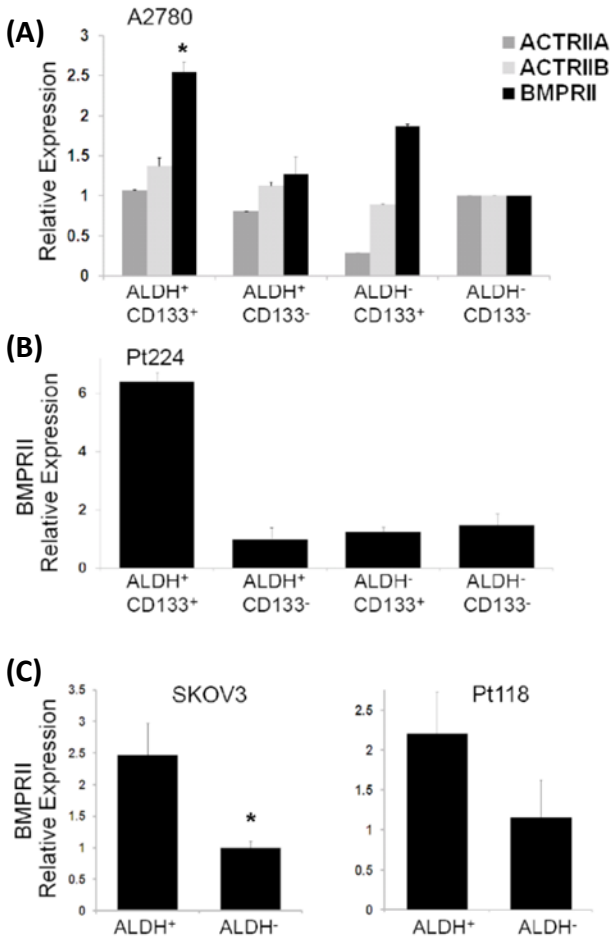

Figure 40: qRT-PCR demonstrating the expression of BMP and Activin receptors in (A) A2780 ALDH+/-CD133+/- cell line populations, (B) Pt224 ALDH+/-CD133+/- patient sample populations, and (C) ALDH+/- cells from cell line (SKOV3) and patient sample (Pt118).

(Figure 41a) in both A2780 cell lines and Pt125 patient samples. However, BMP2 treatment of primary cells in a tumor sphere assay was associated with a 2-3 fold increase in the numbers of ALDH+CD133+ cells (Figure 41b) in three separate patient samples. When A2780 cell samples were FACS sorted and culture in bulk with BMP2 and compared to cultures without BMP2, the proliferation rate of ALDH+ CD133+ cells was increased by 25%, while the growth of ALDH+CD133-, ALDH-CD133+ and ALDH-CD133- cells decreased 2.2, 4.4, and 6.9 fold, respectively (Figure 41c).

Overall this data presents a confusing picture of BMP2 activity. As such, we then evaluated the impact of BMP2 on isolated single cells from the four ALDH+/-CD133+/- cell populations from 3 primary patient samples and 3 cell lines (PEO1, A2780, and OVCAR8) using our single

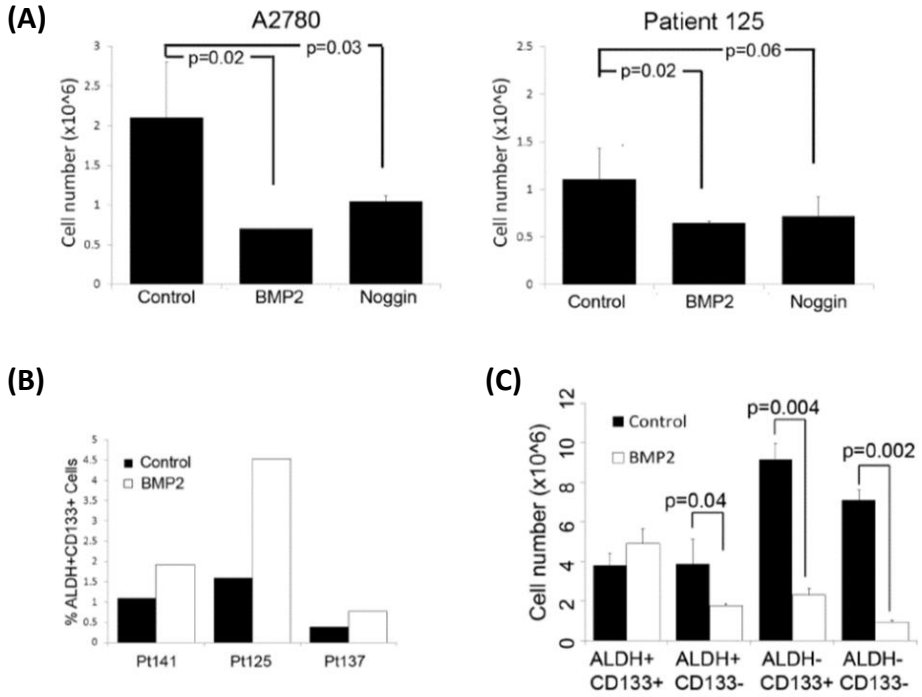

Figure 41: Bulk effects of BMP2. (A) Both BMP2 and BMP2 inhibitor, Noggin, suppress overall cell proliferation in cell line (A2780) and primary sample (Pt125). (B) BMP2 treatment in tumor sphere assay results in great number of CSC in 3 patient samples. (C) In A2780, BMP2 treatment increases ALDH+CD133+ proliferation but suppresses all other ALDH+/-CD133+/- populations.

cell microfluidic platform. In primary patient cells and cell lines, BMP2 treatment of ALDH+CD133+ cells led to a statistically significant increase in the number cells undergoing symmetric division (Figure 42, Figure 43, and Table 3). BMP2 was also associated with a suppression in the proliferation of ALDH-CD133-. ALDH+CD133-, ALDH-CD133+ cells (Table

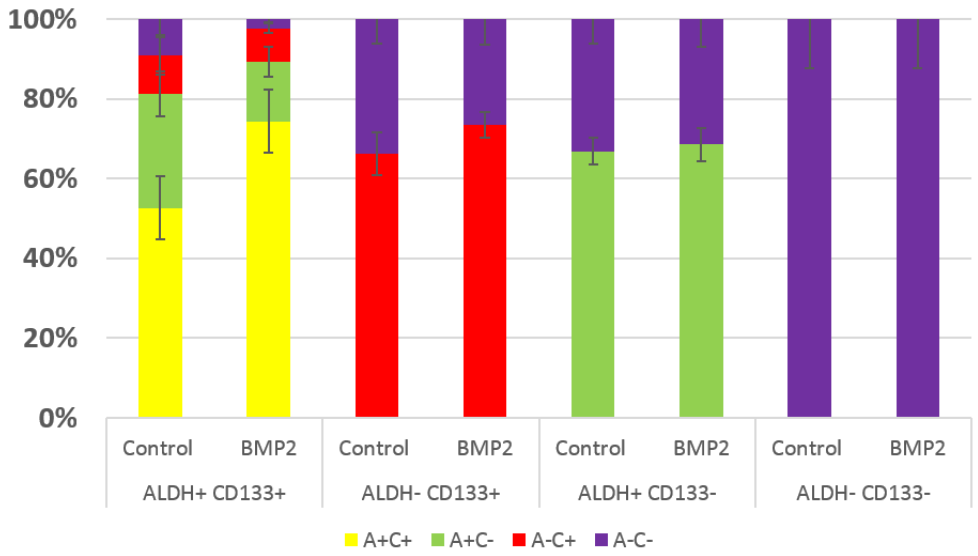

Figure 42: Differentiation potential of ALDH+/- CD133+/- cells in ovarian cancer cell lines (A2780, PEO1, OVCAR8) with and without BMP2 treatment.

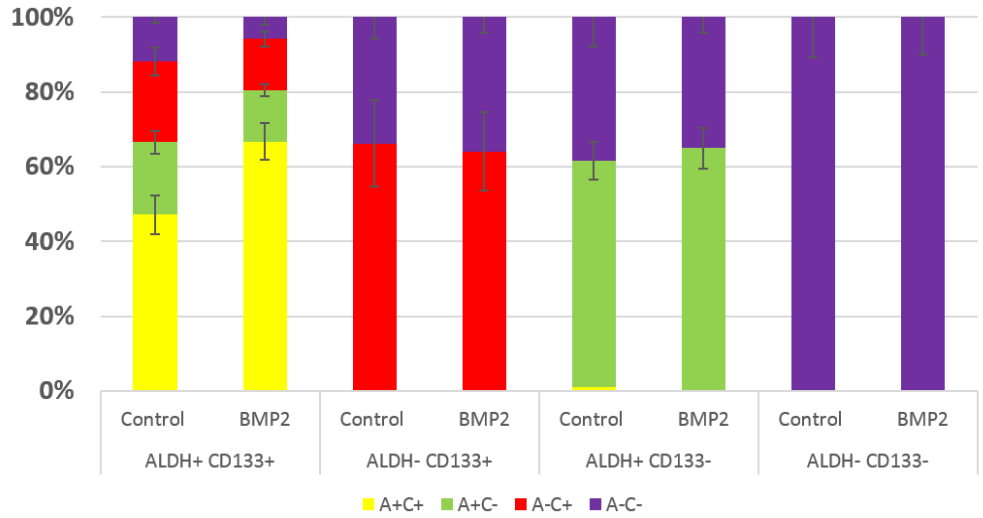

Figure 43: Differentiation potential of ALDH+/- CD133+/- cells in 3 ovarian cancer patient ascites samples with and without BMP2 treatment.

3), but effects were most significant in ALDH-CD133- populations. This data demonstrates that collectively BMP2 promotes CSC self-renewal/proliferation while suppressing the proliferation of bulk tumor cells, helping to harmonize the previously conflicting data. Individual cell lines and patient sample effects are shown in Figure 44-49. Taken together, this data suggests that BMP2 secreted from ALDH-CD133- cells inhibit their own proliferation and increase the symmetric renewal in ALDH+CD133- populations.

Table 3: Aggregated data of effects of BMP2 on ALDH+/- CD133+/- cell lines and primary patient division

Cell Line Data				Daughter Cells				
Cell Type Loaded	**Treatment**	**Evaluable Cells Loaded**	**Total Daughter Cells**	**A+C+**	**A+C-**	**A-C+**	**A-C-**	**None**
ALDH+ CD133+	Control	273	331	174	95	32	30	134
	BMP2	411	433	322	65	36	10	247
ALDH- CD133+	Control	122	312			207	105	39
	BMP2	290	591			434	157	127
ALDH+ CD133-	Control	67	178		119		58	22
	BMP2	203	226		155		71	110
ALDH-CD133-	Control	56	130				130	23
	BMP2	172	143				143	110

Primary Cell Data				Daughter Cells				
Cell Type Loaded	**Treatment**	**Evaluable Cells Loaded**	**Total Daughter Cells**	**A+C+**	**A+C-**	**A-C+**	**A-C-**	**None**
ALDH+ CD133+	Control	328	394	186	76	85	47	146
	BMP2	312	357	238	49	49	21	152
ALDH- CD133-	Control	112	133			88	45	59
	BMP2	107	125			80	45	58
ALDH+ CD133-	Control	100	109	1	66		42	40
	BMP2	83	77		50		27	34
ALDH-CD133-	Control	94	75				75	57
	BMP2	103	78				77	63

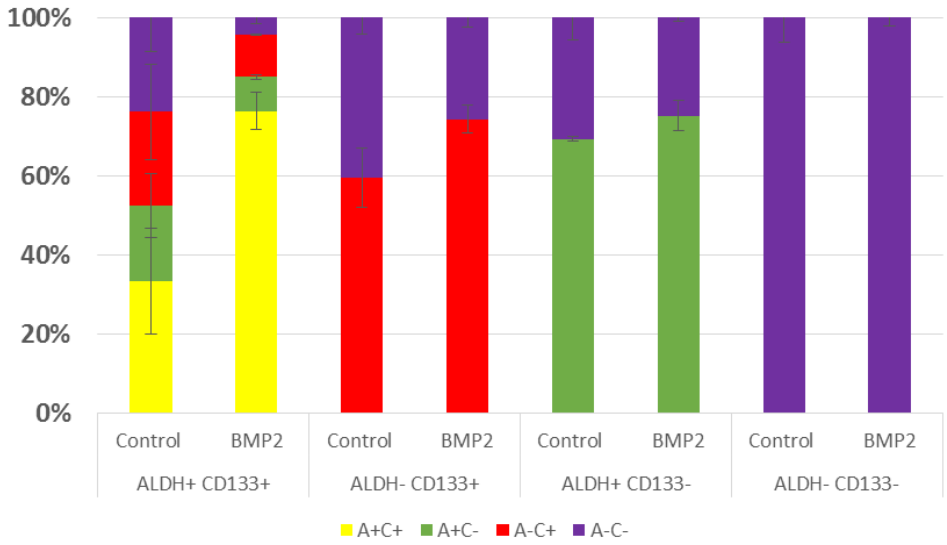

Figure 45: Differentiation potential of PEO1 cell line ALDH+/- CD133+/- with and without BMP2 treatment.

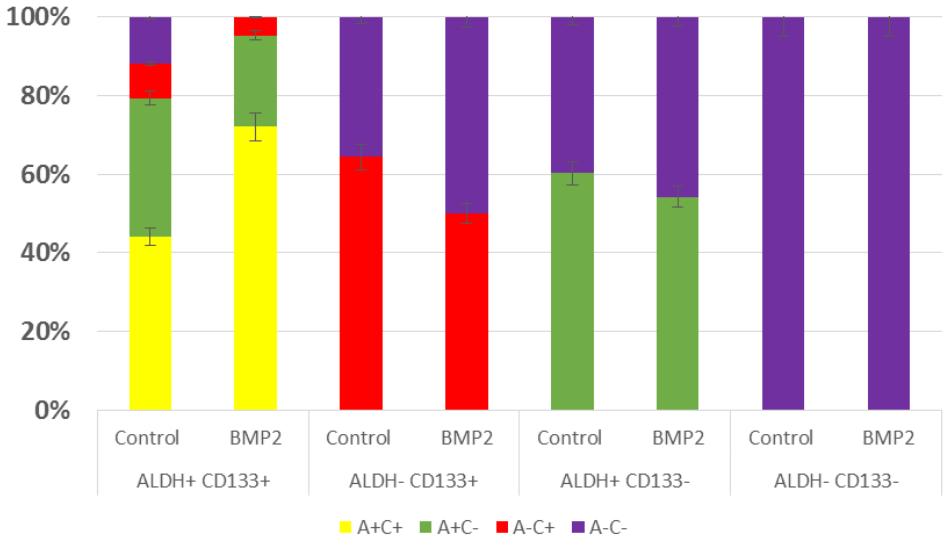

Figure 44: Differentiation potential of A2780 cell line ALDH+/- CD133+/- with and without BMP2 treatment.

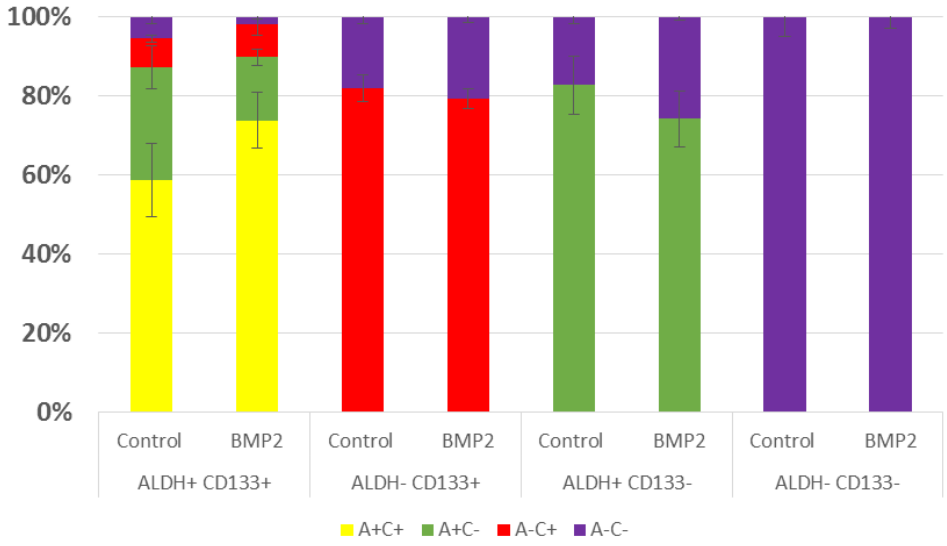

Figure 46: Differentiation potential of OVCAR8 cell line ALDH+/- CD133+/- with and without BMP2 treatment.

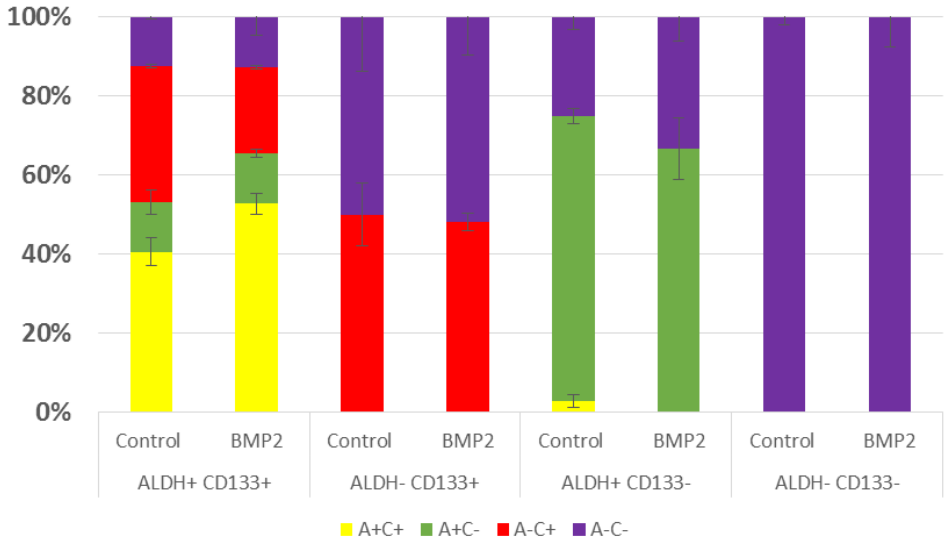

Figure 47: Differentiation potential of Patient Sample 1 ALDH+/- CD133+/- with and without BMP2 treatment.

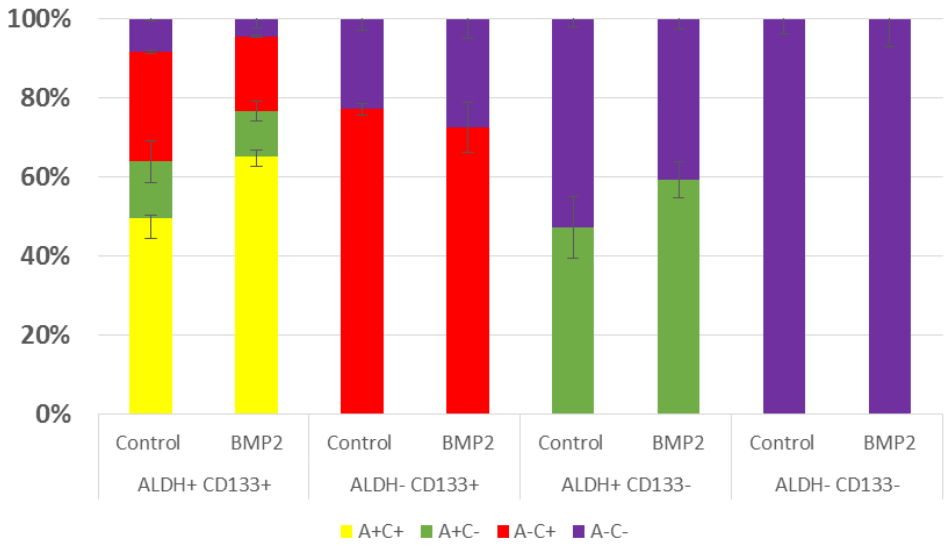

Figure 48: Differentiation potential of Patient Sample 2 ALDH+/- CD133+/- with and without BMP2 treatment.

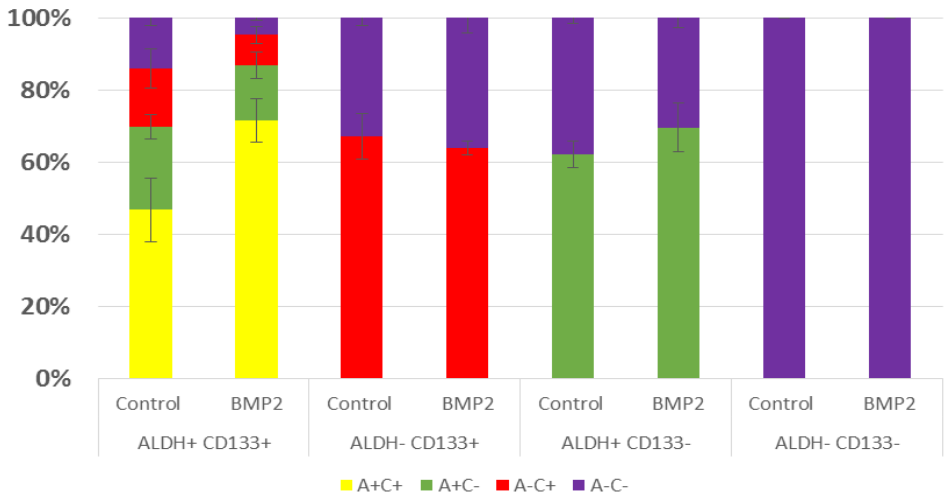

Figure 49: Differentiation potential of Patient Sample 3 ALDH+/- CD133+/- with and without BMP2 treatment.

To confirm the biologic impact of increased CSC self-renewal and suppression of progenitors, our collaborator (Dr. Buckanovich) performed limiting dilution tumor initiation assays. 10 or 100 controls cells or BMP2 treated cells were injected into bilateral flanks of NOD-SCID mice. Both A2780 and SKOV3 BMP2 treated cells showed greater tumor initiation capacity than controls (Table 4). The impact of BMP2 or the BMP2/4 inhibitor Noggin, on SKOV3 and

Table 4: Tumor Initiation rates in A2780 and SKOV3 with BMP2 Treatment

Treatment Groups		Tumors Initiated			
		A2780 Cell Input		SKOV3 Cell Input	
		10	**100**	**10**	**100**
In vitro Treatment	Control	2/5	4/5	0	1/5
	BMP2	5/5	5/5	1/5	5/5
	Cisplatin	ND	1/5	ND	ND
	Cisplatin + BMP2	ND	5/5	ND	ND

A2780 cell growth in tumors formed in NODSCID Mice was also assessed. Treatment with BMP2 in vivo demonstrated a significant increase in tumor growth for both A2780 and SKOV3 tumors, while BMP2 inhibition with Noggin led to a statistically significant reduction in tumor growth (Figure 50). Similarly, when we repeated the above experiment using FACS isolated

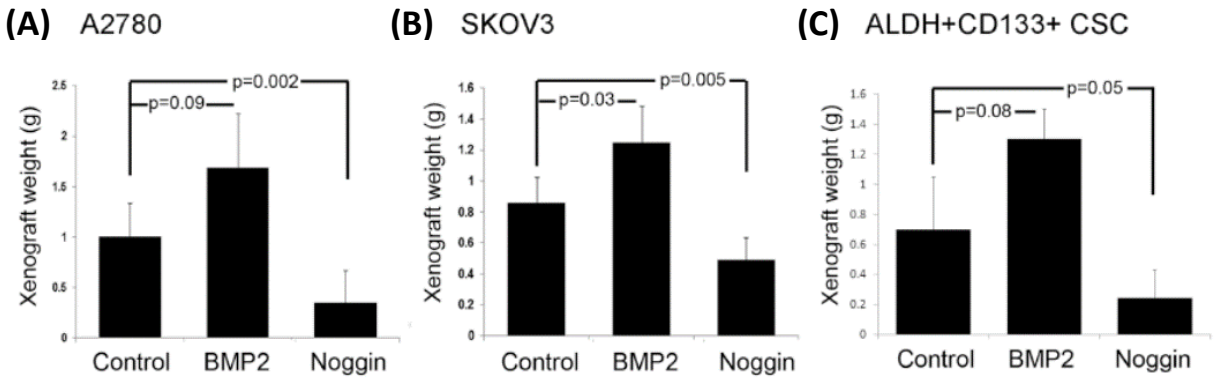

Figure 50: Tumor weights from (A) A2780, (B) SKOV3, and (C) FACS sorted ALDH+CD133+ A2780 cell-derived tumors with or without BMP2 or Noggin treatment (n=10 per group).

ALDH+CD133+ CSC from A2780 cells, BMP2 increased tumor growth while Noggin therapy decreased tumor growth (Figure 50, n=10 per group). This conforms with the data of the differential effects previously observed with in vivo versus in vitro treatment, and suggests BMP2 inhibition may indeed be clinically relevant.

Consistent with this, in vivo treatment with BMP2 results in increased tumor growth and chemotherapy resistance. Inhibition of BMP2 signaling with Noggin or BMP2 knockdown is associated with a reduction in tumor growth and a decrease in cellular proliferation. Additionally, to specifically assess the contribution of tumor cell BMP2 production, our collaborators used shRNA to knockdown BMP2 production in A2780 cells. qRT-PCR evaluation of mRNA levels, and western blot analysis of protein levels confirmed 4-5fold knockdown of BMP2 (Figure 51a & b, n=16 controls and n=8 for BMP2 knockdown). When grown in vivo, BMP2 knockdown tumors demonstrated significantly slower growth (Figure 51c).

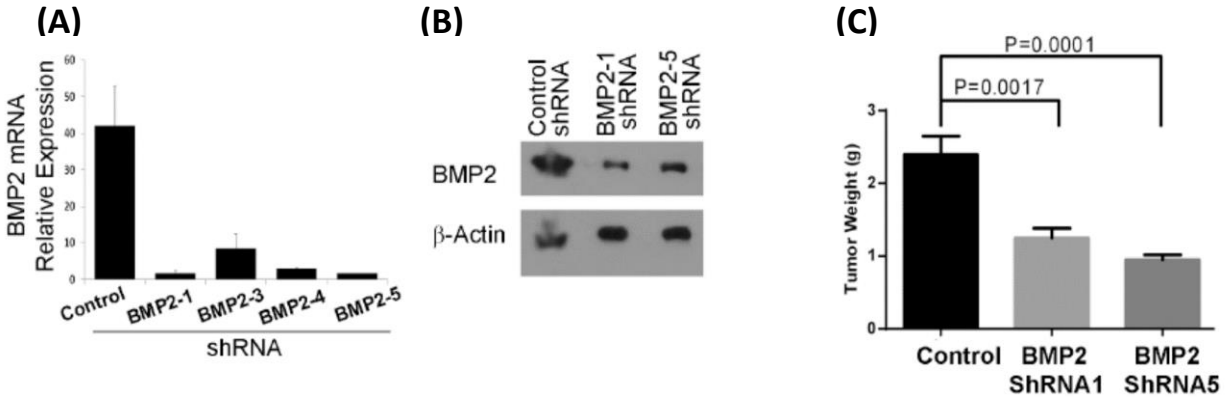

Figure 51: (A) qRT-PCR and (B) western blot demonstrating knockdown of BMP2 in A2780 cells, and (C) tumor weights from cancers initiated from A2780 control and two independent BMP2-shRNA expressing A2780 cells .

As BMP2 influences ovarian CSC proliferation/differentiation it could potentially have a dramatic impact on chemo-sensitivity; by increasing the number of CSCs, BMP2 could increase chemoresistance or, alternatively, by forcing quiescent CSCs into cell cycle, BMP2 could enhance chemosensitivity. Our collaborator, Dr. Buckanovich, observed that, for both A2780 and SKOV3,

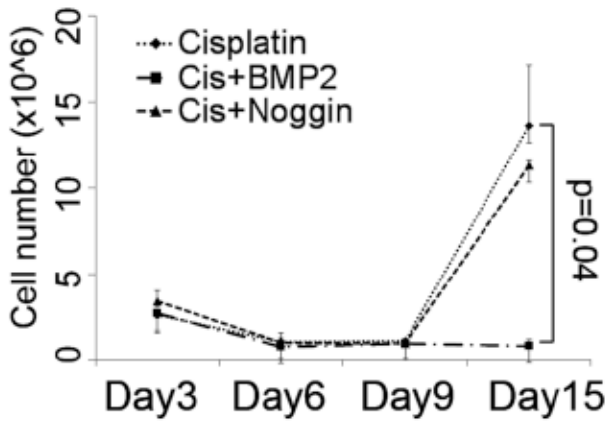

Figure 52: Average cell growth curves of aggregate data from A2780 and SKOV3 cells treated with cisplatin with or without BMP2 or Noggin.

combined treatment with cisplatin and BMP2 demonstrated a significant reduction in cell numbers (Figure 52). Combined treatment with Noggin and cisplatin also lead to a modest reduction in cellular recovery compared to cisplatin treatment alone.

As CSCs are rare but chemoresistant, it is possible the change in total cell numbers does not accurately reflect the number of CSCs. Our collaborators therefore evaluated the absolute number of viable CSCs in A2780 and SKOV3 cells treated with cisplatin with or without BMP2

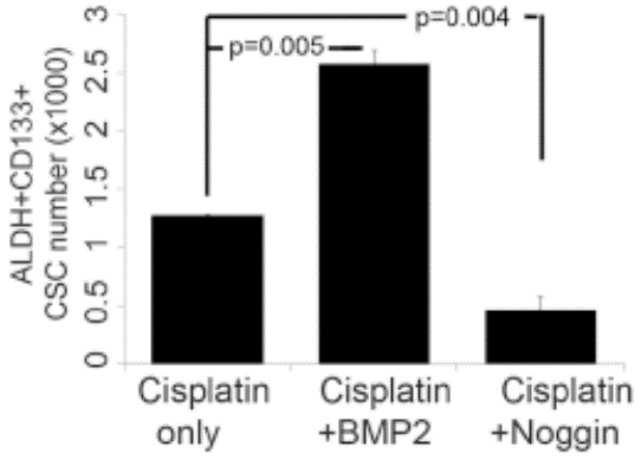

Figure 53: Average absolute CSC number from data aggregated from A2780 and SKOV3 cells six days after cisplatin treatment with or without BMP2 or Noggin.

or Noggin. Despite the significant reduction in total cell numbers, compared to cisplatin treatment alone, treatment with BMP2 and cisplatin was associated with an increase in the absolute number of ALDH+CD133+ CSCs. In contrast, treatment with Noggin and Cisplatin was associated with a decrease in absolute CSC number Figure 53.

Based on these results, it is hypothesized that BMP2 would increase chemoresistance in vivo due to the increase in absolute number of ALDH+CD133+ CSCs. To test this hypothesis, research in Dr. Bucknovich's lab treated A2780 derived mouse xenografts with cisplatin alone or together with BMP2. Tumors treated with BMP2 and cisplatin were significantly larger than tumor treated with cisplatin only (Figure 54). Histological analysis of tumors showed no clear differences in tumor host cells. Combined, this data suggests that BMP2, by promoting CSC self-renewal, also promotes chemotherapy resistance.

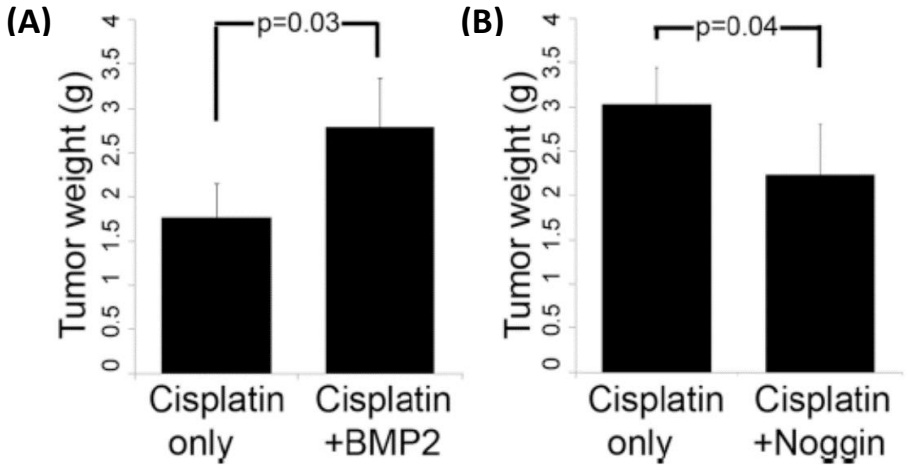

Figure 54: Tumor weights of A2780 tumors treated with (A) cisplatin with or without BMP2 or (B) cisplatin with or without Noggin, a BMP2 inhibitor (n=10 animals/group).

Our data demonstrate a general hierarchical model of ovarian cancer cell differentiation with BMP2 acting as a regulator of CSC division behavior (Figure 55). BMP2 produced by ALDH-CD133- cells promotes ALDH+CD133+ cell self-renewal while inhibiting the proliferation of

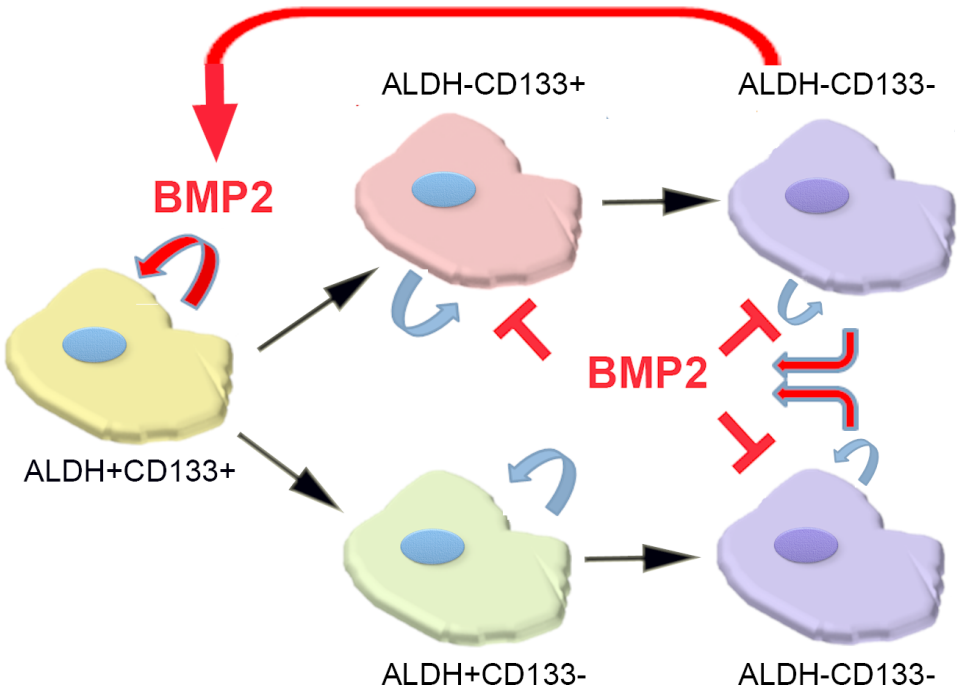

Figure 55: Branched pathway of ovarian cancer cell differentiation hierarchy and BMP2 regulation.

progenitor and bulk cells. However, we have also seen that rare de-differentiation events are possible. While most ALDH+CD133- were not able to give rise to CD133+ cells, we observed one potential de-differentiation event where an ALDH+CD133- cells was able to give rise to an ALDH+CD133+ cell. We also observed the ability of ALDH+CD133- cells to generate CD133+ cells with serial passage of primary cells in vitro. This is consistent with a murine study indicating that in the context of the right combination of oncogenic changes, tumor can be initiated from differentiated epithelial colon cells [89]. Our data is also in line with studies indicating differentiated normal epithelial cells can assume a stem cell phenotype; however, the more differentiated a cell, the less likely it was to de-differentiate. Alternatively, it is possible that there are rare ALDH+CD133- cells that express a third as yet undefined CSC marker that have the potential to differentiate into ALDH+CD133+ cells. Strongly supporting a pro-tumorigenic role of BMP2 in human cancer, use of BMP2 therapy to enhance bone growth has been associated with

a significantly increased incidence of cancer [90]. In an unexpected finding, 20 of 239 patients treated with BMP2, compared to 5 of 224 patients in the control group, developed cancer within three years of treatment. Three patients in the BMP2 group had multiple cancers, compared to none in the controls. One patient developed ovarian cancer and rapidly died of her disease. Given the relatively short latency of tumors after BMP2 therapy, it has been speculated that BMP2 therapy stimulates the growth of pre-existing dormant tumors. These observations are consistent with our results demonstrating that BMP2 promotes ovarian CSC self-renewal. Our data clearly adds to this growing literature indicating a pro-tumorigenic role of BMP2: in vivo treatment with BMP2 promoted tumor growth, and BMP2 knockdown, or inhibition with Noggin, delayed tumor growth. Increase in tumorigenesis could be related to actions on both the tumor cells and the host cells.

BMP2 reduces cancer cell growth and increases chemosensitivity in vitro, yet promotes tumor growth and chemo-resistance in vivo. This reflects the complexity of BMP2 in regulating the distinct ovarian CSC populations; increasing CSC self-renewal while suppressing the production and growth of transient amplifying progenitor cells. Thus, BMP2 treatment in vitro is associated with a decrease in absolute cancer cell numbers due to a reduced proliferation of the bulk ALDH-CD1333- cells. However, BMP2 increases the absolute number of ovarian CSCs. It is likely this increase in absolute number of ovarian CSCs leads to the chemoresistance observed in vivo. This data points out the critical need to evaluate novel therapies impact on CSCs rather than total cell numbers when screening for anti-cancer activity. This highlights the utility of our single cell platform to directly assess CSC division behavior. The microfluidics device allows confirmation of cellular identity by direct observation prior to evaluating differentiation and simple long term tracking in cell lines and patient samples.

2.5 Angiocrine EGFL6 and CSC Differentiation

Like normal stem cells, CSCs also have an important relationship with the vasculature [91]. In most tumors, CSCs reside in a perivascular location tightly associated with tumor endothelial cells [92]. CSCs are highly angiogenic, enhancing their vascular niche. Tumor vessels, which are known to be morphologically, functionally, and molecularly different from normal vessels, provide an abnormal vascular niche and secrete 'angiocrine' factors [93] that promote aberrant stem cell proliferation. Thus, the vascular/CSC niche has been proposed as a therapeutic target [92]. Recent studies identified EGFL6 mRNA as upregulated in tumor vascular cells of epithelial ovarian cancer [94]. Critical in cellular proliferation and differentiation, EGFL6 is primarily expressed in development, with little expression in normal adult tissues [94]. How EGLF6 might regulate CSC regulation, division, and differentiation is currently unknown.

To start the investigation, our collaborators (Buckanovich Lab) first analyzed EGFL6 mRNA expression in the ONCOMINE cancer database [95]. EGFL6 mRNA levels are significantly elevated in all ovarian tumor histologies. With tumor microarray staining with EGLF6 antibodies, EGFL6 protein expression in tumor endothelial cells in the vascular, adipose tissue, and cancer cells themselves was observed. In order to explore the potential function of EGFL6, RNAseq data from 261 TCGA serous ovarian carcinomas were screened and the correlation of expression of EGFL6 to all other genes in the genome was investigated. Spearman correlation was performed comparing expression of EGFL6 to the expression of all other genes in the Ensmbl genome database (55,840 genes). A p-value cutoff of $1x10^{-8}$ was applied to generate a list of the 538 most correlated genes. Interestingly, numerous tumor vascular specific markers (including MXRA, TDO2, TNFAIP6, SEMA3D, and Coll11A1) and EGF like genes (including EGFLAM and MEGF10) were also highly correlated with EGFL6 expression. Gene set

enrichment analysis (GSEA) demonstrated the EGFL6 correlated genes were strongly correlated with **invasive ovarian cancer** and **embryonic stem cell core genes**.

EGFL6 was expressed in HEK293 cells, NIH3T3 cells, and SKOV3 ovarian cancer cells. Western blot analysis confirmed secretion of EGLF6 in transfectants from all three cell lines, and EGFL6 protein was purified to >95% purity from the supernatant. Our collaborators treated ovarian cancer cells with either purified EGFL6, supernatant from EGFL6-expressing HEK293 cells, or supernatant from control transfected HEK293 cells, to assess its effects on ovarian cell proliferation. Purified fusion protein and supernatant from EGFL6 transfected cells were observed to have similar effects. EGFL6 treatment of SKOV3 (Figure 56), OVCAR3 (data not shown), OVCAR8 (data not shown), and primary ovarian tumor cells (Figure 56) was associated with a 30-40% increase in total cell number.

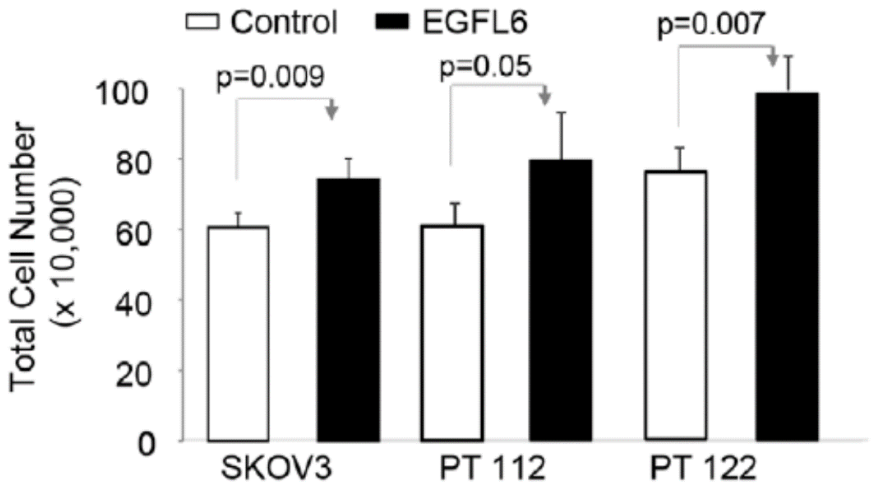

Figure 56: Total cell number for EGFL6 treated SKOV3 cells and primary tumor cells, compared with control.

Given GSEA analysis demonstrates a strong correlation of EGFL6 with core stem cell factors, collaborators next assessed the impact of EGFL6 on ovarian CSCs. As previously discussed, ALDH (or ALDH & CD133) is an excellent marker of ovarian CSCs in SKOV3 cells and primary patient samples [64]. In order to assess effects on CSCs, we looked at ALDH+ cell

behaviors. Treatment of SKOV3 ovarian cancer cells with increasing concentrations of EGFL6 was associated with increasing total cell numbers, but decreasing percentages of ALDH+ CSCs (Figure 57). However, given the increase in total cell numbers, the absolute ALDH+ CSC number remained unchanged (Figure 57).

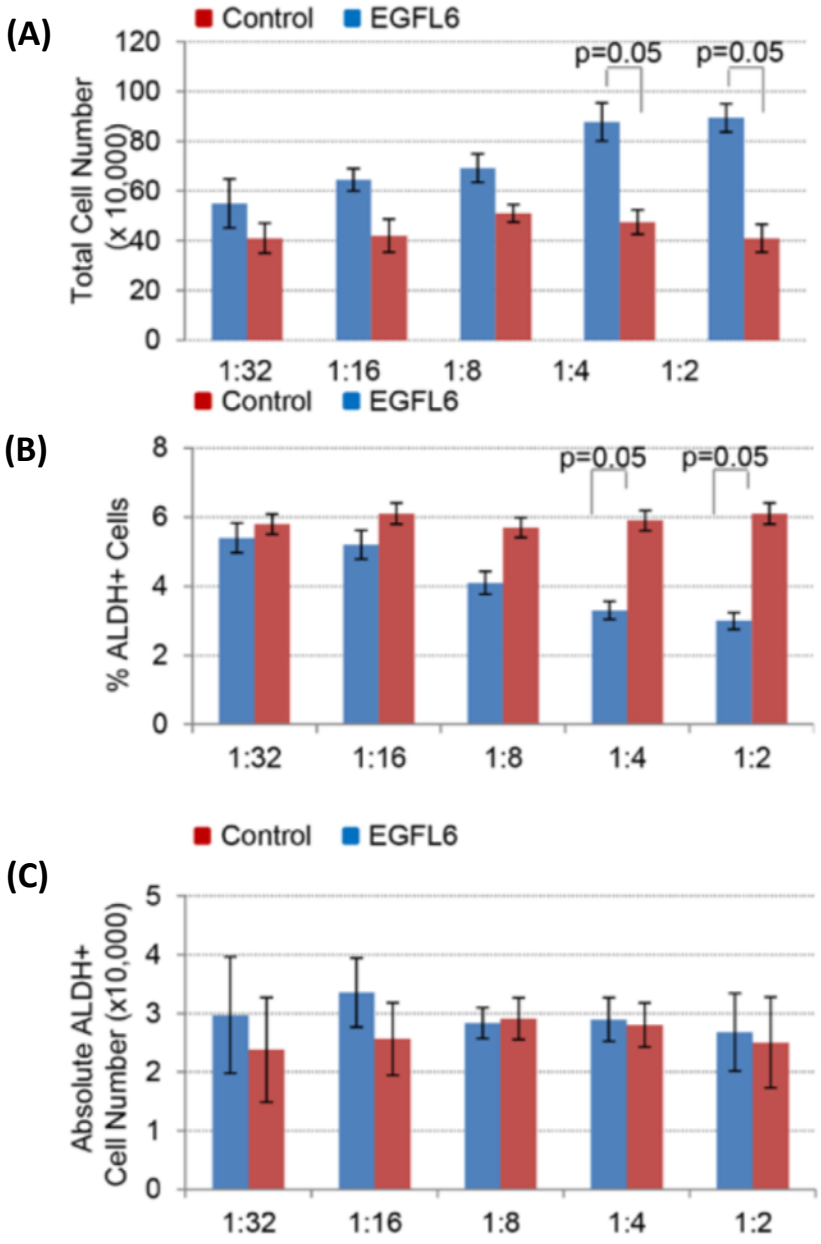

Figure 57: Effect of EGFL6 treatment on SKOV3 ovarian CSC on (A) total cell numbers, (B) percentage of ALDH+ cells, and (C) absolute ALDH+ cell number.

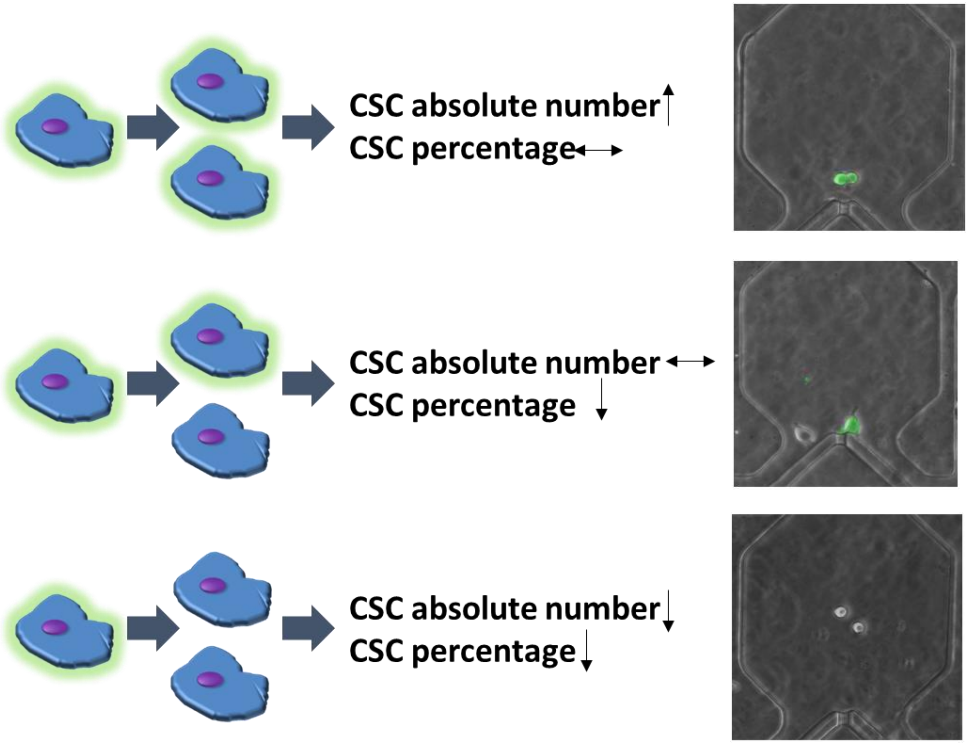

Figure 58: Potential cell divisions of an ALDH+ (green border) cells and the expected changes in CSC number and percentage.

With only a single marker defining CSC populations, dividing CSCs can theoretically undergo at least three distinct types of cell division related to the expression of ALDH: 1) symmetric division (self-renewal) yielding 2 ALDH+ cells, 2) differentiation yielding 2 ALDH(-) cells, or 3) asymmetric division yielding an ALDH+ cell (self-maintenance) and an ALDH(-) cell (Figure 58, ↑=increase, ↓= decrease, ↔ = no change). The finding that EGFL6 increases total cancer cell number and decreases the percentage of ALDH+ cells, while not impacting the absolute number of ALDH+ cells, suggests that it would be consistent with EGFL6 stimulation of ALDH+ CSC asymmetric division. Alternatively, EGFL6 could preferentially promote proliferation of ALDH(-) cells. In order to determine if EGFL6 is promoting asymmetric division, we used our single cell microfluidic device to investigate the division of ALDH+ cells. The same benefits that were present when investigating the effects of BMP2 manifest in this application as well. Cellular

division and the phenotype of progeny can be easily tracked within the device over time. We FACS-sorted ALDH+ and ALDH- SKOV3 cells and loaded them into separate microfluidic devices as previously described. After loading, we confirmed ALDH expression with fluorescent microscopy (Figure 58). Cells were then mock-treated or treated with EGFL6. After 48 hours, live cells were stained using ALDEFLUOR and re-imaged using our fluorescent microscope. Approximately 35% of untreated ALDH- SKOV3 cells demonstrated no cell division (Figure 59),

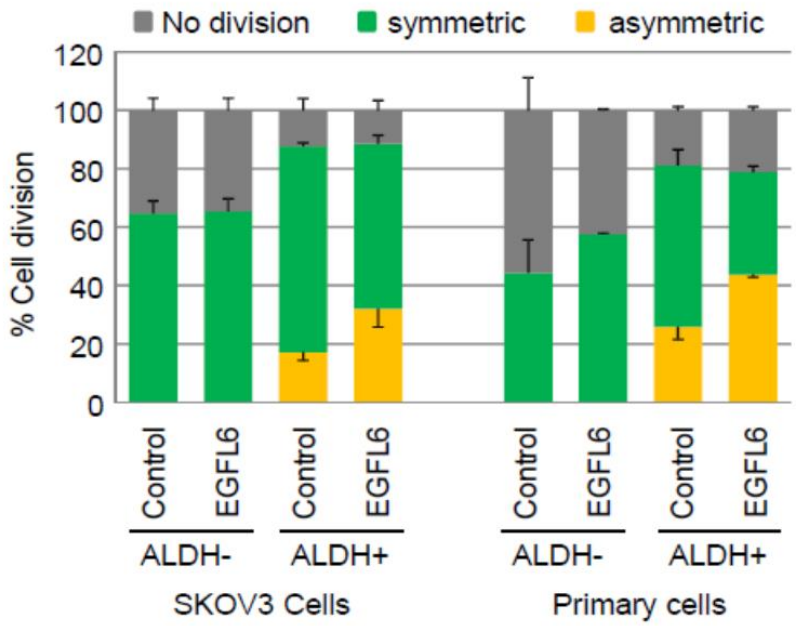

Figure 59: Percentage of observed division events with EGFL6-treatment vs. control conditions for SKOV3 cells (3 days of growth) and primary patient samples (5 days of growth).

while 65% underwent symmetric division to produce two ALDH- cells. Production of ALDH+ daughter cells from ALDH- cells was not observed as is consistent with our BMP2 data. EGFL6 treatment of ALDH- SKOV3 cells had no significant impact on the number or type of cell divisions. Consistent with a stem cell phenotype and unlike ALDH- cells, ALDH+ cells demonstrated the ability to undergo both symmetric division, yielding two ALDH+ cells, and asymmetric division, yielding one ALDH+ cell and one ALDH- cell. EGFL6 treatment of ALDH+ SKOV3 cells resulted in a 2-fold increase in the percentage of ALDH+ cells undergoing

asymmetric division (Figure 59). This was associated with a statistically significant increase in total cell numbers. With EGFL6 treatment, there were on average 6.5 cells/well versus 3.7 cells/well in controls. A total of 325 cells were produced per 50 ALDH+ cells captured with EGFL6 treatment compared to 185 total cells/50 captured cells in the controls. EGFL6 treatment of ALDH- SKOV3 cells had no significant impact on proliferation rates.

These results were confirmed with two separate primary ovarian cancer samples. Primary cells divided more slowly than cancer cell lines, thus division was assessed 5 days after initial loading. For primary cells, we observed that over 50% of untreated ALDH- cells underwent no division over 5 days, while remaining cells underwent symmetric division. EGFL6 treatment of ALDH- cells was associated with a non-statistically significant increase in symmetric divisions. 20% of ALDH+ cells underwent no division. As observed with cell lines, EGFL6 treatment of primary ALDH+ cells was associated with a 1.9-fold increase in the number of ALDH+ cells undergoing asymmetric division (Figure 59). EGFL6 treatment was associated with an increase in total cell numbers (90 EGFL6 treated cells yielded 585 total cells while 82 mock-treated cells yielded 451 cells). However, likely due to the slower growth of primary cells, this did not reach statistical significance.

By identifying the source of EGLF6 effects in cancer cells, our microfluidic approach significantly shrunk the experimental space that needed to be examined. EGLF6 effects were determined to be dependent on the RGD domain using an RGD to RGE mutation assay. RGD signaling was seen to be acting through integrin β3, as EGFL6 effects could be abrogated with integrin inhibitor Echistatin and only β3 was expressed in the ovarian population. Finally, western blot analysis showed that ELG6 affected ALDH+ cell through increasing levels of phospho-SPH2 and phosphor-ERK.

After determining method and mechanism of action, effects of EGLF6 on in vivo tumor growth were assessed by our collaborators. While some EGFL6 expression was observed in tumor cells, EGFL6 is predominantly expressed in tumor vasculature. As such, our collaborators created a new tumor model with EGFL6 expressing human tumor vascular cells. EGFL6 was expressed in human infantile hemangioma stem cells (HemSC). HemSC have been shown to proliferate and generate blood filled human vessels in vivo [96]. When SKOV3 and HemSC-EGFL6 cells were co-injected in vivo, robust human CD31+ tumor vessels which expressed EGFL6 were observed. SKOV3 cells grown with control HemSC-EGFL6 cells demonstrated increased growth compared to SKOV3 cells grown with HemSC controls (Figure 60, n=10/group in two independent experiments). To confirm our findings were not specific to cell lines, primary cells were co-injected from three different primary patient samples (n=2 each) with HemSC-EGFL6 cells or controls HemSC. Similar to that seen with cell lines, EGFL6 expression by Hem-SC cells was associated with more rapid tumor growth (Figure 61).

Together, this data suggests that EGFL6 plays an important role in promoting ovarian cancer cell proliferation, and thus may be a therapeutic target. Following this lead, EGLF6

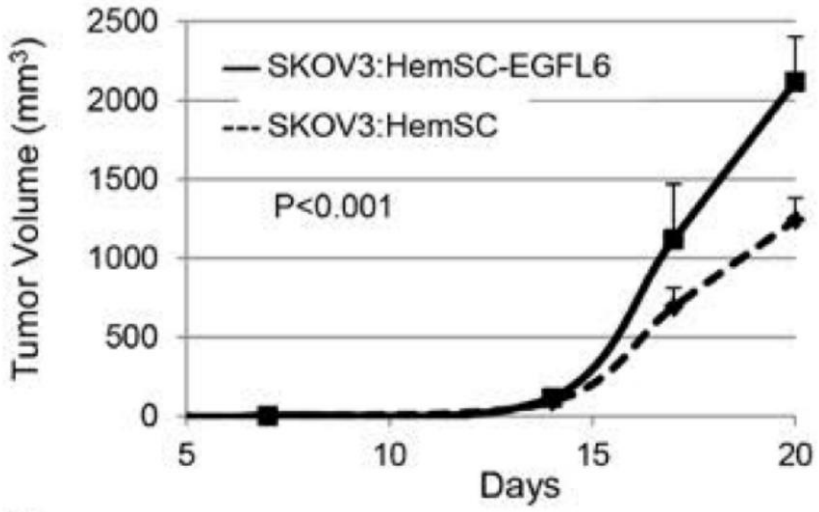

Figure 60: Tumor growth curves of SKOV3- HemSC-EGFL6 tumors vs. SKOV3 HemSC-control tumors.

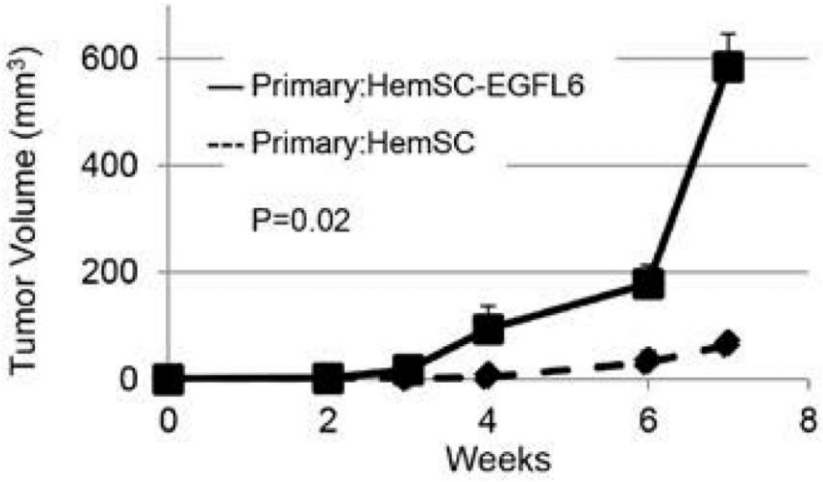

Figure 61: Tumor growth curves of freshly isolated primary patient cells co-injected with HemSC-EGFL6 or HemSC-control.

targeting antibodies have been developed and tested for eventual clinical use. Several successful antibodies show the ability to block EGFL6-mediated reductions in ALDH+ cell percentages, reduce in cellular proliferation rates in cells which endogenously express EGFL6, and block the increased phosphorylation of SHP2 and p-ERK associated with ELGF6 treatment. When looking at effects in vivo, twice weekly intraperitoneal treatment with anti-EGFL6 treatment of SKOV3 flank tumors resulted in a ~2-fold reduction in tumor volume and tumor weight and a reduction in numbers and sizes of nodules. Finally, anti-EGFL6 treatment of SKOV3-HemSC-EGFL6 tumors (to assess the impact of these treatment of the growth promoting effects of vascular EGFL6) was associated with a significant reduction in tumor growth. These results are encouraging to show how data generated from our platform directly led to development of relevant clinical data and directed generation of therapeutic agents.

Though we restricted our focus to applications in cancer and CSC in particular, the microfluidic single cell capture scheme developed by Dr. Chung has the potential to be used for a wide variety of single cell based assays. The user-friendly platform is driven by simple passive

gravity flow, and input-free hydrodynamic capture isolates single cells. It is thus easily deployable in traditional biological or other non-microfluidic laboratories. Many cell types (including primary samples) show robust capture and high viability within the platform. As a result, we were able to make important and clinically relevant discoveries in applications of heterogeneous drug screening, targeted CSC therapy, autocrine BMP2 stimulation of CSC self-renewal, and angiocrine EGLF6 regulation of CSC asymmetric division.

Chapter 3: Surface Patterning for On-Chip Suspension Culture

The utility of microfluidic platforms can often be improved not only by optimizing current performance, but also by expanding their versatility. Robust, user-friendly approaches that can be easily deployed in a variety of laboratory settings and also modified to perform different biological assays can have significant impact. The previous chapter has examined how our single cell capture platform can be used for adherent culture, studying clonal drug response, screening of targeted agents, and CSC division and differentiation behaviors. In this chapter, we will examine surface modification approaches that can be utilized to adapt our platform for suspension culture assays as well.

3.1 Adherent vs. Suspension

At a fundamental level, there are two basic approaches for growing cells in culture: adherent to a substrate and free-floating in the culture media (in suspension). Three dimensional culture is possible in both adherent (matrigel, organotypic) and suspension (spheroid) forms. Adherent culture, as demonstrated in **Chapter 2**, is common for mammalian cells. For most mammalian cells, adhesion to the extracellular matrix (ECM) is essential to maintain cellular homeostasis, and disruption of cell attachment leads to anoikis, a form of programmed cell death [97]. A handful of mamalian cell types, such as hematopoietic-derived cells (i.e. blood), survive in suspension naturally, while others have been modified to survive suspension culture to facilitate higher density cell growth. In contrast, most insect cell lines grow well in adherent culture or suspension.

There are numerous direct methodological differences between adherent- and suspension-based culture approaches when propagating cells in bulk (Table 5). As discussed, adherent culture

Table 5: Differences between adherent and suspension cell culture

	Number of Cell Types	Passaging Requirements	Dissociation Methodoloy	Growth Limitations	Culture Vessel Requirements
Adherent Culture	Appropropriate for most cell types	Periodic passaging requiring replacement culture vessels	Enzymatic or mechanical dissociation; disrupts cell behavior	Limited by culture vessel surface area	Tissue culture treated or extracellular matrix coating
Suspension Culture	Few cell lines (hematopoietic) and primary cultures	Easier passaging, but requires more rigorous cell tracking	No dissociation required	Limited by cell to media concetration ratio	No tissue culture treatment, non-adherent coatings

Adapated from Thermo Fisher Life Technologies Cell Culture Technical Material, 2015

is more widely applicable than suspension methods; however, adherent culture also requires frequent passaging into replacement culture vessels via enzymatic or mechanical dissociation that disrupts cell behavior. Though no dissociation is required, bulk suspension cultures must be rigorously monitored to track cell-to-media ratios to ensure continued cell growth and viability. Many of these prominent methodological differences diminish though when culture is miniaturized for microfluidic assays. Passaging is, more often than not, unnecessary over the course of a single experiment, and in our approach in particular, continuous media perfusion refreshes nutrients and removes waste products to maintain cell health in either culture condition. These advantages allow us to focus on the biological needs of the assay when designing culture conditions within our platform, rather than the methodological restrictions.

In particular, using suspension culture on chip will provide us two major biological advantages over adherent culture. First, suspension sphere culture better recapitulates primary tumor behavior [98, 99]. When plastics and solid substrates are used for adherent culture, primary cells transform, losing important characteristics that they express in vivo. Modifying our single cell capture device substrate for suspension culture will facilitate more physiologically relevant study of heterogeneous single cell behavior from primary patient cells that are capable of

propagation in suspension culture. Second and more importantly, three-dimensional suspension culture in the form of spheres provides a methodology to identify and characterize stem/progenitor cancer cells from multiple cell types [21, 100, 101]. When disassociated into single cell suspension, the vast majority of the cells undergo anoikis, a form of programmed cell death, but CSCs are capable of survival, and proliferate through the formation of spheroids [100]. The integration of suspension culture surfaces within our single cell device would allow their growth from single cells into spheroids, allowing characterization of CSC/progenitor cell sub-populations. We have investigated the two approaches to facilitate single cell suspension culture on chip: topographically patterned superhydrophobic surfaces and polyHEMA patterned suspension culture surfaces

3.2 Topographically Patterned Superhydrophobic Surfaces

Hydrophobic surfaces are already a common part of daily life. From Teflon-coated non-stick pans to stain resistant pants, many surfaces are hydrophobically patterned. From the Greek hydrophobe, meaning "having a horror of water," hydrophobic surfaces seemingly repel water and exhibit high contact angles when drops of water are placed on their surfaces. In some cases, such as with naturally occurring lotus leaves, these surfaces often achieve a superhydrophobic state. These surfaces are those with water droplet contact angles that exceed 150º and a roll-off angle that is less than 10 º [102]. Interestingly, these superhydrophobic effects are a result of physical shapes and interfacial tensions, rather than a chemical interaction. Microscale topographical patterning can increase the contact angle of a naturally hydrophobic material to create a superhydrophobic state [103]. In this state, the fluid is suspended on top of the micro-patterned structures, rather than touching the surface.

In recent years, these superhydrophobic surfaces have become popular for anti-biofouling applications (preventing bacteria adhesion) as well [104, 105, 106]. The same characteristics that make these surfaces useful for preventing bacterial adhesion, such as the small surface to culture media contact area, are also attractive for non-adherent mammalian cell culture. As such, non-adherent mammalian cell culture using hydrophobic surfaces is a natural progression in this respect. By minimizing the surface area in contact with the media, we minimize the area where cells may interact with the surface via focal adhesions. Focal adhesions form on a micrometer scale and mediate cell adhesion [107]. Without the area and binding domains to form focal adhesions, cells cannot adhere to the hydrophobic surfaces. Fortunately, polydimethylsiloxane (PDMS), the material used in the fabrication of our microfluidic channels, is hydrophobic, and thus by introducing micropatterns in PDMS, we can form PDMS-based superhydrophobic surfaces. A PDMS superhydrophobic suspension culture surface can be integrated with our single cell capture channels by oxygen plasma bonding to create robust suspension culture single cell microfluidic devices. A topographical approach to non-adherent culture is also attractive due to its long term stability (patterns do not degrade over time) and physical mode of action (rather than through chemical modifications), as introduced chemicals may alter cell behavior.

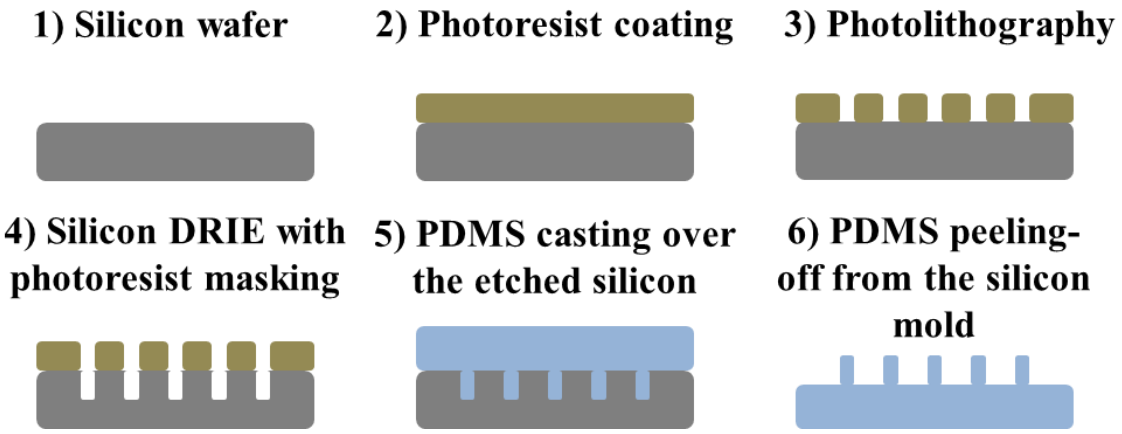

Figure 62: Soft lithographic fabrication of PDMS hydrophobic surfaces.

Hydrophobic PDMS surfaces were fabricated using standard soft lithography techniques as shown in Figure 62. Silicon wafers were coated with photoresist and patterned with photolithography to form various hollow pillars such as circular, triangular, square, and honeycombs [108]. We investigated multiple topographies to find the optimal micropattern. The silicon was then etched with deep reactive ion etching (DRIE) to a depth of 15μm. PDMS was poured onto the wafer, cured, and detached from the silicon mold. SEM images of the etched silicon pattern and confocal laser images of the fabricated PDMS honeycomb surface were taken to observe feature structure and verify fidelity (Figure 63).

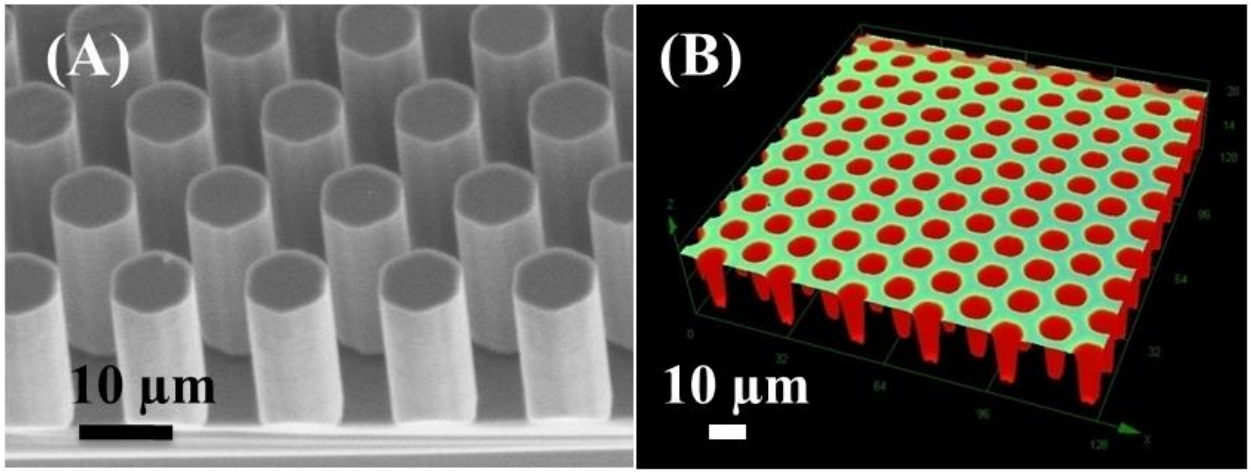

Figure 63: (A) SEM image of DRIE etched negative honeycomb pattern in silicon and (B) confocal laser microscopy image of the fabricated PDMS honeycombs.

Of particular interest is the relationship between the micropatterns and the resulting contact angle to observe the hydrophobicity of the fabricated PDMS surfaces. The ratio of the total surface area compared to the area of the contacting surface (the microstructures) should be a key factor in determining hydrophobicity. Contact angles were measured by pipetting a 10 μL droplet of deionized (DI) water onto the various PDMS patterns. The contact angle of the surfaces varied from ~110° to 150° depending on their geometries, as shown in Figure 64. In total, 13 separate

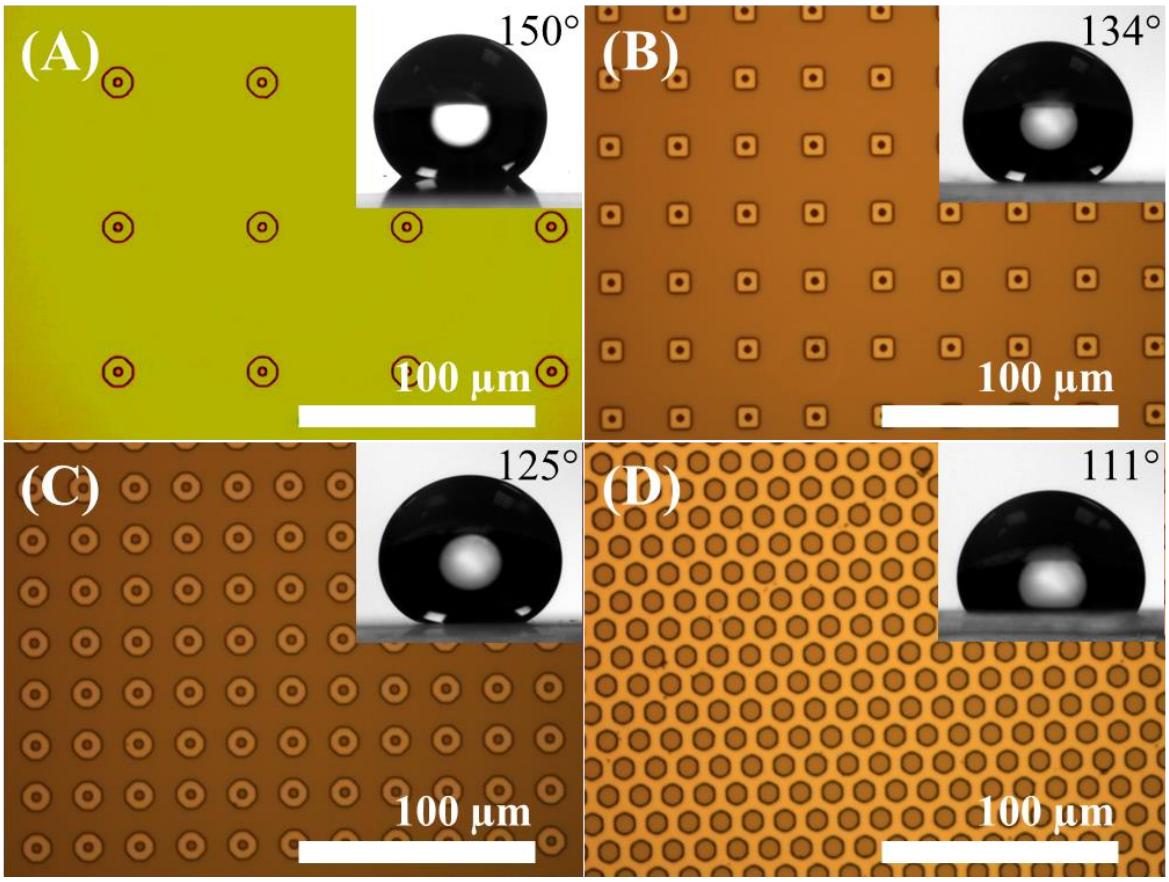

Figure 64: Optical images of 10µL droplets on hydrophobic surfaces with droplet contact angles and the corresponding patterns (A-D) of masks used in fabrication.

hydrophobic patterns were tested, including four different designs (circular, triangle, square, and honeycomb) in two different structural sizes of 7.5 and 10 µm with a pitch variation from 10 µm to 50 µm. As expected, increasing pitch between micro-pillars reduces the contact surface area and therefore increases the resulting contact angle. Decreasing the pillar size likewise causes an increase in contact angle (Figure 66). Superhydrophobicity (>150° contact angle) was achieved using 7.5 µm pillars with a pitch of 50 µm.

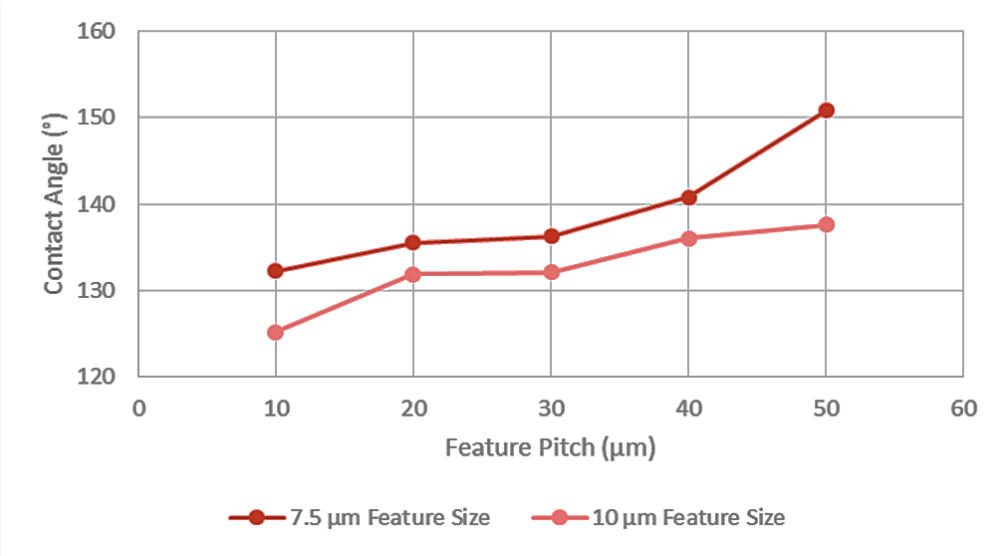

Figure 66: Changes in hydrophobicity on pillar surfaces with varying pattern feature size and pitch.

As discussed in Chapter 2, in long term culture, PDMS surfaces exhibit mild cell toxicity; however, cleaning the surface prior to culture removes any residual uncured PDMS and reduces this toxicity significantly. Unfortunately, these cleaning treatments can affect surface characteristics. The standard cleaning procedure thermally ages the PDMS surface, to ensure minimal adsorption and thorough curing, and submerges it is a variety of cleaning solvents (EtOH,

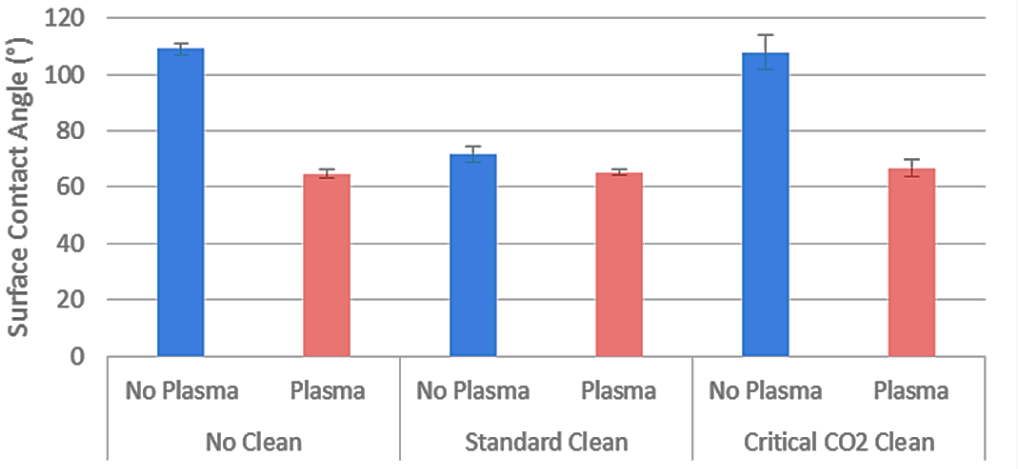

Figure 65: The effects of cleaning protocols on hydrophobicity of 10µm pitch 10µm feature size PDMS honeycomb surface.

Tween, etc). In order to monitor the effects of cleaning on surface hydrophobicity, the contact angle of a 10μm-pitch-10μm feature size honeycomb surface was measured after these steps. Standard solvent cleaning procedures resulted in an undesirable reduction in contact angle (Figure 65). As an alternative cleaning method, brief treatment with supercritical carbon dioxide, a supercritical fluid, was performed. Supercritical carbon dioxide has low toxicity and negligible environmental impact, and more importantly, carbon dioxide cleaned surfaces show similar long term viability to those treated with liquid solvents without a reduction in contact angle (Figure 65). As expected, post cleaning plasma treatment for bonding reduces contact angle to comparable levels (60º) in all cases. This plasma effect fades within 24 hours after bonding is complete, returning surface hydrophobicity to post clean values. Supercritical carbon dioxide treatment provides a methodology to clean PDMS surfaces for improved cell viability without affecting long-term hydrophobicity.

In order to validate successful suspension culture on the various patterned PDMS surfaces, we formed microwells by bonding an additional open circular PDMS layer, created using a biopsy punch, to the patterned PDMS hydrophobic surface. We cultured three different types of cells (C2C12 myoblasts, 10T1/2 fibroblasts, and SUM159 breast cancer cell lines) in bulk to assess the

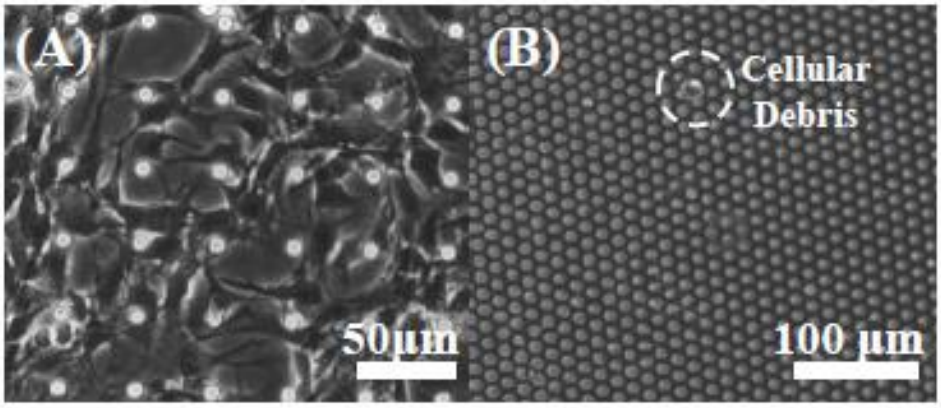

Figure 67: (A) C2C12 myoblast culture on hydrophobic PDMS patterns with attachment on hydrophobic pillar surface and (B) anoikis on honeycomb patterns.

culture conditions. These cell lines were chosen as they have particular surface requirements: C2C12 myoblasts readily undergo anoikis in non-adherent culture only, 10T1/2 fibroblasts require adhesion but also readily aggregate when culture in high concentration, and SUM159 cancer cells contain a large pool of progenitor/CSC that are capable of anchorage independent growth and proliferation. Prior to loading into the makeshift hydrophobic wells, all the three types of cells were cultured in Dulbecco's Modified Eagle Medium (DMEM) with 10% fetal bovine serum. For loading, cells were trypsinized (trypsin with .05% ethylenediaminetetraacetic acid) and suspended. After loading into the non-adherent wells, we cultured the cells with mammary epithelial cell basal medium supplemented with B27, insulin, lipid concentrate, hydrocortisone, cholesterol, and epidermal growth factor.

Figure 67 and Figure 68 show the morphology of cells (C2C12 and 10T1/2, respectively) grown on example hydrophobic surfaces. When cultured on the hollow pillars, both C2C12 and

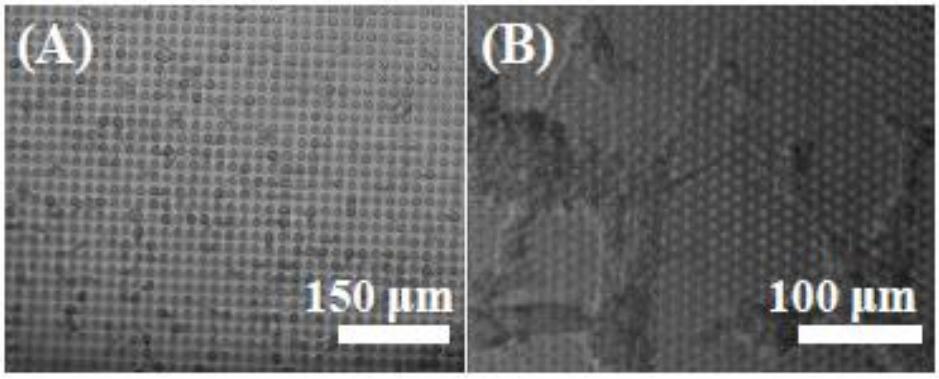

Figure 68: (A) 10T1/2 fibroblast culture on hydrophobic PDMS patterns with attachment observed on hydrophobic pillar surface and (B) forced aggregation on honeycomb surface

10T1/2 cells attached to the bottom surface despite high hydrophobicity (high contact angle). Fluid clearly penetrated the microstructures as the cells adhered to the bottom substrate. Low contact angle honeycomb structures, on the other hand, actually prevented C2C12 cells from attaching to the bottom surface (causing cell death), and fibroblasts (10T1/2 cells) were forced into aggregates.

This is interesting as the honeycomb surface showed the lowest measured contact angle, defying expectations of the relationship between suspension culture performance and hydrophobicity.

When we investigate the underlying physics, however, the picture becomes clear. The high-pitch, small-feature structures are highly susceptible to Cassie-Baxter to Wenzel State transitions [109], and underwent such transitions during culture. A Cassie-Baxter state, where the fluid is suspended on top of the microstructures, is needed to minimize cell-surface contact and prevent cell adhesion. In order to maintain a Cassie-Baxter state, contact line forces must overcome body forces of the fluid weight and the microstructures must be tall enough to prevent the liquid that bridges the structures from touching the substrate [110]. In the case of the high-pitch, small-feature structures, the body forces of the fluid greatly exceeded the capillary surface forces at the interface due to the large volume of fluid used for cell culture and the humid culture environment. This results in the fluid touching the substrate, wetting it, and causing a transition to a Wenzel state, where the liquid covers the entire surface. The honeycomb surface is better able to resist these Cassie–Baxter to Wenzel transitions (Figure 69). Another benefit of these honeycomb structures

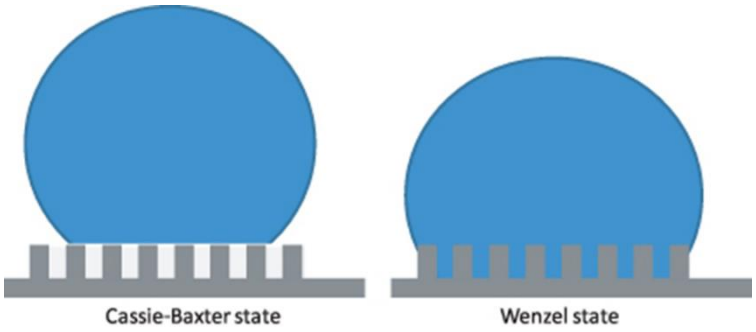

Figure 69: Cassie-Baxter to Wenzel state transitions result in a decrease in hydrophobicity and an increase in the volume of fluid interacting with the surface as fluid displaces air-pockets in the micropatterned features.

is their "non-communicating" nature [111]. Within the honeycomb micropatterns, the columns of trapped air are isolated from one another. Wenzel state transitions or wetting in one patterned area does not "communicate" or affect another. "Communicating" or open pillar structures readily

transfer collapse of the superhydrophobic state once wetting occurs in a single location. In the end, measured hydrophobicity mattered less for successful non-adherent culture than robust maintenance of Cassie-Baxter states in cell culture conditions.

After identifying the ideal topographic pattern, SUM159 breast cancer cells were cultured and monitored on the surfaces in macro-scale wells (formed from flat surfaces of PDMS punched with 6 gauge biopsy punches and bonded to the topographically patterned PDMS) over 6 days to monitor for sphere formation (Figure 70). Surface hydrophobicity was maintained (no observable Cassie–Baxter to Wenzel transition) and SUM159 cells were unable to attach to the bottom surface. Only a subset of SUM159 cells, the progenitor/CSC population, were capable of resisting anoikis, proliferating (Day 1), and forming small single cell derived spheres (Day 6). In this bulk trial, ~42% of single SUM159 cells were capable of forming spheres.

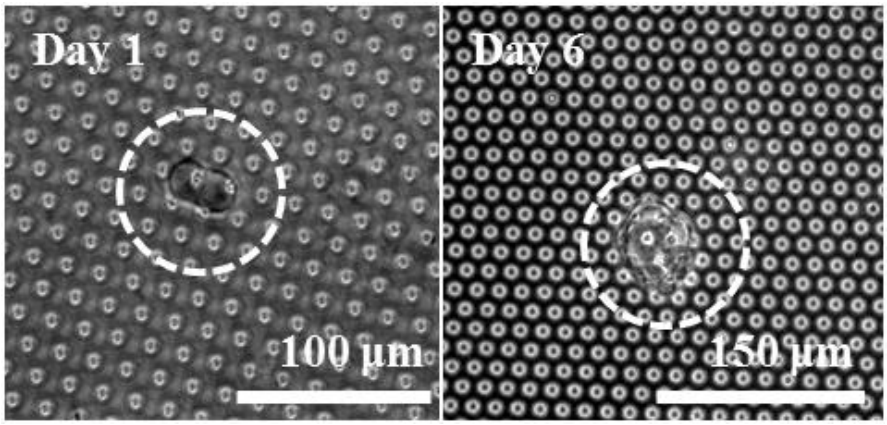

Figure 70: Growth of a SUM159 sphere on honeycomb surface over the course of 6 days of culture.

Next, the non-adherent topographically-patterned surface was integrated with the single cell capture scheme to facilitate robust and user-friendly single cell suspension culture. The microfluidic component of the integrated device was fabricated with standard soft lithography using a silicon wafer, patterned with SU-8 to create a mold [49]. PDMS was poured over this mold and cured to form a hardened negative cast. The cast was peeled from the silicon surface, and this fluidic layer was then bonded over the patterned hydrophobic surface using an oxygen plasma

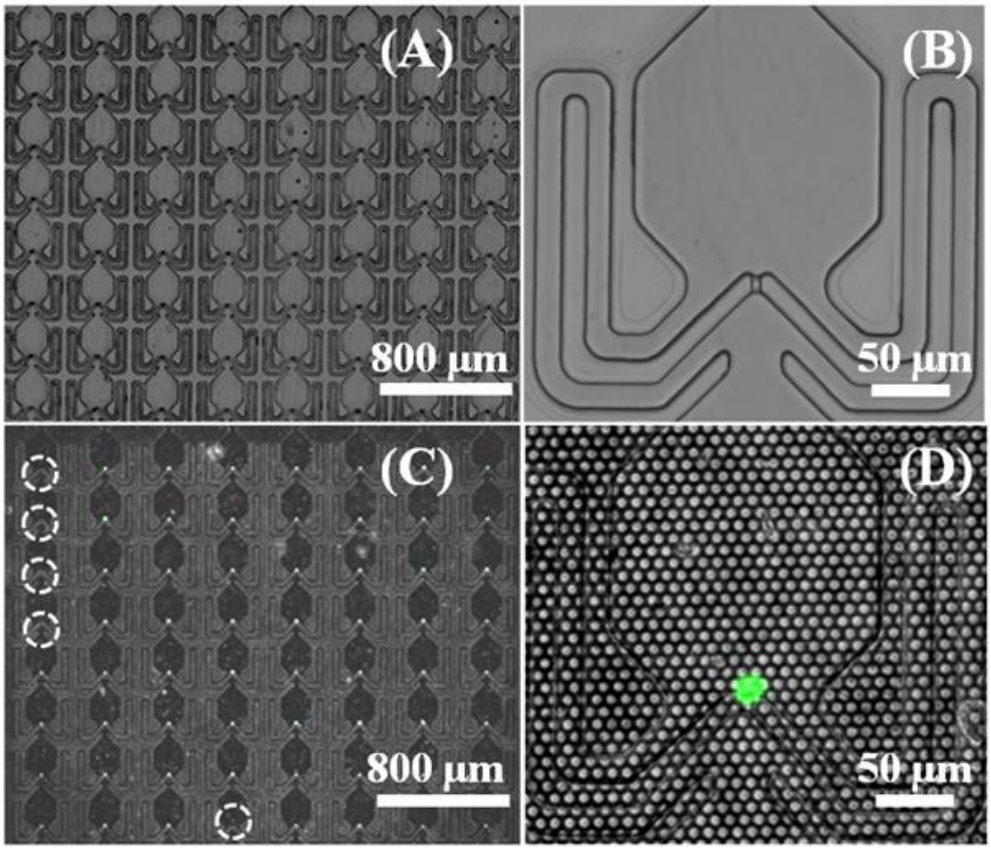

Figure 71: Overview of 64-microwells high-throughput single-cell capture device (A) before and (C) after surface integration with magnified view of the single microwell for single cell capture (B) with and (D) without pattern and cell capture (cells stained with Cell Tracker Green).

treatment. As both surfaces are fabricated from PDMS, this provides a strong fluidic seal for the channels. Figure 71 shows the single cell channels prior to surface integration and after. When SUM159 suspensions were loaded into the device as previously describe in Chapter 2, we achieved a capture rate of >90%. The micropatterned surface had no effect of device performance or capture (Figure 71 c-d). With continuous media perfusion provided by gravity flow, the cells can be cultured for over 2 weeks, which is more than adequate time for sphere formation from single cells.

The integrated microfluidic platform automates single cell placement and permits easy tracking of single cells because the cells are geometrically confined in each microwell inside the

microfluidic device. In traditional culture plates, tracking single cells within the large area is very time consuming, extremely slow and laborious. Additionally, microfluidic integration allows for continuous perfusion of culture media to the growing sphere. In the standard 96-well plate technique, media may be only changed by exposing the culture environment and replacing the media that has been lost through evaporation. This process causes imbalances in pH and solute concentrations, both of which are critical parameters for successful sphere formation. Within the integrated microfluidic platform, media can be continuously perfused through the microwells by gravity driven flow. More importantly, this platform provides a method for robust and high throughput single cell-derived spheroid formation. To the best of our knowledge, this is the first demonstration of both 1) using hydrophobic surfaces within microfluidics for sphere formation and 2) robust single cell-derived sphere formation on-chip.

3.3 PolyHEMA Patterned Suspension Culture Surfaces

While the integration of topographically-patterned PDMS hydrophobic patterns into our single cell capture platform facilitates successful long-term chemical-free single cell-derived sphere formation, it has several disadvantages that were not anticipated during the development. First, the fabrication of the hydrophobic pattern master requires expensive deep reactive ion etching, greatly increasing the cost of what would otherwise be an inexpensive device. In addition, as can be observed in Figure 71d, the micropatterned structures interfere with traditional optical microscopy, resulting in poor resolution for imaging the cells and spheres of interest. As an alternative to the topographical approach, we have developed a poly(2-hydroxyethyl methacrylate) (polyHEMA) based surface modification for single cell suspension culture.

To achieve suspension culture in our single cell platform, we used poly(2-hydroxyethyl methacrylate) (polyHEMA) as a non-adherent coating material [112]. PolyHEMA, originally invented for use in contact lens, is a water absorbing polymer, capable of forming a flexible hydrogel in aqueous environments. It has demonstrated good bio-compatibility, and many polyHEMA co-polymers have seen widespread use since as early as the 1960's [113]. Despite its versatility and biocompatibility, polyHEMA structures or coatings have been of limited use in cell culture applications, specifically only for bulk surface modification [114, 115]. When exposed to water (50% by weight), polyHEMA methyl groups turn outwards facilitating swelling and sterically block cell adhesion to the substrate (Figure 72). As the 2-hydroxyethyl methacrylate

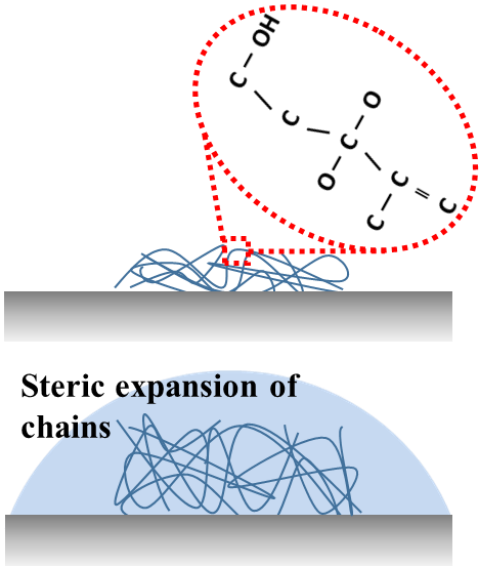

Figure 72: Mechanism of action for PolyHEMA non-adherent culture.

chains have no cell binding sites and streically block the surface, cells are unable to adhere, creating environments for suspension culture. In these culture applications, PolyHEMA is traditionally deposited by simple bulk evaporation into tissue culture dishes. PolyHEMA is first dissolved in ethanol, and then the solution is added to a cell-culture dish. After spontaneous evaporation of ethanol from the solution due to its volatility, polyHEMA is left and forms a thin

film on the dish [116]. This method facilitates high throughput production of polyHEMA coatings, but it is unable to provide control for thickness or shape. As our single cell capture devices are composed of a patterned PDMS layer bonded to bottom glass substrate, we wish to coat and bond the glass substrate to facilitate non-adherent culture. Although polyHEMA has been used for suspension culture in bulk for more than 30 years, it has not been previously integrated with microfluidic technology due to two major challenges that arise with the conventional process. First, large surface roughness, resulting from the uncontrolled nature of the ethanol evaporation, will lead leads to poor bonding with the PDMS and induces severe leakage (Figure 73a). Second, due to the non-uniformity of film thickness, thicker polyHEMA coatings (~ 30 mm) are needed to prevent pinholes or openings in the coating where cells may adhere. These thick coatings are problematic as polyHEMA can absorb 50% water (w/w) and expand [117]. The expanded polyHEMA hydrogel can block the fluidic channel and degrade device performance and yield.

In order to overcome these issues, my colleague, Dr. Yu-Chih Chen, developed an alternative two-step process involving: spin coating and reflow. In our alternative process, polyHEMA (Sigma-aldrich, MO, USA) was dissolved at 60 mg/mL in 95% ethanol at 65°C overnight. 50 µL/cm^2 was pipetted onto a glass substrate and coated using a 2 step spin process (Solitec spinner): (1) 500 rpm for 10 second (spread), and (2) 1000 rpm for 60 second (spinning).

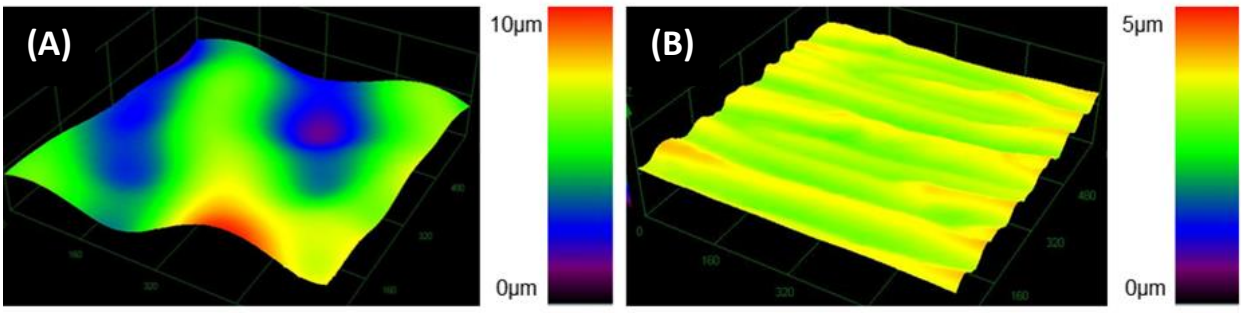

Figure 73: LEXT 3D surface profile of polyHEMA coated substrate fabricated by (A) conventional evaporation process or (B) spin coating and reflow process.

The thickness of polyHEMA layer can be precisely controlled by the spin speed. The spin-coating process was repeated twice to avoid any pinholes on the surface. Although the rapid spinning speed may result in quicker evaporation of ethanol, leaving possible hills and valleys along the radial direction, these issues can be alleviated by reflowing the polyHEMA film at an elevated temperature after spin coating (Figure 73b). As the glass transition temperature of polyHEMA is around 100°C, the polyHEMA film was reflowed at 150°C, below the burning temperature of polyHEMA (200°C) (Figure 74). The surface-roughness root-mean-square (RMS) of the conventional coating process is greater than 3 μm, while that of the spin-coated films is less than 0.2 μm. Compared to the conventional evaporation process, which generates high peaks and deep valleys, the thin and uniform polyHEMA films, created through the spin coating and reflow process, should reliably bond with the PDMS after oxygen plasma activation, creating a robust non-adherent culture environment within the microfluidic platform.

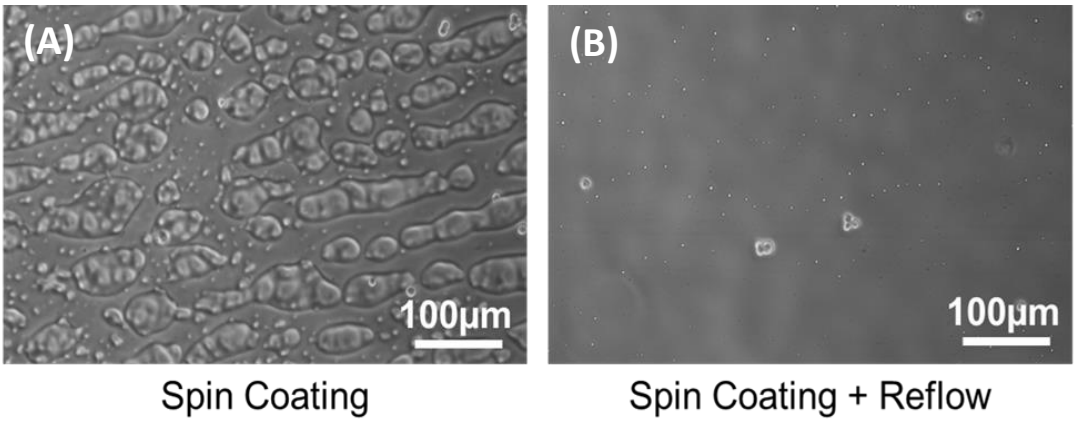

Figure 74: PolyHEMA spin-coated surface (A) with and (B) without reflow process.

After characterizing coating quality, suspension cell culture was then performed on polyHEMA coated surfaces (polystyrene cell culture dishes) to test coating performance. MDA-MB-231 breast cancer cells cultured for 24 hours on substrates without polyHEMA coating exhibited spreading morphology under brightfield microscopy (Figure 75). In contrast, MDA-MB-

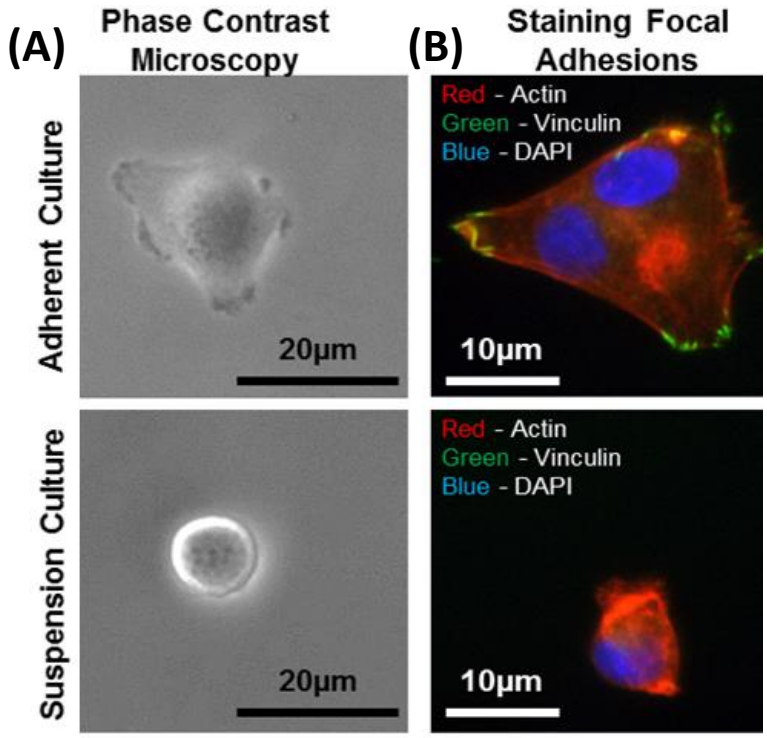

Figure 75: (A) Phase contrast and (B) fluorescent microscopy images of MDA-MB-231 cells that were cultured on non-coated or polyHEMA coated substrates to assess cell adhesion via morphology and focal adhesion staining.

231 cells cultured on the polyHEMA-coated surfaces did not seem to spread and cells maintained a rounded morphology under the same examination. In order to obtain a more objective measure of cell attachment, fluorescent staining of cellular focal adhesions was performed. Focal adhesions serve as the link between internal cytoskeletal networks and the ECM; thus, their absence may be a good indicator whether a cell is truly cultured in a suspension environment [118]. MDA-MB-231 cells were cultured to 50-60% confluence, trypsinized, seeded into 60 mm petri-dishes (polyHEMA coated and non-coated), and cultured for 24 hours. Millipore's Actin Cytoskeleton and Focal Adhesion Staining Kit (#FAK100) was used to stain actin (TRITC-conjugated Phalloidin), nucleus (DAPI), and anti-vinculin. For staining, cells were fixed with 4% paraformaldehyde in PBS for 15-20 minutes at room temperature. After washing, cells were permeabilized with 0.1% Triton X-100 in PBS for 5 minutes at room temperature, washed, and

then blocked with 3% BSA for 30 minutes. Cells were stained with anti-vinculin antibody at room temperature for 1 hour, washed in PBS, and simultaneously incubated with TRITC-conjugated phallodin and FITC conjugated secondary antibody. After washing, nuclei were stained with DAPI for 1-5 minutes at room temperature. Cells cultured on a normal tissue-culture plastic expressed distinct vinculin focal adhesion clusters, while cells cultured on polyHEMA-coated surfaces did not (Figure 75). No adherent cells or cells with distinct extracellular vinculin clusters were observed in the polyHEMA-coated dishes, confirming a robust non-adherent environment for sphere formation

This data together demonstrates our ability to fabricate uniform polyHEMA coatings that are suitable for microfluidic integration and robust suspension cell culture. However, another problem remains: PDMS cannot be bonded to polyHEMA through traditional microfabrication methodologies. In its pre-swelled state, compact polyHEMA coatings can be weakly bonded to PDMS via plasma oxygenation, but once water is introduced and a hydrogel is formed, all bond integrity is lost. Tape liftoff (placing tape to pattern the substrate prior to spinning polyHEMA) can provid an imprecise was to exclud polyHEMA coatings in certain areas, but resolution and margins are poor (~1 cm). A more precise methodology for polyHEMA patterning is required for successful patterning within microwells.

To this end, we developed a novel method for patterning PolyHEMA utilizing a variation of standard polydimethylsiloxane (PDMS) soft lithographic stamping. With this process, we have demonstrated precise micron-scale patterning of polyHEMA on both glass and polystyrene substrates, facilitating fabrication of large scale polyHEMA patterns for device integration. Using this process, we can also create cell culture arrays made from polyHEMA itself. These large-scale microwell arrays were used to capture and culture single SUM159 breast cancer cells in both

adherent and non-adherent environments. The unique chemical composition of polyHEMA allows its use in migration blocking, suspension culture, and even, if so desired, as a master for subsequent lithographic processing.

PDMS patterns were fabricated for soft lithographic **[33]** stamping of polyHEMA using a SU8 master, as shown in Figure 76a. Silicon wafers were Piranha cleaned and spun with SU8

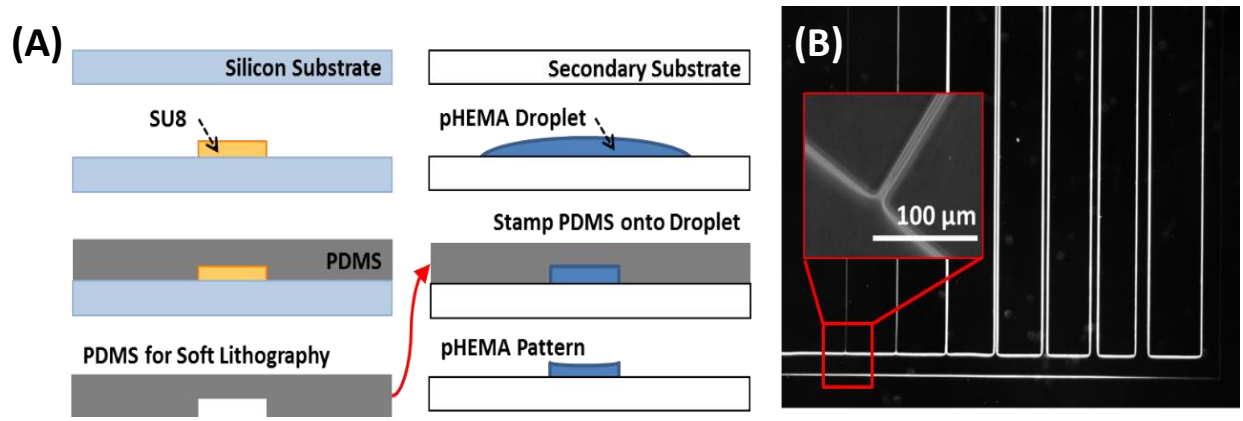

Figure 76: (A) Soft lithographic patterning process for polyHEMA structures and (B) example large- and small-feature fabrication.

(MicroChem) negative photoresist before they were patterned by UV-exposure and development. PDMS (10 to 1 ratio with curing agent) was poured over the mold, cured, and demolded to create the final PDMS lithographic stamp. 100µL of the polyHEMA (Sigma Aldrich) solution (60 mg/mL in 95% ethanol) was pipetted onto the secondary substrate (glass or polystyrene) and the PDMS stamp was pressed onto the droplet. This process excludes the excess polyHEMA, as the PDMS forms a tight seal with the secondary substrate due to the hydrophobicity of the PDMS stamp. This exclusion is especially important to achieve well-defined, highly-precise polyHEMA features (µm in resolution). As PDMS is gas permeable, it allows for evaporation of ethanol through the stamp, and thus deposition of solid cross-linked polyHEMA on to the substrate after stamping.

As shown in Figure 76b, PolyHEMA pattern sizes ranging from 2μm to 500μm have been successfully demonstrated with this process. Inset illustrates accurate small feature reproduction. Many factors affect the resulting PolyHEMA patterns. The shape of polyHEMA patterns will be solely determined by the PDMS stamp pattern itself. However, there are three factors (stamp channel height, stamping temperature, and stamping duration) that will affect the vertical aspects of the pattern. Stamp channel height alone does not dictate the resulting pattern height as a large portion of the volume in the channel (95%) is ethanol that will evaporate. In order to pattern 3μm thick polyHEMA, patterns of 30-40μm are required. By elevating the stamping temperature, we modulate the concavity of the deposited polyHEMA features. In order to deposit flat rectangular polyHEMA patterns, stamping temperatures must be kept below 50ºC and stamping time (to allow thorough ethanol evaporation) is increased.

When patterned, polyHEMA can also be used as a cell migration blocking structure. Fabricating polyHEMA cell migration blocking structures is quicker, cheaper, and easier compared to other methods such as etched trenches or tall-patterned photoresist walls. As a proof of concept, multiple polyHEMA structures were shown to prevent the migration of GFP-expressing MDA-MB-231 cells (Figure 77) despite proliferation and crowding. To test the migration blocks in microfluidic devices, we incorporated 3 μm-tall polyHEMA migration blocks into single cell capture microfluidic devices to prevent well-to-well migration. These migration blocks will allow us to maintain pure clonal colonies over long culture periods by restricting cell movement. These features were able to constrain cell growth without significantly disrupting gravity-driven flow in channels.

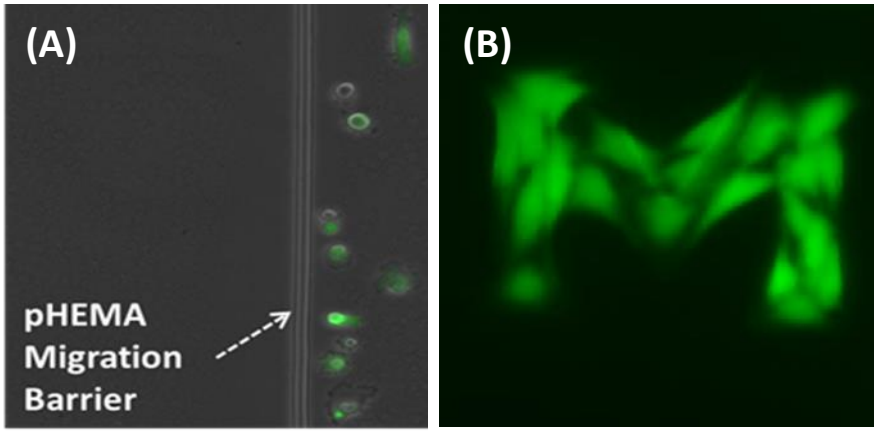

Figure 77: PolyHEMA structures preventing GFP-expressing MDA-MB-231 cells from in (A) linear blocking strcutures or (B) Michigan "M" patterns.

As our stamping process also provides us the ability to modulate feature concavity, we can create curved micropattern-features in a single stamping step by changing only stamping temperature. Arrays of concave polyHEMA microwells have been created by depositing polyHEMA at elevated temperatures (>50^{0}C), as shown in Figure 78. The thickness progressively increases from the center of the microwell toward edges due to wall-fluid interactions. Elevated temperatures increase ethanol evaporation rates, so that only thin layers are deposited in the center

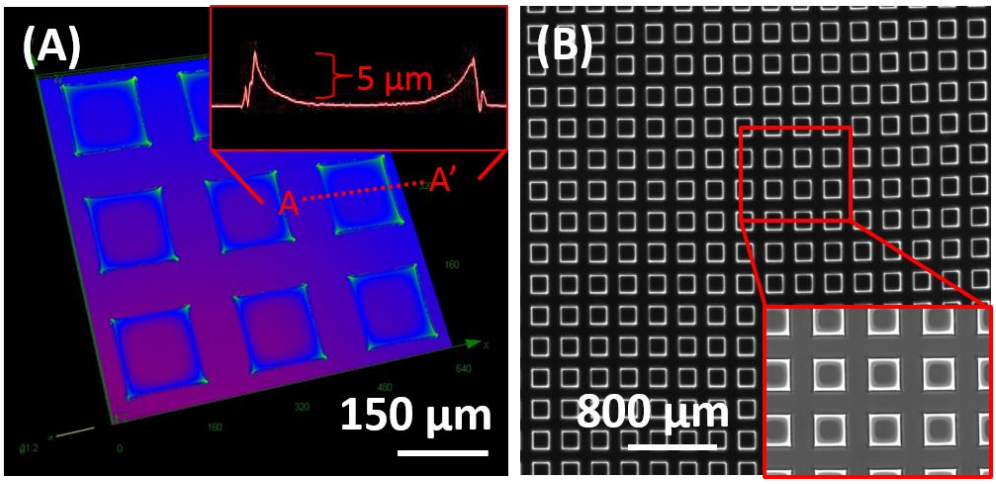

Figure 78: (A) LEXT laser interferometer image of concave polyHEMA microwell structures and (B) phase contrast microscope image of large scale (~2,000) polyHEMA microwell arrays.

of the stamp feature and the rest of the polyHEMA is pulled towards the walls of the PMDS stamp. This effect is even more pronounced at increased temperatures (>80^{0}C), resulting in complete depletion of polyHEMA at the center of the fabricated wells. By stamping at two temperatures with the same pattern, we created arrays (Figure 78, Figure 79) of >2,000 adherent (exposed glass) or non-adherent (concave polyHEMA) microwells. Single SUM159 cancer cells were seeded into the microwells through gravity settling (Figure 79a) and suspension concentration control, where they grew into adherent colonies (Figure 79b) or spheroids (Figure 79c), depending on the microwell architecture. This settling procedure is probabilistic, but with enough wells (>2,000 in our case) sufficient numbers of single cells are captured in individual microwells80. Residual cells can be easily removed through gentle washing. These high-throughput arrays are extremely simple and inexpensive to fabricate and thus useful in a variety of cell culture assays (e.g. single cell phenotyping, clonal analysis, spheroid drug assays). However, in our application, their utility is limited due to the probabilistic loading procedure. In both our adherent and suspension culture applications, cell numbers are limited due to availability of primary patient samples and the rarity

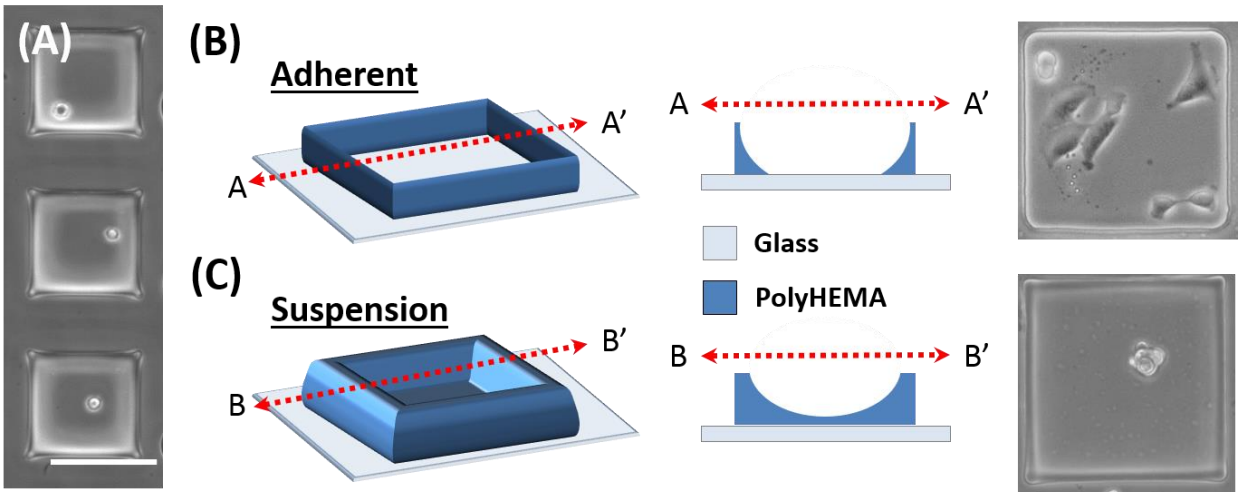

Figure 79: (A) Loading of single SUM159 cells into polyHEMA microwells. Schematic representations of two microwell designs and example clonal culture in each: (B) adherent and (C) suspension polyHEMA microwells .

of certain subtypes of interest (such as CSC). As a result in the long term, an active capture scheme with greater single cell capture efficiency and rates is more desirable.

In aqueous environments, polyHEMA absorbs water and a hydroxyethyl side turns outward, facilitating flexibility, swelling of the polymer chains, and becomes a non-adherent surface. However prior to wetting, a non-polar methyl group is turned outward, making the deposited polyHEMA hard and compact. Due to the unique geometries that we can achieve via temperature controlled stamping, polyHEMA also has utility in its non-polar dry state. Dry polyHEMA can serve as a reusable master for further PDMS lithography (Figure 80). This approach has several distinct advantages. First, the chemical properties of dry polyHEMA facilitate de-molding of small PDMS features without any silanization. This is important for culture applications with sensitive cells (such as single cell culture or primary cells directly from patients), where the residual silane decreases viability. As discussed, by controlling stamping temperature, we can create concave features in the deposited polyHEMA. These can be used to

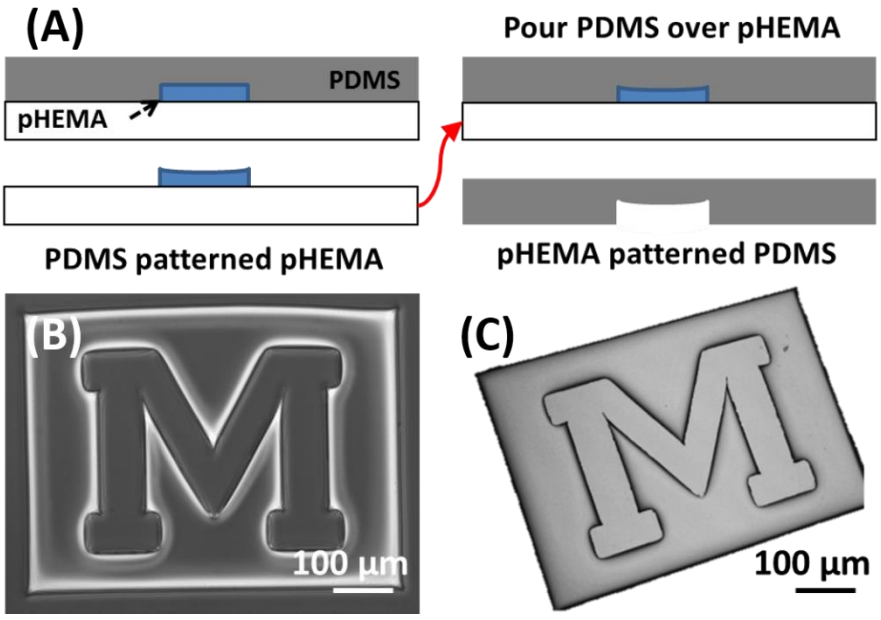

Figure 80: (A) Fabrication of novel PDMS structures from a polyHEMA master with (B) bright-field image of polyHEMA-cast PDMS and (C) LEXT laser interferometer image of PDMS molded from polyHEMA master.

fabricate a variety of novel concave and convex features in the secondary PDMS molds. These types of features, useful in microfluidic valves, pumps, and even microlenses, are often difficult to create with standard microfabrication technologies, but here they can be created in a single step.

PolyHEMA is a versatile polymer and hydrogel, and we have demonstrated methodologies to create robust spin-coated surfaces and unique micropatterned features. Combined with our topographically-patterned PDMS surfaces, we have created several surface patterning methods for on-chip suspension culture, each with their own advantages. Hydrophobic topographically-patterned PDMS surfaces provide a long term, chemical-free approach for suspension culture, but are expensive to fabricate and obscure optical imaging. Spin-coated or stamped polyHEMA patterns are inexpensive to fabricate, but introduce chemical surface modifications and require more precise control of fabrication parameters to achieve robust suspension culture. These various characteristics can be leveraged when required by the biological needs of the target assays. Initial single cell-derived sphere formation testing was performed with patterned PDMS surfaces. But once it was determined that the results from polyHEMA patterns matched well with those observed from PDMS (no apparent chemical disruption), the rest of the work for suspension culture in the following chapter was performed with polyHEMA coated devices.

Chapter 4: Single Cell-Derived Sphere Formation for CSC Analysis

Targeted therapy looks to be a promising addition to the currently standing cancer treatment triumvirate (surgery, chemotherapy, and radiation) due to the growing body of literature showing the importance of cancer cell heterogeneity and rare cell subpopulations [11, 119, 13] Targeting specific cell subtypes, CSC in particular, has great potential for therapeutics [13, 28, 29]. By eliminating CSC or other initiating cells through targeted therapy, we may cause natural cancer regression through loss of growth potential. Without targeted therapy, cancer relapse will occur through CSC division and proliferation [6]. Sadly, this presents a problem as this heterogeneity is still poorly understood and identification of CSC is no easy task. These cells are often identified using cell surface markers (CD133, CD44, CD24, etc.) and assays for enzymatic activity (Aldeflour). However in many cancers, there is considerable evidence that several subpopulations of stem like cells may exist within one tumor, and that their identification would require the use of many cell markers in combination with other identifying characteristics [120, 121]. Certain characteristics markers that denote "stemness" in one type of cell may be absent in another [122]. There is a great need for marker-free, simple, user-friendly methods to screen heterogeneous CSC behavior in a large number of cells.

4.1 Mammosphere Assays and CSC Identification

First utilized for the identification of neurostem cells, in vitro sphere formation assays have also been suggested as a marker-free methodology for culture and identification of mammary cancer stem-like cells [21, 100, 101]. At their most basic level, these are anoikis (a Greek

neologism meaning “the state of being without a home”) based assays. For normal cells, adhesion to the extracellular matrix (ECM) is essential to maintain cellular homeostasis, and disruption of cell attachment leads to anoikis, a form of programmed cell death [97]. While there are numerous

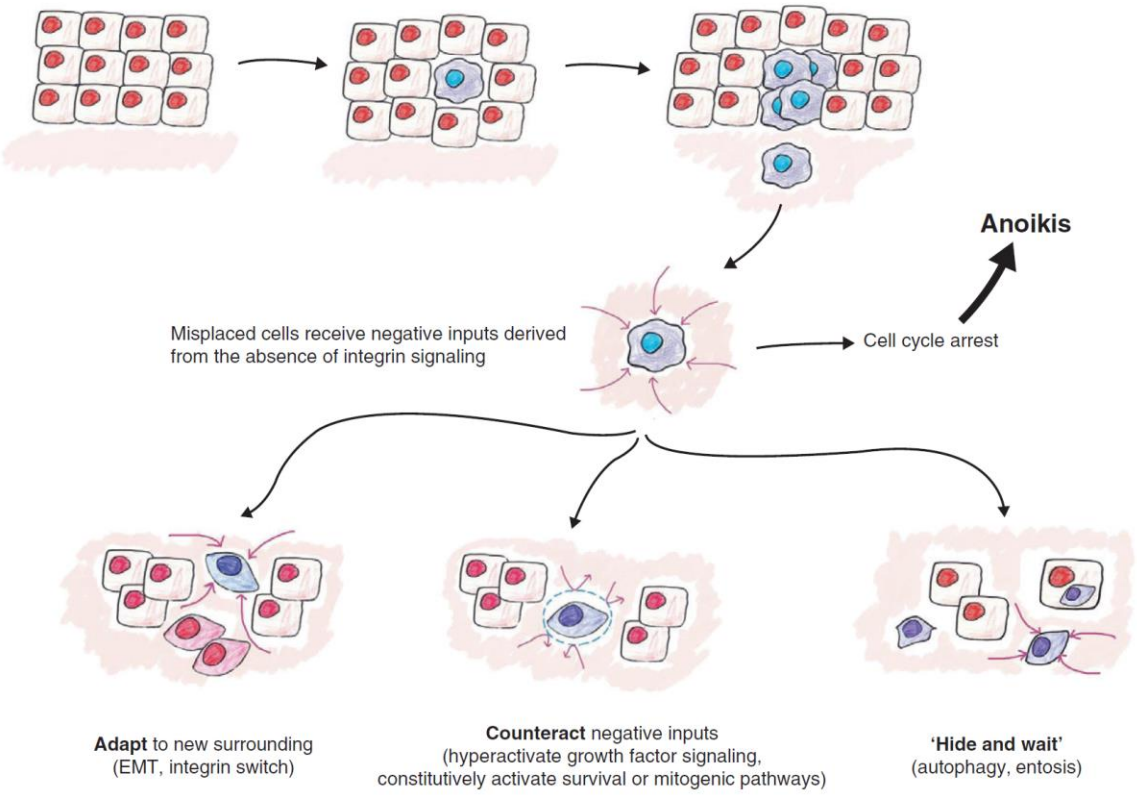

Figure 81: When bulk tumor cells detach from the matrix, signals encourage anoikis, but CSCs have many strategies (such as EMT, integrin switching, hyperactive growth, or quiescence) to compensate for or circumvent anoikis signals (Guadamillas, 2011).

mechanisms that can be involved in resistance to anoikis (Figure 81) [123], it has been shown that when breast cancer cells are cultured in suspension, bulk non-stem cells undergo anoikis, while only stem-like cells survive and proliferate to form spheres. Stem-like cells are anoikis resistant and capable differentiation. As such, the formation of these mammospheres can be used to identify cells with these stem-like characteristics, and serial sphere formation can be used to enrich for CSC within a population (Figure 82).

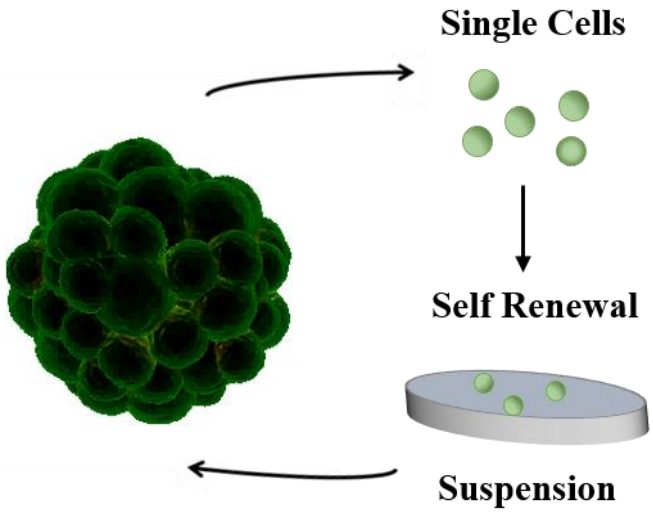

Figure 82: Single cell-derived mammospheres approach for CSC identification and enrichment.

In practice, there are a number of issues hindering the utility of these assays [124]. For proper selection, cell aggregation must be prevented, so that anchorage dependent cells cannot adhere together to survive and proliferate. In conventional culture methods, such as dishes or plates, cell seeding density must be expertly controlled. Many laboratories utilize fluorescent activated cell sorting tools to assist in single cell deployment and density control, but cellular stains are required with a priori knowledge of markers. This process also greatly affects cell viability and has a high seed rate error. In many cases, density control does not even solve the problem. Even with proper methodology it has been reported that many mammospheres are not single cell derived, but in fact, aggregation of the seeded cells [125, 126]. Although anti-aggregation additives (e.g. Heparin) can be used to mitigate this, cell behavior can be significantly affected [127]. In conventional culture platforms, reliable media exchange can also be a problem. Cells can be easily lost or disrupted when replacing the media; as a result, the duration of the assay is limited by nutrient depletion and waste buildup. Finally, studies performed in neurospheres (the neuronal mammosphere analog) suggest intermediate progenitor cells may also form spheres, but with

different proliferation rates. Only looking at sphere formation rates alone may result in overestimated CSC frequency [128, 129]. Robust single cell-derived sphere formation, tracking, and downstream sphere analysis are needed to identify and study potential CSC in mammosphere assays, and a microfluidic approach is ideal to address these needs.

There are a number of microfluidic approaches for performing sphere assays on-chip, including hanging droplet methods [130, 131, 132] that have greatly increased assay throughput and micro-rotation flow [133]. But these platforms accomplished sphere formation mostly through cell aggregation, rather than single cell growth as required for mammosphere-based CSC identification (Figure 83). While droplet-based and two-phase systems can isolate single cells in

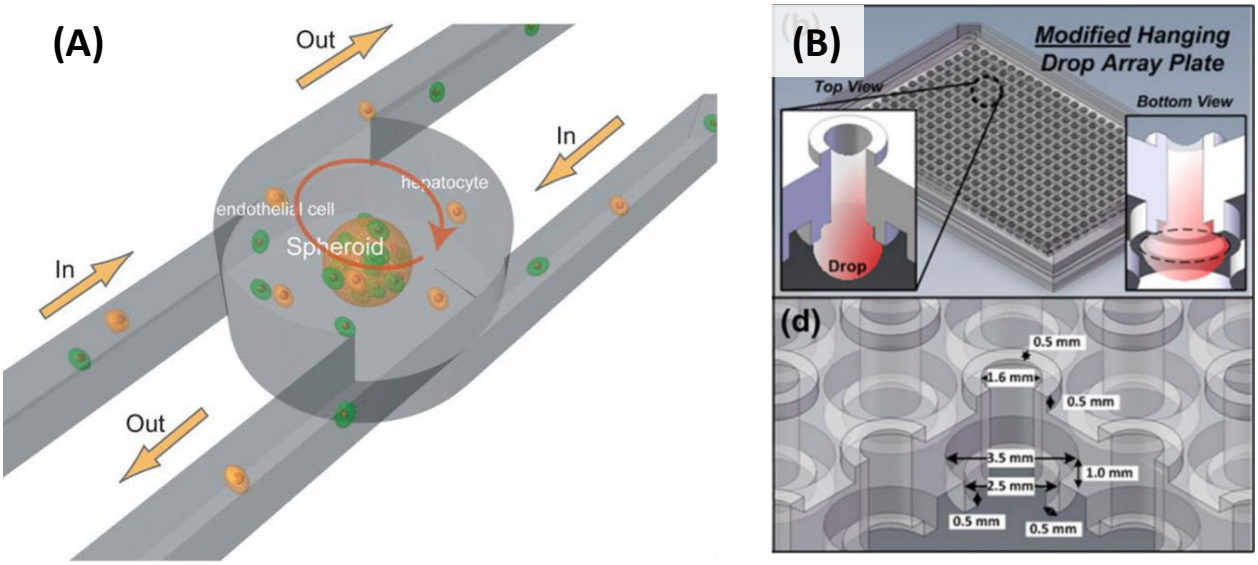

Figure 83: Example microfluidic platforms for on-chip sphere formation using (A) micro-rotational flow to aggregate cells of multiple types via intersecting flow paths** [133] **and (B) droplet aggregation in a high throughput microfluidic hanging drop approach** [130]**.

suspension, it is difficult to continuously provide fresh media to each droplet, preventing long term culture [134]. Methods for on-chip mammosphere formation must provide reliable and scalable single cell capture, robust long-term (>2 weeks) culture, and continuous media perfusion in order to facilitate successful single cell derived sphere formation. The robust single cell capture platform

demonstrated and validated in Chapter 2 is capable of addressing each of these requirements, when integrated with the novel surface modification techniques for on-chip suspension culture from Chapter 3. These devices will help dimish the issues surrounding reliable mammosphere formation and help more widespread adoption of this assay for CSC identification.

4.2 Single Cell-Derived Spheres

In our initial implementation, topographically patterned PDMS hydrophobic honeycomb surfaces were integrated in our 64-well single cell capture device. A critical step in our surface fabrication is actually the demolding of the PDMS patterns from the DRIE patterned silicon master. As a result of the small feature size and thermal expansion that occurs during PDMS curing, it is not trivial to pull the PDMS microstructures from the mold without tearing the surface. If the surface is torn, it cannot be properly bonded to the channel layer due to non-uniformities, and suspension culture will not be achieved where patterns have been damaged. If the topographical patterns are formed on a thick layer of PDMS, these problems are exacerbated as there is not enough flexibility in the thicker PDMS to facilitate pulling the patterns from the mold without breaking the silicon. As such when integrating honeycomb patterns, DRIE patterned masters were spin-coated with PDMS rather than having PDMS poured directly onto the mold. PDMS was mixed in a 10:1 ratio with the curing agent (Slygard, Dow Corning) and degassed. Wafers were ramped to 500 rpm within 15 seconds to spread the PDMS and then spun at 1000 rpm for 60 seconds, resulting in ~150μm PDMS layers. Thin layers were more easily peeled from the substrate, releasing intact micropatterns though care still needed to be taken to not rip the thin PDMS. These thin patterns could not be directly integrated with the channel layers due to their obvious fragility, so they were cut and placed on a glass microscope slide as support. Non-covalent

forces were enough to robustly adhere the thin PDMS to the glass slide, so oxygen plasma treatment was not performed. This conveniently allowed repositioning of the pattern if it was initially wrongly positioned. Afterwards, the patterned PDMS on a glass slide support layer was treated with oxygen plasma and bonded to the single cell capture channel layer.

After integration, suspensions of SUM159 breast cancer cells were loaded into the device using the methods previously described. Briefly, cells were harvested from a petri-dish with 0.05% Trypsin/EDTA and centrifuged. Cells were then re-suspended at $0.5x10^6$cells/mL in culture media, and 100 µL of the cell solution was injected into the inlet of device. Within 5 minutes, the cells were hydrodynamically captured, and the cell solution was replaced with cell-free culture media. Due to the robust hydrodynamic capture mechanism, single cell capture was not disrupted by the surface patterns and greater than 90% of the 64 microwells captured single cells (Figure 84). SUM159 cells were then cultured for 10 days in serum-free MEBM (Lonza, Allendale, NJ)

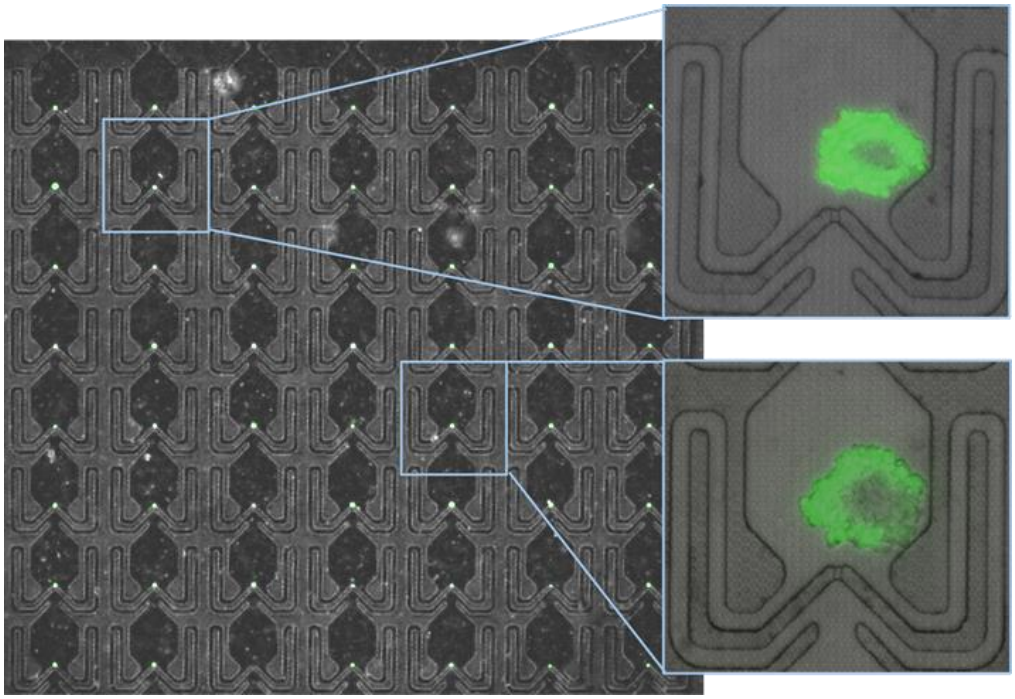

Figure 84: Single cell capture and sphere formation after 10 days from SUM159 (Cell Tracker Green) breast cancer cells in the microfluidic platform with the patterned PDMS on the bottom surface.

supplemented with B27, 20 ng/ml bFGF, 20 ng/ml EGF, 5 ug/mL insulin, 1 mM lipid concentrate (Invitrogen), 1 ug/mL hydrocortisone, 100uM mercaptoethanol, 10uM cholesterol, and 1% penicillin/streptomycin, and sphere formation was observed (Figure 84 inserts). To our knowledge, this is the first microfluidic chip that has shown successful clonal (**single cell derived**) sphere formation. It is also the first demonstration of sphere culture with topographically patterned PDMS substrates. Sphere rates obtained utilizing our platform for SUM159 breast cancer cells were quite comparable to those obtain with a serial dilution method (~54%) (Table 6). Claudin-low SUM159 cells are known to have a large progenitor cell pool, resulting in higher sphere formation than average. So while mammosphere assays with SUM159 cells may overestimate the stem-cell pool and be less biologically relevant, SUM159 cells are useful for device characterization and debugging due to their high sphere rates.

For further characterization, one Luminal A and another Claudin-low basal cancer line were selected (MCF-7 and MDA-MB-231, respectively). After loading and culture in the same conditions, mammosphere formation rates for these lines were calculated (Table 6). These values match more accurately with the cancer stem-like cell pool expected.

Due to the low sphere formation rates expected (a few percent), we wish to increase the throughput of our mammosphere assays, so that more spheres could be observed and statistically

Table 6: Single cell-derived sphere formation rates of breast cancer cell lines on topographically patterned PDMS.

Cell Lines	Sphere Formation Rate (%)
SUM159	54.69%
MCF-7	3.45%
MDA-MB-231	1.28%

significant observations could be made. With our topographically patterned PDMS surfaces, however, this is problematic. Cell Tracker dyes were used for cell and sphere visualization as the patterns obstruct or obscure brightfield images of the microwells, but it is not ideal to require stains for visualization. Complicated assay and staining protocols may affect cell behavior and sphere formation. So in order to better visualize and image spheres, simplify assay protocols, and reduce cost, we moved to our alternative polyHEMA patterning method developed by Dr. Yu-Chih Chen, presented in Chapter 3.3. Glass microscope slides were patterned with polyHEMA via the methods previously described and bonded to form 1,024 high throughput single cell capture devices (Figure

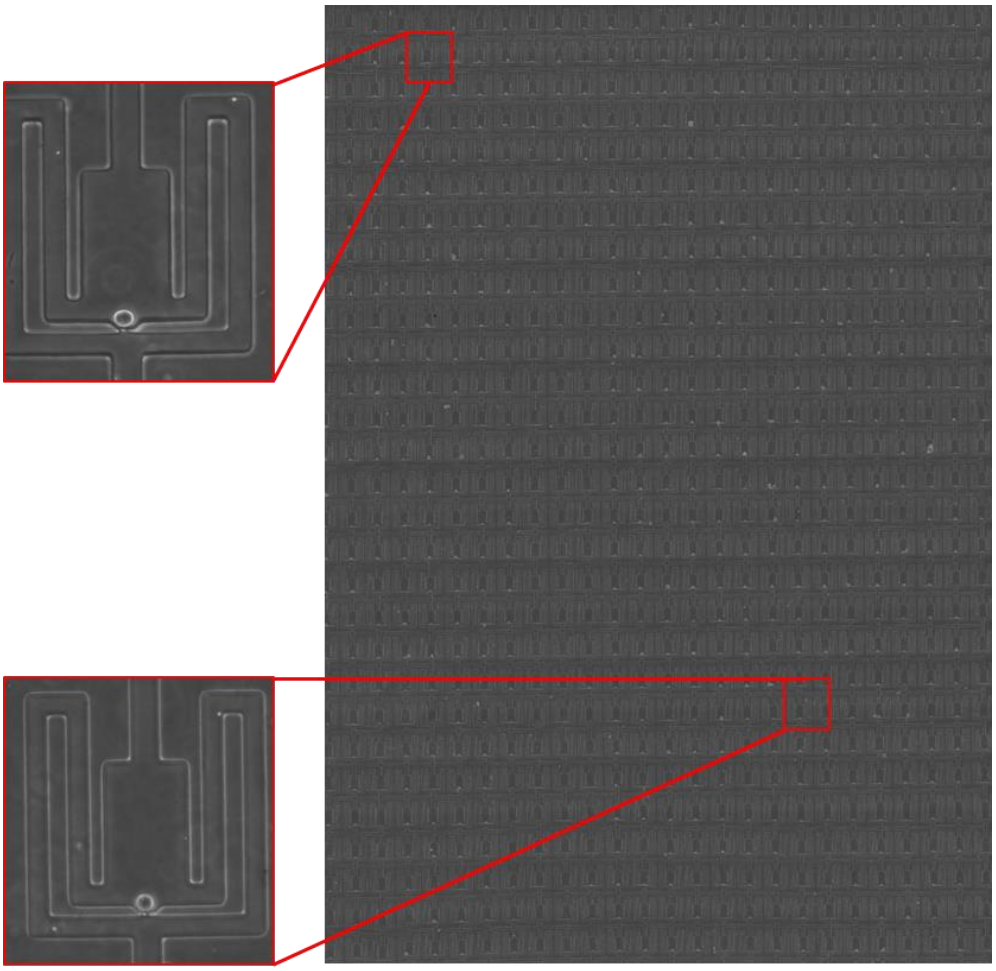

Figure 85: High throughput single cell device integrated with polyHEMA coating with captured T47D single cells.

85). With these devices, we can overcome many of the current issues with single cell derived mammosphere assays by improving single cell seeding and control and throughput (needed due to the rarity of CSC and low sphere formation rates).

First, Dr. Chen and I wished to confirm similar performance as our topographically patterned approach, as different sphere formation rates in SUM159, MCF-7, and MDA-MB-231 may indicate issues with our assay. After loading and culture on-chip, successful sphere formation was observed and sphere formation rates were recorded (Table 7). Sphere formation rates in SUM159 (55.4% polyHEMA vs. 54.7% patterned), MCF-7 (3.1% polyHEMA vs. 3.45% patterned), and MDA-MB-231 (1.4% polyHEMA vs. 1.28% patterned) were comparable between the two approaches. The polyHEMA approach, however, afforded increased throughput (16 times), allowing us to see statistically significant variations from the spheres as well. Differences in the sphere formations between the two approaches fall with

Additional cell lines were tested with our high throughput platform including T47D (Luminal A breast cancer line), SUM149 (inflammatory breast cancer line), and HCC38 (Claudin low basal cancer line). Compared to SUM159 cells, other lines have lower-sphere-forming

Table 7: Single cell-derived sphere formation rates of breast cancer cell lines and breast cancer derived PDX samples using polyHEMA coated single cell platform

Cell Lines	Sphere Formation Rate (%)	PDXs	Sphere Formation Rate (%)
SUM159	55.4±6.8	**PDX# 2147**	1.8±1.3
MCF-7	3.1±2.5		
T47D	2.8±1.1	**PDX# VARI068**	0.8±0.6
SUM149	1.8±0.8		
HCC38	1.2±0.8		
MDA-231	1.4±0.6		

potential (Table 7) and result in overall smaller spheres. Images of example spheres in the polyHEMA coated high throughput microfluidic device for SUM159, T47D, MCF7, and MDA-MB-231 cells are shown in Figure 86.

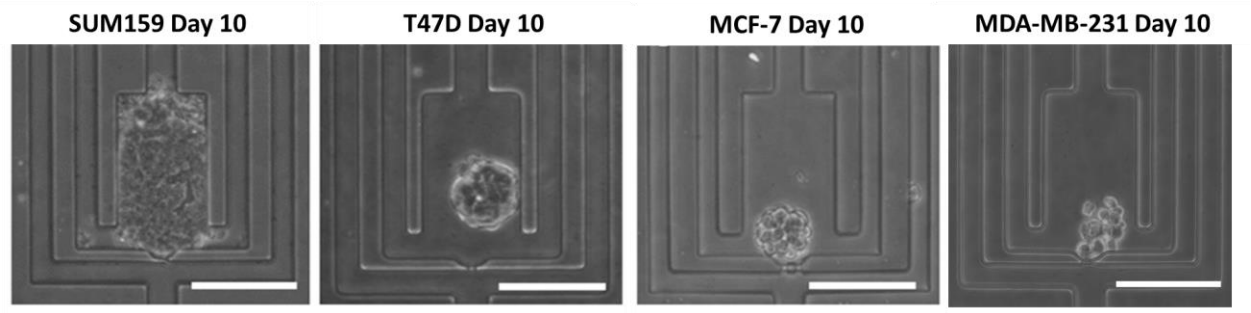

Figure 86: Example sphere formation from four separate breast cancer cell lines (SUM159, T47D, MCF-7, and MDA-MB-231).

In addition to cell lines, single cells from breast cancer patient derived xenografts (PDX) were tested in the platform. While not still not as clinically relevant as a true primary tumor biopsy, PDXs conserve original tumor heterogeneity, molecular signals, and phenotypes, making them ideal for our application [135]. PDXs were prepared and sorted by our collaborator, Dr. Sean McDermott, in the laboratory of Dr. Max S. Wicha with the protocol as follows. Female NOD/SCID mice, 4-8 weeks old, were prepared for surgery the day before injection by using Nair exfoliant to remove hair around the incision site. Mice were anesthetized using isoflurane inhalation with a vaporizer. The incision site was disinfected with betadine and a midline incision was made between the fourth and fifth nipples and then angled toward the nipples. The skin was loosened from the body wall. Patient-derived xenograft (PDX) breast cancer cells (VB, 2147, VARI-068) were suspended in 50μL of 1:1 DMEM:Matrigel (BD Biosciences) and injected into the inguinal fat pad using a syringe with 18 gauge needle. The skin was secured with 9mm wound clips and clips removed after 7-10 days.

After time for tumor growth, PDX-bearing mice with ~1cm diameter tumors were euthanized by CO2 asphyxiation. Tumors in the inguinal mammary fat pad were excised, weighed, and <1g tumor in 60mm dish was minced with a razor blade to <2mm pieces. Minced tumor was transferred to a C-tube (Miltenyi Biotec, Auburn, CA) and digested with the Human Tumor Dissociation Kit (Miltenyi Biotec) following the manufacturer instructions. Briefly, each C-tube contained 4.7mL RPMI-1640 media, 200µL reagent H, 100µL reagent R, and 25µL reagent A. Tumors were digested on the gentleMACS Octo Dissociator with heating elements for 1hr using the medium tumor setting. Following digestion, 10mL of RPMI-1640 was added to each C-tube, filtered through a 70µm strainer (Corning) into a 50mL conical, and the C-tube rinsed with 10mL RPMI-1640. Samples were centrifuged at 337g for 10min at 4C. Pellets were suspended in 10mL RPMI-1640, filtered through a 40µm strainer (Corning), and combined with 10mL rinse of 50mL tube. Samples were counted on Luna FL (Logos Biosystems, Annandale, VA) using AO/PI and manufacturer instructions. Samples were depleted of mouse cells using the Mouse Cell Depletion Kit (Miltenyi Biotec). Briefly, $1x10^6$ cells were suspended in PBS/0.5% BSA, centrifuged at 337g for 5min at 4C, and suspended in 80µL PBS/0.5% BSA. 20µL of the mouse cell depletion cocktail was added and incubated 15min in the refrigerator. While incubating, a LS column (Miltenyi Biotec) was equilibrated on a MultiMACS Cell24 Separator Plus (Miltenyi Biotec) with 3x1000µL PBS/0.5% BSA. Following 15min incubation, 400µL PBS/0.5% BSA was added to each sample. The 500µL sample was applied to the LS column and the flow through collected in 5mL FACS tube (Corning). LS columns were washed 3 times with 1000µL PBS/0.5% BSA and collected into same 5mL FACS tube. Samples were centrifuged at 337g for 5min at 4C, suspended in 5-10mL PBS/0.5% BSA, and counted on Luna FL using AO/PI. These methods produced healthier mouse cell free PDX samples

After the final sorting step, PDX samples were loaded on chip and cultured in supplemented MEBM media. Two separate PDXs successfully formed spheres on chip (Figure 87), showing a slightly lower sphere formation rate as compared to the tested cell lines (Table 7). Though slower growing, PDXs were easy to culture for a longer period in our device to observe sphere formation. With definite single sphere spatial confinement and continuous media perfusion supplied by the gravity flow, the PDXs were continuously monitored over 28 days (Figure 87).

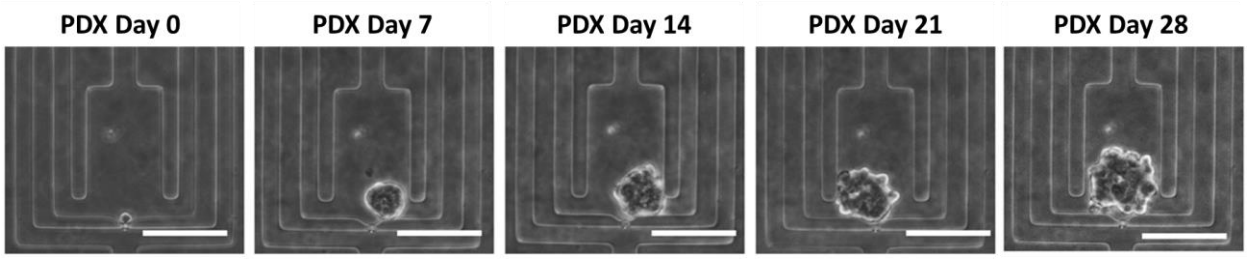

Figure 87: 4 week sphere formation from single patient derived xenograft cells.

For good measure, 3 additional non-breast cancer cell lines (A549 human alveolar adenocarcinomic, SKOV3 human ovary adenocarcinoma, and C6 rat glioma) were assayed on chip to assess their sphere formation potential (Table 8). These experiments demonstrated our capacity to perform high-throughput and robust single cell sphere formation assays with a wide variety of cell types and even models of primary breast cancer cells

Table 8: Single cell-derived sphere formation rates of non-breast cancer cell lines

Cell Lines	Sphere Formation Rate (%)
A549	0.6±0.3
SKOV3	2.3±2.1
C6	2.6±2.1

4.3 Heterogeneity of Single Cell Sphere Formation

A major advantage of our single cell mammosphere assays is the ability to enumerate CSCs independent of cell surface markers. Marker-based identification of CSCs is challenging, as certain characteristics markers, that denote "stemness" in one type of cell, may be absent in another [122]. There is also considerable evidence that several subpopulations of stem-like cells may exist within one tumor that may each express different cell surface markers. Their identification and separation would require the use of many cell markers in combination with other identifying characteristics [120, 121]. More recently, Liu et al [136] reported two important distinct CSC populations in breast cancer, where plasticity existed to allow transitions between the populations. CSC were reported to transition between epithelial and mesenchymal states, reflective of their normal stem cell counterparts. Mesenchymal-like (epithelial-mesenchymal transition [EMT]) CSC are identified as CD24- CD44+. They are primarily quiescent and localized at the tumor invasive front. Epithelial-like (mesenchymal-epithelial transition [MET]) CSC, on the other hand, express ALDH, are proliferative, and are located more centrally within tumors. As such, it will be interesting to examine the single cell sphere formation potential of these independent CSC states to observe whether mammosphere assays select for particular types of CSC. T47D breast cancer cells were stained and FACS sorted into 3 separate populations: ALDH+, CD44+/CD24-, and bulk tumor. Each population was loaded into devices, and their resulting sphere formation rates were observed (Figure 88). ALDH+ T47D cells exhibit significantly higher sphere formation potential as compared to CD44+/CD24- or bulk T47D. This is not unexpected, because ALDH+ CSCs are associated with extensive proliferation. ALDH+ were also shown to have greater potential for self-renewal and multilineage differentiation capacity [136], so successful sphere formation is expected. What is unexpected, however, is greater sphere formation in the bulk population as

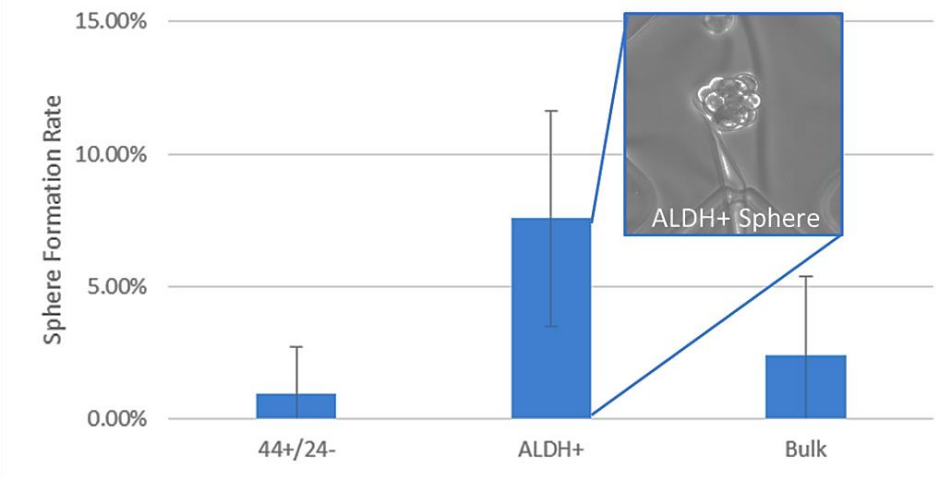

Figure 88: Sphere formation rates of ALDH+ and 44+/24- breast cancer stem-like cells from T47D cell lines.

compared to CD44+/24- CSCs. It may be possible that there is a contaminating CD44+/24- or ALDH+ population in the FACS sort. Post loading staining was not performed to verify state (as was done in the case of investigating ovarian CSCs) prior to sphere formation, as staining directly after loading was shown to negatively impact cell viability. To overcome this or prevent this in the future, double FACS sorting may be needed.

Alternatively, this may be a result of the CD44+/24- cell's supposed quiescence, but our collaborators have reported that in adherent culture, CD44+/CD24- form robust colonies. In order to ensure that culture conditions or cell viability issues were not the source, adherent and suspension culture were performed on the same device for CD44+/CD24- cells. Patterning of polyHEMA facilitates precise spatial localization of suspension culture environments. A subset of microwells on the glass slide were patterned for suspension culture while others remained uncoated and were utilized for adherent culture, facilitating easy side by side comparison in the same chip and removing issues of device-device variation. It was observed that adherent culture greatly resuscitated CD44+/24- growth potential. 14% of seeded adherent CD44+/24- cells grew into colonies, while only 3% showed sphere formation potential with the same device, indicating that

the observed results accurately represent sphere formation potentials in ALDH+ and CD44+/24- populations. However, the biological reason for these results is still not clear. To further investigate the relationship between conventional 'stemness' markers and sphere formation potential, we also examined Notch, which has been suggested to identify yet another population of cancer cells with stem cell activity [137].

There are considerable similarities between healthy stem cells and cancer stem-like cells. In particular, canonical stem cell pathways such as Wnt and Notch have been shown to be critical for the regulation CSC behaviors (e.g. survival and self-renewal) [138]. In fact, high Notch expressing cells have been shown to possess higher tumor initiating potential [139, 140]. Correlating Notch expression with mammosphere formation in our microfluidic assay could provide more insight into the overall assay utility and Notch signaling in CSC. To monitor Notch pathway activation, our collaborators in the lab of Dr. Max Wicha transduced T47D cells with a lentiviral (pGreenFire1) Notch reporter. This reporter contaied multiple Notch response elements upstream of a minimal CMV promoter, regulating destabilized GFP. Lentiviruses were prepared using 3rd generation helper plasmids to generate VSVG pseudotyped particles (roughly $1x10^7$ units/mL) by the University of Michigan Vector Core. 500,000 T47D breast cancer cells/well ($50,000/cm^2$) were plated in a 6-well plate, transduced the following day at a MOI of 10 for 24hr. Transduction efficiency was ~90% at 1 week post transduction based on FACS analysis of eGFP from cells transduced with pGreenFire-CMV. GFP+ cells were collected by flow cytometry sorting using a MoFlo Astrios cytometer to insure all cells contain the lentiviral vector. Following cell culture, GFP- (Notch-) cells were generated from GFP+ (Notch+) cells after reaching equilibrium.

To measure single cell sphere formation from Notch+ and Notch- T47D cells, we loaded unsorted cells into suspension microfluidic chips and cultured them in serum-free media as

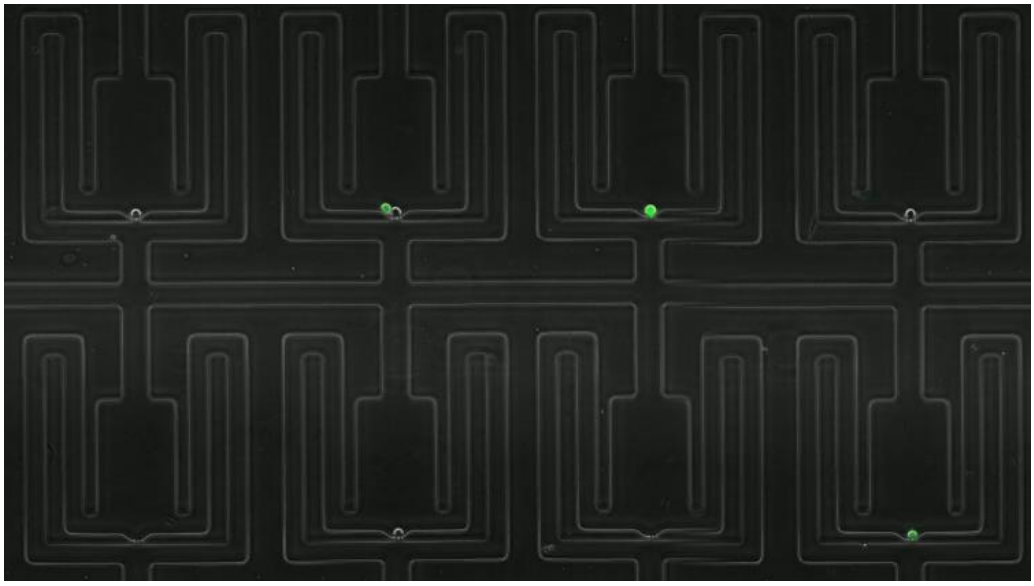

Figure 89: Capture of heterogeneous T47D Notch (Notch+, GFP Green) cells in integrated high throughput platform.

previously reported. Despite the heterogeneous population with only two populations of interest, no pre-sorting is necessary due to the robust single cell capture and large throughput of the platform Figure 89). After culture for 14 days, both Notch+ and Notch- T47D cells formed spheres (Figure 90), but the average size of Notch+ cell spheres was significantly higher. The sphere formation rate of Notch+ cells was also significantly higher (Figure 90). Additionally, spheres formed from Notch- cells contained no Notch+ cells, while spheres formed from Notch+ cells contained both. Much like as was observed with higher bulk sphere formation with CD44+/CD24-, the ability of Notch- cells to form spheres is surprising, as the absence of Notch suggests that the source cell is likely not stem-like. However, Notch- cells forming smaller and less frequent spheres may confirm a previously mentioned complication for mammosphere CSC asssays: progeneitor cell sphere formation. This highlights the needs for our assay (and mammosphere assays in general) to facilitate continuous cell tracking and further downstream analysis as well. Genetic expression analysis of the spheres will provide a way to differentiate progenitor derived spheres and true stem-like cell derived spheres.

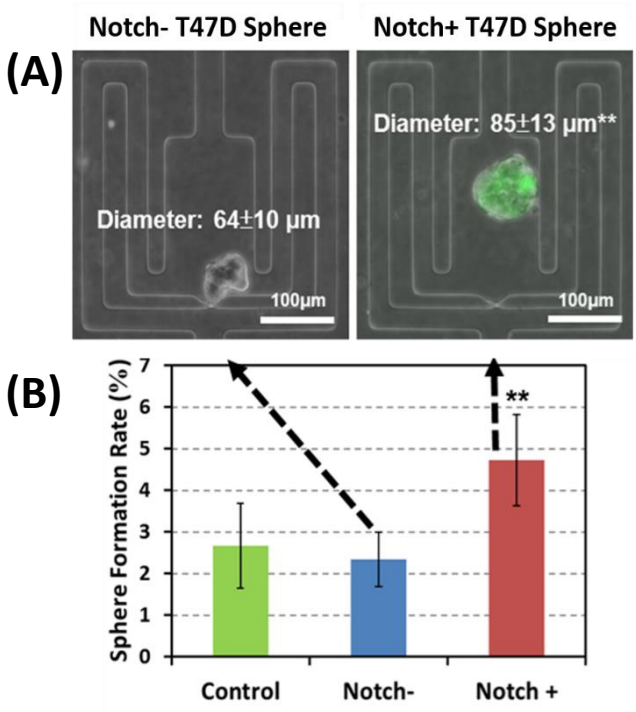

Figure 90: Differential cancer sphere formation from Notch+ and Notch- T47D cells was observed after 14 days with Notch+ cells forming spheres with (A) larger average size and (B) more spheres compared with Notch- cells.

Fortunately, polyHEMA fabrication facilitates simple sphere retrieval after assays are performed. Though spin coating and reflow of polyHEMA coatings improves the bonding between the substrate and the top patterned PDMS layer, the bond strength between polyHEMA and PDMS is still weaker as compared to PDMS-PDMS or PDMS-glass bonding. Consequently, to retrieve the spheres, the top layer can be peeled off over a culture substrate, releasing the spheres inside. For Notch+ and Notch- sphere comparisons, single cell-derived spheres were formed on-chip and cultured as normal. The spheres were retrieved and placed in a polyHEMA coated non-adherent 384-well plate (Figure 91). At the time of sphere retrieval, there is no risk of non-sphere forming cells contaminating the retrieved sample, as the non-adherent environment has induced anoikis and death. After anoikis, non-sphere forming cells remnants can be washed out of the arrays by the gentle perfusion flow. The microwell dimensions limit the size that the spheres can grow to on chip, and a larger pool of cells is needed for use with the Fluidigm C1 and Biomark HD for

multiplexed single cell genetic expression analysis. So, the single cell-derived sphere were kept and grown in the non-adherent well for an additional 2 weeks, providing sufficient cell numbers for single cell gene expression analysis.

Two spheres of interest (one Notch+ derived and one Notch- derived) were dissociated into

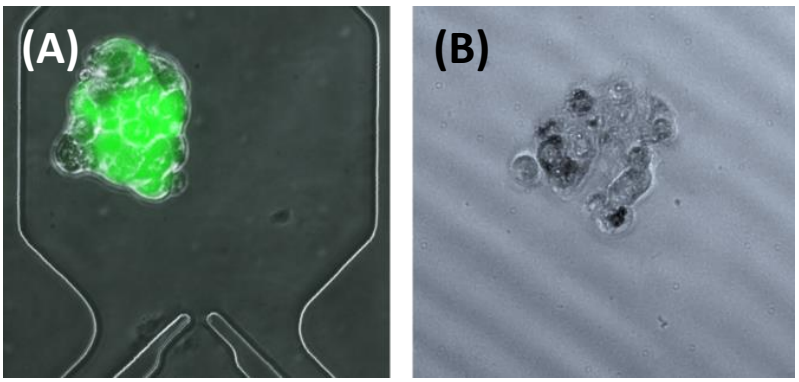

Figure 91: Notch+ T47D sphere (A) in device and (B) after retrieval from device for downstream analysis.

single cells via trypsinization and mechanical force (pipetting) and loaded into the Fluidigm C1/Biomark HD for multiplexed gene expression analysis of a 96-gene CSC signature. Our collaborators in the Wicha lab used microarray and RNA-sequence gene expression analyses of isolated CSC populations from breast cancer cell lines and PDX samples to the panel used in these screens. This 96 genes is capable of clustering and differentiating CSCs from non-stem cells. As the Fluidigm C1 does not capture every single cell that is loaded, the data generated is not for each individual cell, but instead a statistically representative subset of the single cells. All the chambers of C1 chip were examined under the IX83 fluorescent microscope to record the status of captured cells in each chamber. Single cells underwent lysis, RNA release, reverse transcription, and finally cDNA pre-amplification for 96 target gene transcripts in the C1 chip. The pre-amplified cDNAs from each single cell were analyzed by BioMark HD instrument that generates nearly 10,000 qPCR data-points in a single run using a 96 x 96 chip and TaqMan assays. Gene expression data were

analyzed using SINGuLAR and R script to generate PCA, HeatMap and Violin plots based on the Log2Expression value for each gene per single cell.

Single cell expression data of the genes that are statistically different between the two (Notch+ and Notch-) spheres is shown as a heatmap and violin plot (Figure 92). As hypothesized, cells within the Notch+ derived spheres are enriched for more stem-related genes as compared to

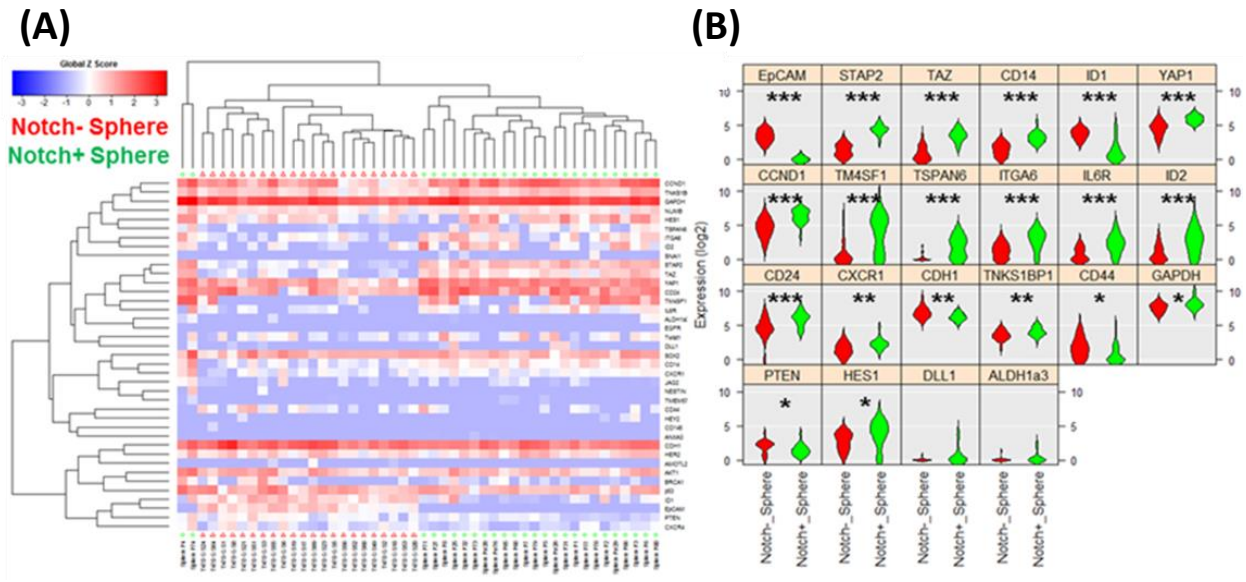

Figure 92: Single cell expression data in both (A) heat map and (B) violin plot form showing differences between Notch+ and Notch- derived spheres in statistically significant genes: stem related genes are significantly upregulated in Notch+ spheres.

the Notch- sphere. Though dissociated from a clonal sphere, we see heterogeneity in the form of a small population of ALDH1a3 high expressing cells within the Notch+ derived sphere cells. When analyzed separately, these cells show markedly different expression of genes such as βCatenin, CXCR1/4, and p53 to name a few (Figure 93). These cells represent a rare sub-population that would have been ignored in non-single cell based approaches. When separating based on ALDH1a3 expression, only a single Notch- derived cell was also scored as ALDH high, indicating a relatively less possible stem-ness in the population as compared to the Notch+ derived spheres.

Downstream single cell genetic analysis provides a wealth of information, not available through culture assays alone.

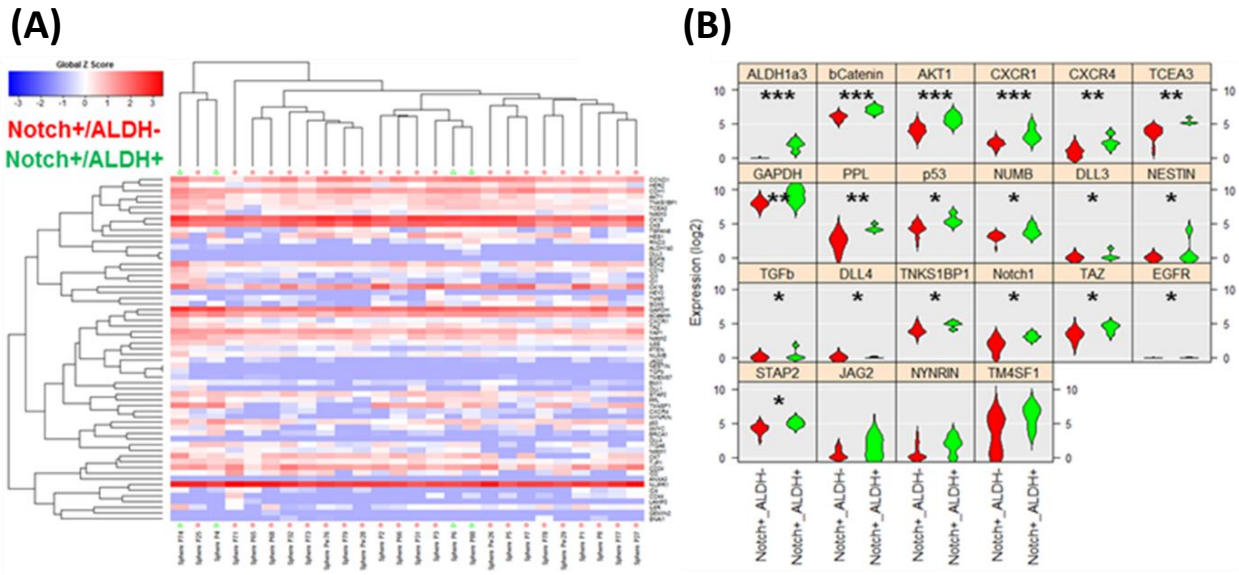

Figure 93: Single cell expression data in both (A) heat map and (B) violin plot form showing differences between ALDH1a3 high Notch+ derived and ALDH1a3 low Notch+ derived cells: ALDH high cells show further upregulation of stem related genes and demonstrate significant heterogeneity in a clonal population.

In performance of mammosphere assays as shown here, our microfluidic device improves on the conventional approach on several fronts. First, the integrated hydrodynamic capture scheme simplifies single cell seeding. Each single cell is captured in its own microchamber, preventing any possible aggregation from skewing sphere formation readout. In conventional approaches, pipetting fresh media or removing waste can disrupt/remove cells, complicating or outright preventing media exchange over the long culture period. In contrast, the presented platform provides a continuous perfusion of media from gravity flow for long-term culture. 96- or 384- non adherent culture plates (10cm by 8cm) are often the culture platform of choice for conventional mammosphere assays; our microfluidic approach contains 1,024 chambers for single cell sphere formation in an order of magnitude smaller area (1 cm by 3 cm). With this device, we successfully

performed single cell-derived sphere assays for A549, C6, HCC38, MCF-7 MDA-MB-231, SKOV3, SUM149, and SUM159 cell lines and 2 patient derived xenograft samples.

In the same study, we also examined the relationship between Notch expression and single cell sphere formation. The throughput and reliability facilitated the use of unsorted Notch reporting cells. In this experiment, we observed Notch+ and Notch- cells both forming spheres, though at significantly different rates, suggesting that there could be non-stem progenitor cells forming a portion of the resulting spheres. Subsequent genetic analysis allowed us to identify numerous genes of interest that were different between the two clonal spheres. HES1 and DLL1 are both upstream controllers of Notch signaling through PTEN, so their upregultaion here in the Notch+ derived population is consistent with previous literature [139]. Other genes that are upregulated, such as YAP1, TM4SF1, TSPAN6, ITGA6, and IL6R, have been correlated with increases in stemness and tumorigenic potential, suggesting a true stem-like cell source or at least higher stem-like potential in Notch+ derived spheres compared to Notch- [140, 141, 142, 143]. Upregulation in CXCR1 is particularly convincing on this front, as it has been shown to be almost exclusively expressed in the cancer stem-like cell population as compared to bulk tumor cells [144]. The overall decrease in CD44 and EpCAM, though, is unexpected. Overexpression of Notch-1 has been shown to contribute to the CSC self-renewal capacity and an acquisition of an EMT-like (epithelial to mesenchymal transition) state. These changes were facilitated by activation of both CD44 and EpCAM46, which contradicts the results seen here. It is possible that our sphere culture skews the CSCs within the sphere into a more MET-like (mesenchymal to epithelial transition) state. Media choices (serum versus serum free) and culture conditions (2D adherent versus spheres in suspension) greatly affect single cell expression, but further experimentation will be needed to validate this hypothesis.

Due to the single cell resolution of our data, we are also able see a small population of cells expressing aldehyde dehydrogenase (ALDH) isoform 1a3 within the Notch+ derived sphere cells. Enhanced ALDH activity is a hallmark of cancer stem-like cells, and ALDH1a3 activity, in particular, significantly contributes to aldefluor positive expression in mouse hematopoietic stem cells and human breast cancer CSC [145]. Within these cells, CXCR1, CXCR4, and p53, all CSC related genes, are all significantly upregulated as compared to other Notch+ derived cells. It is possible that these cells are progeneitor/stem cells (or early descendants) that asymmetrically divided to give rise to the other cells and the heterogeneity observed in the sphere; significant insight into initial tumorogenesis could be gleaned from further study. In addition to the 4 identified ALDH1a3 high Notch+ derived cells, 1 cell was identified to have increased ALDH1a3 expression in the Notch- derived sphere. Though we could not perform ANOVA to determine what genes were significantly different as compared to the other cells in the clone as there was only one cell identified, the ALDH activity hints at greater stem potential, even though it was derived from a Notch- source. Analysis of such rare cells might provide previously unobtainable insight into clonal heterogeneity or possible de-differentiation events.

This highlights the potentially exciting applications for our methodlogy in the investigation of inter- and intra- clonal heterogeneity. Intra-clonal heterogeneity, in particular, is a major challenge in the cancer therapy due to the difficulty of study this phenomena. Spheres formed from our device are clonal in nature, thus allowing us to 1) identify potential CSC through our high throughput mammosphere assay and then 2) dissociate and analyze the resulting sphere to study the clonal progeny of the CSC source.

Additionally by introducing biological agents of interest or stromal cell conditioned media, we can see how various factors influence clonal evolution, epigenetic regulation in the progeny,

or, more generally, CSC sphere formation. Initial steps have been taken to investigate our platform with conditioned media, biological agents, and drugs of interest.

4.3 Microenvironmental Effects on Sphere Formation

As seen in Chapter 2, the microenvironment heavily regulates CSC behavior, even in breast cancer [146, 147]. In metastasis, it is believed that particular microenvironments are needed to stimulate secondary tumor formation [147], driving CSC transition and proliferation. Therefore factors secreted by the microenvironment should have significant effects on tumor sphere formation. While we currently lack the ability for co-culture on chip, we can investigate microenvironemental effects on sphere formation through the use of conditioned media. "Conditioned" media is media harvested from other cultured cells containing metabolites, growth factors, and extracellular matrix proteins secreted into the medium by the cultured cells. When placed in conditioned media for growth, the new cell population is influenced by the secreted factors of the cells used to condition the media. Often used as an alternative to serum media, conditioned media can also be used to study possible signaling between cell types, but only in one directional manner from the conditioned cells to those cultured in the conditioned media. As microenvironments are believed to secrete signals that cause proliferation and tumor growth in metastasizing CSCs, this unidirectional communication may be appropriate for preliminary tests. Whether or not conditioned media from different sources can affect sphere formation will provide valuable information about CSC and how they might be regulated by their microenvironment.

In particular, we are interested in how conditioned media from endothelial cells and fibroblasts may affect the CSC subtypes. In previous work performed in the Wicha lab, it was seen that breast cancer CSCs existed in different transition states (EMT vs MET) [136] and that these

states can be characterized by different CSC markers (CD44/24 and ALDH). More basal cell lines (SUM149, SUM159, MDA-MB-231) have a greater percentage of CD44+/CD24- CSCs compared to ALDH+ CSCs and are thus more EMT-like. It was hypothesized by our collaborator in the Wicha lab, Dr. Michael Brooks, that different types of microenvironmetal signals would be required to activate these different CSC states. Endothelial or vascular niches may have a great effect on EMT like cells, while fibroblasts stromal cells may have little effect. If so, the opposite should be true for luminal lines (T47D, MCF-7), which are higher in ALDH expression and more MET-like. In these experiments, the effects of the possible different microenvironments were simulated using conditioned media from endothelial and fibroblast cells.

As a preliminary test SUM149 breast cancer cells were trypsinized and plated in non-adherent 96 multiwell plates through limiting dilution in order to assess the effects of conditioned media using conventional methods. On average, 3 cells were deployed per well with a distribution from 1-10. Cells were cultured for 3 weeks for mammosphere formation in supplemental MEBM media, human fibroblast cell conditioned MEBM media, or human endothelial cell conditioned MEBM media. Due to the limitation of dilution deployment, cell aggregation most likely occurred

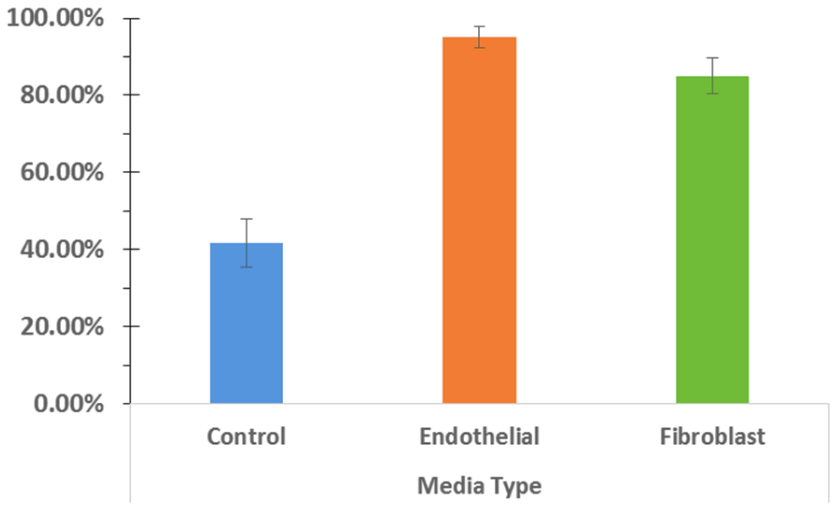

Figure 94: SUM149 sphere formation in limiting dilution culture under the influence of conditioned media.

within the microwells, causing significantly higher sphere formation rates (Figure 94). However, a significant change was observed with conditioned media culture. Both endothelial and fibroblast conditioned media caused an increase in sphere formation. Sphere formation increased from 40% in supplemented MEBM to 95% in endothelial conditioned media (P-value $2.52x10^{-11}$) and to 85% in fibroblast conditioned media (P-value $4.45x10^{-7}$). While endothelial media did in fact have a greater effect, the overall difference was slight compared to comparing control media versus any form of conditioned media.

To test this hypothesis with true single cell derived spheres, SUM149 cells were loaded into our single cell sphere formation assay and cultured for 2 weeks with different media conditions (control supplemented MEBM, endothelial conditioned media, and fibroblast conditioned media). In the single cell assay, sphere formation rates were more comparable to the expected CSC rates and matched well with previously obtained values (1-2%) (Figure 95). Endothelial conditioned media in this case, did not result in a significant increase in sphere formation and fibroblast

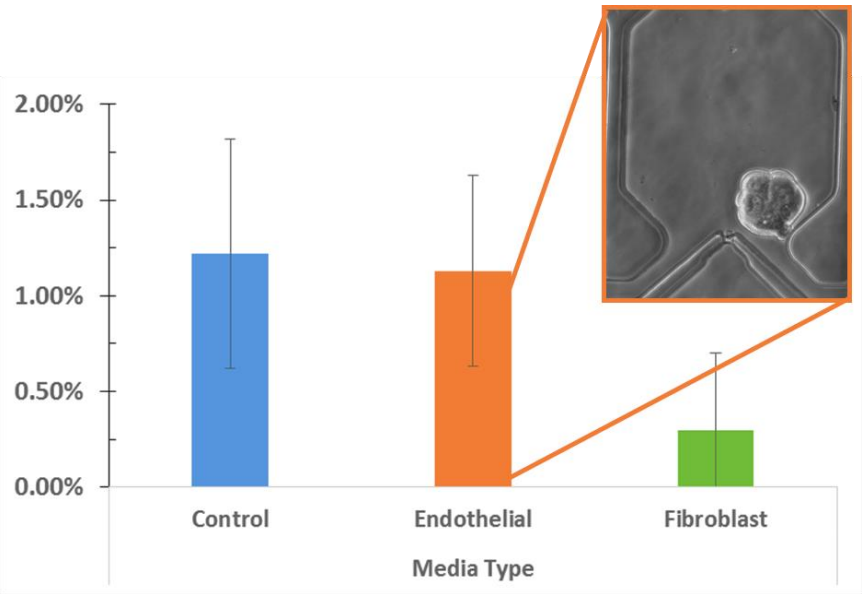

Figure 95: SUM149 sphere formation in single cell microfluidic assay under the influence of conditioned media from endothelial and fibroblast cells.

conditioned media reduced overall sphere formation. This is unexpected based on the results observed in bulk. While endothelial conditioned media resulted in greater sphere formation than fibroblast conditioned media in both experiments as expected, whether it outperformed control MEBM media was not consistent. Interestingly when both experiments were repeated with another breast cancer cell line, HCC38, that has a greater ALDH+ population, no changes in sphere formation rates were observed in any conditions. It is clear that CSC percentages and composition can greatly alter cancer responses to microenvironmental and stromal signaling.

Due to the large various and ambiguous effects between the bulk and single cell sphere derived culture, we do not have sufficient information to confirm or reject our current hypothesis. It is possible that reciprocal signaling is required to observe these interaction as it has been suggested that feedback loops are required [148]. Integrated simultaneous adherent-suspension co-culture on chip would be required to study such phenomena and may provide an interesting next direction for our mammosphere assays.

4.4 High Throughput Spheroid Drug Screening

Importantly, we have begun assessing sphere formation as a drug screening readout. To develop CSC targeted therapies, assays that are capable of assessing single cell behavior and differentiating bulk cells from stem cells are critically important. In more conventional assays for screening agents targeted for CSCs, cells are FACS sorted using a cell surface marker and deployed in multiwall plates in bulk. However as mentioned, there are a large number of potential markers that could be used, confounding results and screening [120, 121]. Instead, actual cell behavior and phenotype via our single cell sphere formation assay can be used to assess the population composition for drug screening. Drugs of varying types and doses that reduce sphere formation rates without changing bulk viability can be identified as possible CSC or progenitor targeting

agents. Chemicals of interested can be used to pre-treat the bulk population prior to device loading or introduced on chip during cell growth by simply pipetting the solution into the inlet, making our assay compatible with existing chemical library systems.

One chemical of particular interest for its effects on breast cancer CSCs is the antibacterial ionophore Salinomycin. Salinomycin was a part of a small subset of drugs discovered in a screen of nearly 16,000 agents to show CSC targeting ability. It was shown to target CSCs in mice at least

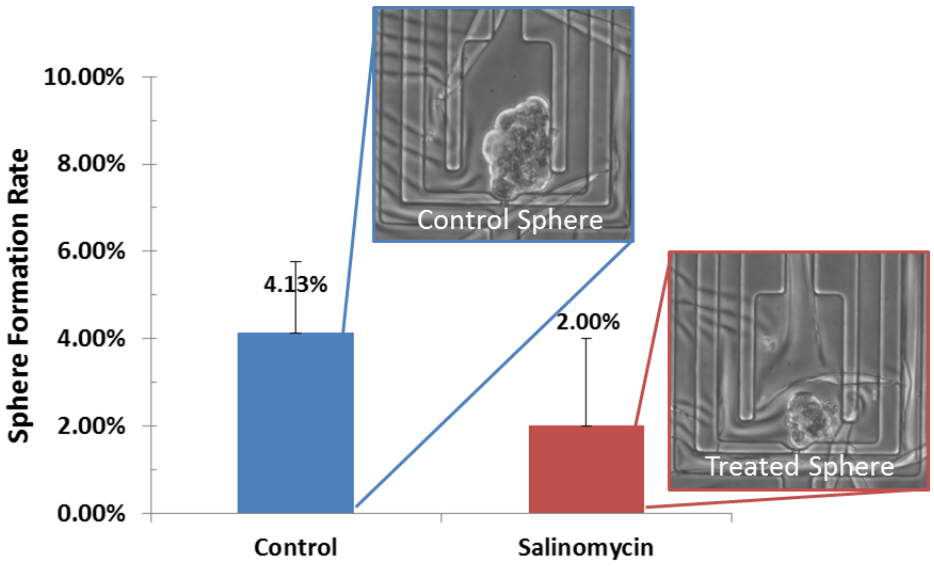

Figure 96: Treatment with 10μM salinomycin resulted in a 2-fold decrease in T47D single cell sphere formation. Spheres formed under treatment were also reduced in size.

2 orders of magnitude more effectively than conventional chemotherapeutic paclitaxel [149, 150]. It will be an important evaluation of our assay to see if salinomycin treatment will disrupt sphere formation. For this assay, T47D were treated in bulk with 10μM salinomycin or given only supplemental MEBM culture media 1 day prior to loading. T47D cells were trysinized, loaded into the devices, and cultured for 14 days to observe single cell derived sphere formation (Figure 96). Untreated T47D cells formed spheres at a rate similar and within the standard deviation of the

previously observed rates (~3-4%). Salinomycin treatment resulted in a 2 fold decrease in sphere formation. Cells that did form spheres had significantly reduced final spheres size (2x).

In adherent culture, no statistically significant difference in viability between the two populations was observed. More tests need to be screened to confirm the reliability of the assay as a drug screening tool, but these result demonstrate the ability of our approach to detect CSC targeting agents without a priori knowledge of CSC markers. With an approximate 100 by 200 μm area, each microwell occupies little space. This packing density will facilitate even higher throughput, and for inlet architecture to be designed to match the automated pipette layout. In this way our approach can be used for screening of chemical libraries. Microfluidic gradient generators are ubiquitous [151] and could be easily integrated to facilitate simultaneous dosage and chemical screening. This will be integrated screening platform could be an important long term goal for this assay.

Chapter 5: Conclusions

5.1 Summary

The goal of this research was to develop and deploy microfluidic assays capable of probing single cell behavior. Single cell technologies have been revealed to be increasingly important, as cell populations that were previously considered homogeneous are seen to be heterogeneous. As such, considerable effort is being put to forward to develop single cell tools across many biological fields. In cancer in particular, single cell tools will be critical for the investigation of cancer stem-like cells. Here, we have presented adherent and suspension based microfluidic assays with the ability to probe the behavior of these cancer stem-like cells.

A microfluidic single cell capture scheme developed by Dr. Jaehoon Chung in our lab provides the foundation for my single cell assay research. Dr. Chung performed clonal drug screening on populations of PC3 prostate cancer cells with integrated migration control. To demonstrate its more widespread applicability, I extended its application to perform on-chip targeted drug screening of ovarian cancer CSCs and increased the throughput of assays while maintaining device performance. Through drug screening, two novel targeted agents were identified to outperform conventional chemotherapy and the currently accepted targeted therapy, disulfiram, in their ability to disrupt CSCs. Additionally, I showed that through proper preparation and modification primary patient ovarian cancer cells could be cultured on chip, something very few microfluidic platforms have successfully demonstrated. This optimized single cell assay was then utilized to investigate CSC hierarchies in ovarian cancer and how different biological factors regulate differentiation within these hierarchies.

Through the development of topographically patterned hydrophobic PDMS surfaces, I also demonstrated successful non-adherent culture. Parameters were optimized to maintain non-adherent conditions despite cell culture environments. To create cheaper alternative non-adherent culture surfaces, processes to deposit and pattern polyHEMA coatings were developed and optimized. Both types of non-adherent coating were successfully integrated with our single cell capture scheme without degradation in device performance.

With these integrated non-adherent single cell devices, I could successfully perform mammosphere assays on chip. Such assays provide the ability to select and enrich CSCs without the use of FACS or cell surface markers, while conventional assays suffer from low throughput and poor single cell control. Our microfluidic assay improves single cell-derived mammosphere throughput by an order of magnitude (100s in plates to 1000s on-chip) and ensures single cell-derived sphere formation for proper CSC enrichment. With this approach, I investigated the relationship between traditional CSC markers and sphere formation, genetic heterogeneity, and the effects of conditioned media on sphere formation. Most interestingly, using our sphere formation assays as a drug screening tool can provide significant impact for the development of CSC targeted drugs.

These presented results demonstrate the ability of microfluidic approaches to improve on traditional biological assays without increasing complexity. Novel findings that were not possible with conventional bulk methods were presented, showing the unique applications of single cell based approaches, especially in regards to cancer stem-like cell behavior. The developed new technologies to probe rare CSC behaviors such as differentiation, genetic expression, and sphere formation may be applied to advance patient care and evolve our current understanding on cancer and its treatment in the future.

5.2 Contributions

This research contributes both to the technology of single cell and microfluidic assays in general and to the knowledge of cancer stem-like cells in their division, differentiation, drug response, and sphere formation behavior.

In regards to the contributions to the microfluidic assays:

- Single cell capture platforms were optimized for higher throughput and for culture of patient derived xenographs and other primary samples. Device cleaning protocols and extracellular matrix compositions were optimized to improve cell viability. Without the ability to culture primary samples, microfluidic impact is limited.
- Superhydrophobic topographic PDMS patterns were developed and characterized for integration with microfluidic single cell culture, and the relationship between surface characteristics and suspension culture performance was studied.
- Alternative polyHEMA-based coating techniques were developed for on-chip single cell suspension culture. Spin coating and soft lithographic polyHEMA patterning methods allow the fabrication of unique microstructures and simplify the fabrication of high-throughput single cell-derived sphere formation devices.
- Suspension culture surfaces (PDMS and polyHEMA) were integrated with the high-efficiency single cell capture scheme, creating a robust and highthroughput on-chip mammosphere assay. The developed microfluidic devices have shown the ability to form single cell-derived mammosphere in a reliable and high-throughput manner.

In regards to cancer stem-like cells biology:

- Differentiation hierarchies of ovarian cancer stem-like cells defined by ALDH and CD133 were directly observed and characterized. Hierarchical behavior and the possibility for de-differentiation events were observed synthesizing previous observations about CSCs.
- BMP2 was identified as a major controller of CSC differentiation behavior. Previous research suggested conflicting roles for BMP2 in its effect on cancer, but through direct microfluidic observation, evidence was generated that clarified the effects while supporting both claims. BMP2, produced from ALDH-CD133- negative cancer cells, drives ALDH+CD133+ cell to self-renew while suppressing bulk cell proliferation. In this way it can both suppress proliferation when treated in dish while also having a negative clinical effect in vivo by increasing the CSC population.
- EGFL6 was seen to play a major role in CSC division behavior. The tumor vascular niche is known regulate CSC fate, and it was seen that EGLF is expressed in ovarian tumor vasculature and isolated cancer cells. Single cell microfluidic culture demonstrated that EGFL6 promotes cancer cell proliferation by stimulating ALDH+ CSCs to undergo asymmetric division. As a direct result, EGFL6-blocking antibodies were found to represent a potential therapeutic.
- After identification of cells at the top of CSC hierarchies, single cell drug screening was performed on-chip. By culturing single CSCs we can observed the effects of targeted agents directly on the target population. Through this methodology, two novel ALDH targeting agents were identified that outperform currently available anti-CSC drug and general chemotherapeutic approaches.

- With our single cell derived sphere assay, we showed a direct correlation between traditional CSC markers and single cell-derived sphere formation. Using this same approach, drugs of interest and microenvironemental factors were screened for their effects on CSCs in a marker-independent manner. The demonstrated sphere assay is compatible and easily modified for use with chemical library screening, facilitating cheaper and faster identification of CSC-targeting agents.
- Integrating our sphere assay with Fluidigm single cell genetic expression analysis, we directly observed clonal heterogeneity within spheres and how different expression patterns could be observed between progenitor-derived and true CSC-derived single cell mammospheres.

5.3 Future Work

The immediate goal for our adherent single cell microfluidic assay would be to translate the devices and assays into the labs of biological collaborators. Heterogeneity and single cell behaviors are important in many fields apart from cancer including immunology [152], cardiology [153], and hematology [154], to name a few, and its clinical impact is growing. Tools are needed to facilitate single cell characterization for widespread use at a low cost with compatibility with current biological laboratory practices. We have demonstrated a robust single cell capture scheme and user-friendly high throughput devices using this scheme. Devices have small analytical footprints and are cheap to manufacture. Assays with our approach can be performed with no external equipment, save a pipette, and single cell capture is performed without any user input, lowering expertise requirements. These factors together make our approach ideal for deployment in a variety of lab settings.

In fact, several collaborators have already begun using these assays in their lab. The lab of Dr. Ronald Buckanovich has begun investigating the effects of vascular endothelial growth factor (VEGF) on ovarian CSC and our single cell assays will provide the capability to monitor single CSC response. Additionally, they are interested in understanding CSC quiescence. In many cases, CSC can adopt a slow cycling phenotype. This quiescent potential of CSCs represents an inherent mechanism that at least partially explains chemotherapy resistance and recurrence in post-therapy cancer patients [155]. It is likely that understanding mechanisms that control quiescence and encourage CSC to enter cycling will be key components of future therapies that target CSC and have the potential to eradicate tumors. Quiescence in CSC is particularly hard to study due to CSC rarity and the ease by which quiescent cells are often 'overgrown' by their cycling kin. Our devices are uniquely well suited to monitor quiescent cells due to robust single cell capture and definite spatial confinement. We have even already observed viable quiescent primary ovarian cells on chip for over 12 days (Chapter 2.3), and further data has been generated with cell lines. Devices have already been used to examine head-and-neck cancer stem-like cells here in the School of Dentistry, in the lab of Dr. Jacques Nor.

Preliminary device sharing, however, has had mixed success. While useful data has been generated, non-microfluidic technicians and personnel have had difficulty controlling single cell loading. Cell concentration control and device preparation seem to be able to greatly affect device capture. High cell concentrations can result in significant clogging and non-specific capture. While low cells numbers should theoretically have no effect on capture, low capture efficiency (and rate) is clearly observed with low cell number. Further device and (possibly more important) protocol optimization is required for devices to be broadly useful for end users. Reducing capture sensitivity

to cell concentration will likely be the most important step, and members in our lab have already begun investigating measures to improve capture efficiency with low cell numbers.

In regards to our single cell derived sphere assays, it is our immediate goal to validate our mammosphere assays through in vivo validation. Seminal work in cancer stem-like cells suggests that single cell derived sphere formation identifies and enriches for breast cancer stem-like cells [100, 101]. Implantation of aggregate mammospheres in NOD SCID mice results in great tumor initiation (the gold standard assays for CSCs) than implantation of a similar number of bulk aggregates or cells, implying greater stemness. However, due to the low throughput of conventional techniques for single cell-derived sphere formation, there is little information regarding how true single cell-derived spheres compare to aggregates in tumor initiation potential. Aggregates spheres will be formed in conventional multi-well plates and implanted in one side of a mouse mammary fat pad. In the other side, we can inject a single cell derived sphere of a comparable size. Using 15-20 mice, we can directly compare tumor initiating potential between the two approaches with greater initiation indicating greater enrichment of CSC populations. We expect higher tumor initiation potential in our single cell-derived spheres; this data would providing extremely convincing evidence for oncologists and cancer biologists of the utility and improvements of our microfluidic approach over conventional dish-based methods.

In the long term, we expect that our high-efficiency single cell capture scheme can be optimized for a variety of approaches through changing architectures (e.g. valve integration for chemical sensing assays) or through other surface patterning approaches. Here we demonstrated how integration of hydrophobic surfaces or polyHEMA coatings could be used to facilitate mammosphere assays and other sphere screening approaches with the single cell capture scheme as the foundation. But due to the robustness of the scheme, a variety of other modifications are

possible without disrupting device performance and advantages. For example, sensing structures or chemicals can be patterned into our microwells to monitor single cell behavior. Professor Jinsang Kim here at the University of Michigan has developed a versatile polydiacetylene-liposome based microsensor that exhibits a shift in color and fluorescence when stressed [156, 157], and some initial testing was performed for integrating such sensors. One application of interest is single cell adhesion force measurement, which could provide useful information about morphogenesis and viability [158, 159]. Mechanosensors can be created from surface bound liposomes, chemically modified to contain RGD cell binding domains (Figure 97). APTES-based

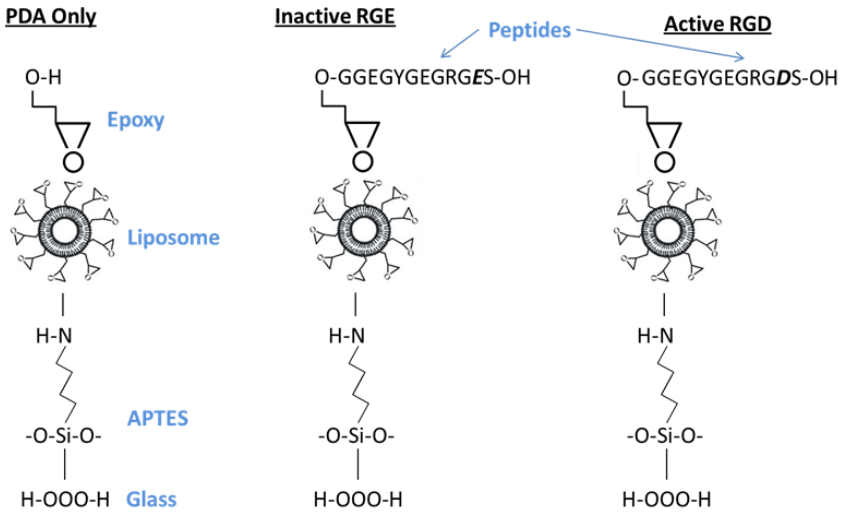

Figure 97: Schematic of PDA liposome -based mechanosensing surface modifications with control, active, and inactive cell RGD binding domains.

glass surface chemistry facilitates simple integration into glass bond PDMS device. PDA-liposomes can also be created that do not facilitate cell-adhesion (Epoxy or inactive RGE domains), and these can be used control spatial localization of cell adhesion. When a surface is completely covered with the sensing chains, cells are sterically blocked from the surface and can only adhere through interaction with RGD domains on the sensor. As the cells adhere and exhibit traction forces, the PDA liposome connecting the active domain to the glass surface experiences

stress and fluoresces. This fluorescence is directly proportional to the stress and reversible, providing a way to accurately and dynamically monitor cell adhesion. Preliminary testing was performed in bulk culture (Figure 98), but initial sensor designs created considerable surface debris

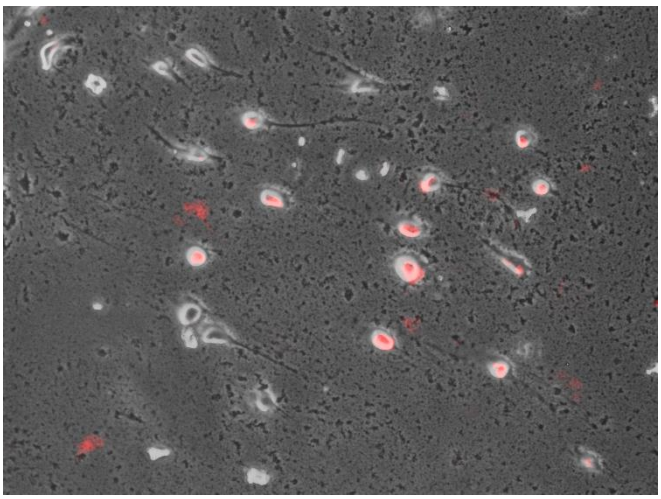

Figure 98: PDA-Liposome modified glass surface for direct sensing of cell adhesion, where red fluorescence indicates where cell adhesion is stressing PDA-based liposome sensors.

causing the approach to be too insensitive and nonspecific. However, we believe sensor optimization is possible, and this is only one example of potential sensing methodologies that could be easily integrated with our microfluidic capture scheme.

Finally, our single cell derived mammosphere assay has great potential for use as a high throughput screening tool. Sphere formation as a readout allows us to directly assess drugs effect on the stem and progenitor population without the need to FACS sorting or use of stem-related surface markers. This type of readout also allows us to observe targeting effects independent of any cytotoxic effects in the cells. The single cell capture scheme is simple to array into high throughput assays due to the hydrodynamic capture and small microwell footprint. Device inlets can be easily photopatterned to match the structure of 96-well plates to even facilitate use of our device with chemical screening libraries. In this way, our assay could greatly speed the

identification of CSC targeting drugs. Identifying ways to target CSC and their effects is critical for the development of solutions to manage, if not cure, cancer when it arises providing hope for millions worldwide.

References

[1] "Cancer Facts and Figures," American Cancer Society, Atlanta, Georgia, 2014.

[2] A. Johnson, B. Alberts, D. Bray, J. Lewis and K. Roberts, Essential Cell Biology, 4th Edition, New York, NY: Garland Science, 2013.

[3] B. Alberts, A. Johnson, J. Lewis, M. Raff, K. Roberts and P. Walter, Molecular Biology of the Cell, Fifth Edition, New York, NY: Garland Science, 2007.

[4] S. Clancey, "DNA Damage & Repair: Mechanisms for Maintaining DNA Integrity," *Nature Education,* vol. 1, no. 1, p. 103, 2008.

[5] T. Reya, S. Morrison, M. Clarke and I. Weissman, "Stem cells, cancer, and cancer stem cells.," *Nature,* vol. 414, pp. 105-111, 2001.

[6] J. Zhou and Y. Zhang, "CSC: Models, mechanisms and implications for improved treatment.," *Cell Cycle,* vol. 7, no. 10, pp. 1360-1370, 2008.

[7] M. Shehata, "The Father of Medicine: A Historical Reconsideration," *Journal of Medical Ethics,* vol. 12, pp. 171-176, 2004.

[8] S. Mukherjee, The Emperor of All Maladies: A Biography of Cancer, New York, NY: Scribner, 2010.

[9] T. Lawrence, R. Ten Haken and A. Giaccia, "Principles of Radiation Oncology," in *Cancer: Principles and Practice of Oncology. 8th ed.* , Philadelphia, PN, Lippincott Williams and Wilkins, 2008.

[10] D. Miller, "A tribute to Sidney Farber – the father of modern chemotherapy," *British Journal of Haematology,* vol. 124, no. 1, pp. 20-26, 2006.

[11] D. Bonnet and J. Dick, "Human acute myeloid leukemia is organized as a hierarchy that originates from a primitive hematopoietic cell.," *Nature Medicine,* vol. 3, pp. 730-737, 1997.

[12] M. Zhang, F. Behbod, R. Atkinson, M. Landis, F. Kittrell, D. Edwards, D. Medina, A. Tsimelzon, H. S. J. Green, A. Michalowska and J. Rosen, "Identification of tumor-initiating cells in a p53-null mouse model of breast cancer.," *Cancer Research,* vol. 68, p. 4674, 2008.

[13] N. Maitland and A. Collins, "Prostate CSC: A New Target for Therapy.," *JCO,* vol. 26, no. 17, pp. 2862-2870, 2008.

[14] P. G, J. Tzeng, J. Doll, R. Greig, D. Rieman and I. Zeidman, "Evolution of tumor cell heterogeneity during progressive growth of individual lung metastases," *Proceedings of the National Academt of Sciences,* vol. 79, no. 21, pp. 6574-6578, 1982.

[15] B. Ljungberg, RStenling and G. Roos, "DNA content in renal cell carcinoma with reference to tumor heterogeneity," *Cancer,* vol. 56, no. 3, pp. 503-508, 1985.

[16] T. Lapidot, C. Sirard, J. Vormoo, B. Murdoch, T. Hoang, J. Caceres-Cortes, M. Minden, B. Paterson, M. Caligiuri and J. Dick, "A cell initiating human acute myeloid leukaemia after transplantation into SCID mice," *Nature,* vol. 367, pp. 645-648, 1994.

[17] S. Mukherjee, "The Cancer Sleeper Cell," *The New York Times,* 29 October 2010.

[18] B. Bryder, D. Rossi and I. Weissman, "Hematopoietic Stem Cells: The Paradigmatic Tissue-Specific Stem Cell," *Am Journal Pathol*, vol. 169, no. 2, pp. 338-346, 2006.

[19] B. Beck and C. Blanpain, "Unravelling cancer stem cell potential," *Nature Reviews Cancer*, vol. 13, pp. 727-738, 2013.

[20] M. Al-Hajj, M. Max S. Wicha, A. Benito-Hernandez, S. Morrison and M. Clarke, "Prospective identification of tumorigenic breast cancer cells," *Proceedings of the National Academy of Sciences,* vol. 100, no. 7, pp. 3983-3988, 3983-3988 2003.

[21] S. Singh, I. Clarke, M. Terasaki, V. Bonn, C. Hawkins, J. Squire and R. Dirks, "Identification of a Cancer Stem Cell in Human Brain Tumors.," *Cancer Research,* vol. 3, no. 63, p. 5821, 2003.

[22] C. O'Brien, A. Pollett, S. Gallinger and J. Dick, "A human colon cancer cell capable of initiating tumour growth in immunodeficient mice," *Nature*, vol. 445, p. 106–110, 2007.

[23] S. Zhang, C. Balch, M. Chan, H. Lai, D. Matei, J. Schilder, P. Yan, T. Huang and K. Nephew, "Identification and characterization of ovarian cancer-initiating cells from primary human tumors," *Cancer Research,* vol. 68, no. 11, p. 4311–4320, 2008.

[24] C. Li, D. Heidt, P. Dalerba, C. Burant, L. Zhang, V. Adsay, M. Wicha, M. Clarke and D. Simeone, "Identification of pancreatic cancer stem cells," *Cancer Research,* vol. 67, no. 3, pp. 1030-1037, 2007.

[25] S. Lang, F. Frame and A. Collins, "Prostate cancer stem cells," *J Pathology,* vol. 217, no. 2, p. 299–306, 2009.

[26] T. Schatton, G. Murphy, N. Frank, K. Yamaura, A. Waaga-Gasser, M. Gasser, Q. Zhan, S. Jordan, L. Duncan, C. Weishaupt, R. Fuhlbrigge, T. Kupper, M. Sayegh and M. Frank, "Identification of cells initiating human melanomas," *Nature,* vol. 451, p. 345–9., 2008.

[27] W. Matsui, Q. Wang and J. Barber, "Clonogenic multiple myeloma progenitors, stem cell properties, and drug resistance," *Cancer Research,* vol. 68, no. 1, pp. 190-197, 2008.

[28] D. Dexter and J. Leith, "Tumor heterogeneity and drug resistance.," *JCO,* vol. 4, no. 2, pp. 244-257, 1986.

[29] J. Geisler, S. Rose, H. Geisler, G. Miller and M. Wiemann, "Drug resistance and tumor heterogeneity.," *Journal of Gynecologic Oncology,,* vol. 7, pp. 25-28, 2002.

[30] S. Halldorsson, C. Lucumi, R. Gómez-Sjöberg and R. Fleming, "Advantages and challenges of microfluidic cell culture in polydimethylsiloxane devices," *Biosensors and Bioelectronis,* vol. 63, pp. 218-231, 2015.

[31] R. Willis, "Sorting out the mess," *Modern Drug Discovery,* vol. 7, no. 11, 2004.

[32] C. Chaffer, I. Brueckmann, C. Scheel, A. Kaestli, P. Wiggins, L. Rodrigues, M. Brooks, F. Reinhardt, Y. Su, K. Polyak, L. Arendt, C. Kuperwasser, B. Bierie and R. Weinberg, "Normal and neoplastic nonstem cells can spontaneously convert to a stem-like state," *Proceedings of the National Academy of Sciences,* vol. 108, no. 19, pp. 7950-7955, 2011.

[33] Y. Xia and G. Whitesides, "Soft Lithography," *Angewandte Chemie Int. Ed.,* vol. 37, pp. 550-575, 1998.

[34] E. Choban, L. Markoski, A. Wieckowski and P. Kenisa, "Microfluidic fuel cell based on laminar flow," *Journal of Power Sources,* vol. 128, no. 1, pp. 54-60, 2004.

[35] P. Hung, P. Lee, P. Sabounchi, R. Lin and L. Lee, "Continuous perfusion microfluidic cell culture array for high-throughput cell-based assays.," *Biotechnol Bioeng,* vol. 89, no. 1, pp. 1-8, 2005.

[36] L. Kim, M. Vahey, H. Lee and J. Voldman, "Microfluidic arrays for logarithmically perfused embryonic stem cell culture.," *Lab Chip,* vol. 6, no. 3, pp. 394-406, 2006.

[37] F. Balagaddé, L. You, C. Hansen, F. Arnold and S. Quake, "Long-term monitoring of bacteria undergoing programmed population control in a microchemostat.," *Science ,* vol. 309, no. 5731, pp. 137-140, 2005.

[38] V. Chin, T. P. S. Sanga, J. Scheel, F. Gage and S. Bhatia, "Microfabricated platform for studying stem cell fates.," *Biotechnol Bioeng,* vol. 88, no. 3, pp. 399-415, 2004.

[39] V. Lecault, M. Vaninsberghe, S. Sekulovic, C. Hansen and e. al., "High-throughput analysis of single hematopoietic stem cell proliferation in microfluidic cell culture arrays," *Nature Methods,* vol. 8, pp. 581-586, 2011.

[40] L. Yu, H. Huang, X. Dong, D. Wu, J. Qin and B. Lin, "Simple, fast and high-throughput single-cell analysis on PDMS microfluidic chips.," *Electrophoresis,* vol. 29, no. 24, pp. 5055-5060, 2008.

[41] A. Wheeler, W. Throndset, R. Whelan, A. Leach, R. Zare, Y. Liao, K. Farrell, I. Manger and A. Daridon, "Microfluidic Device for Single-Cell Analysis," *Analytical Chem,* vol. 75, pp. 3581-3586, 2003.

[42] E. Brouzes, M. M. N. Savenelli, D. Marran, M. Twardowski, J. Hutchison, J. Rothberg, D. Link, N. Perrimon and M. Samuels, "Droplet microfluidic technology for single-cell high-throughput screening," *Proceedings of the National Academy of Sciences,* vol. 106, no. 34, pp. 14195-14200, 2009.

[43] Y. Huang, S. Joo, M. Duhon, M. Heller, B. Wallace and X. Xu, "Dielectrophoretic Cell Separation and Gene Expression Profiling on Microelectronic Chip Arrays," *Analytical Chem.,* vol. 74, no. 14, pp. 3362-3371, 2002.

[44] B. Taff and J. Voldman, "A Scalable Addressable Positive-Dielectrophoretic Cell-Sorting Array," *Analytical Chem.,* vol. 77, no. 24, pp. 7976-7983, 2005.

[45] J. Jaeger, K. Uhlig, T. Schnelle and T. Mueller, "Contact-free single-cell cultivation by negative dielectrophoresis," *Journal of Physics D: Applied Physics,* vol. 41, no. 17, p. 5502, 2008.

[46] P. Chiou, A. Ohta and M. Wu, "Massively parallel manipulation of single cells and microparticles using optical images," *Nature,* vol. 436, pp. 370-372, 2005.

[47] A. Skelley, O. Kirak, H. Suh, R. Jaenisch and J. Voldman, "Microfluidic control of cell pairing and fusion," *Nature Methods,* vol. 6, pp. 147-152, 2009.

[48] A. Rowat, J. Bird, J. Agresti, O. Rando and D. Weitz, "Tracking lineages of single cells in lines using a microfluidic device," *Proceedings of the National Academy of Sciences,* vol. 106, no. 43, pp. 18149-18154, 2009.

[49] J. Chung, Y. Kim and E. Yoon, "Highly-efficient single-cell capture in microfluidic array chips using differential hydrodynamic guiding structures," *Applied Physics Letters,* vol. 98, p. 123701 , 2011.

[50] J. Chung, P. Ingram, T. Bersano-Begey and E. Yoon, "Traceable clonal culture and chemodrug assay of heterogeneous prostate carcinoma PC3 cells in microfluidic single cell array chips," *Biomicrofluidics,* vol. 8, p. 064103, 2014.

[51] C. Klein, T. Blankenstein, O. Schmidt-Kittler, M. Petronion, B. Polzer, N. Stoeckklien and G. Riethnuller, "Genetic heterogeneity of single disseminated tumour cells in minimal residual cancer," *The Lancet,* vol. 360, no. 9334, pp. 683-689, 2002.

[52] B. Brehm-Stecher and E. Johnson, "Single-Cell Microbiology: Tools, Technologies, and Applications," *Microbiol. Mol. Biol. Rev.,* vol. 68, no. 3, pp. 538-559, 2004.

[53] H. Li, X. Chen, T. Calhoun-Davis, K. Claypool and D. Tang, "PC3 Human Prostate Carcinoma Cell Holoclones Contain Self-renewing Tumor-Initiating Cells," *Cancer Research,* vol. 68, p. 1820, 2008.

[54] M. Pfeiffer and J. Schalken, "Stem Cell Characteristics in Prostate Cancer Cell Lines," *European Urology,* vol. 57, no. 2, pp. 246-255, 2010.

[55] D. Brunette, "Spreading and orientation of epithelial cells on grooved substrata," *Experimental Cell Research,* vol. 167, no. 1, pp. 203-217, 1986.

[56] C. Oakley and D. Brunette, "Response of single, pairs, and clusters of epithelial cells to substratum topography," *Biochemistry and Cell Biology,* vol. 73, no. 7-8, pp. 473-489, 1995.

[57] C. Chen, M. Mrksich, S. Huang, G. Whitesides and D. Ingber, "Micropatterned Surfaces for Control of Cell Shape, Position, and Function," *Biotechnology Progress,* vol. 14, no. 3, pp. 356-363, 1998.

[58] C. Nelson, S. Raghavan, J. Tan and C. Chen, "Degradation of Micropatterned Surfaces by Cell-Dependent and -Independent Processes," *Langmuir*, vol. 19, no. 5, pp. 1493-1499, 2003.

[59] X. Jiang, D. Bruzewicz, A. Wong, M. Piel and G. Whitesides, "Directing cell migration with asymmetric micropatterns," *Proceedings of the National Academy of Sciences*, vol. 102, no. 4, pp. 975-978, 2004.

[60] C. T. Y. Fan, S. Takayama, E. Meyhofer and K. Kurabayashi, "Electrically Programmable Surfaces for Configurable Patterning of Cells," *Advanced Materials*, vol. 20, no. 8, pp. 1418-1423, 2008.

[61] V. Liu, W. Jastromb and S. Bhatia, "Engineering protein and cell adhesivity using PEO-terminated triblock polymers," *Journal of Biomedical Materials Research*, vol. 60, no. 1, pp. 126-134, 2002.

[62] C. Fan, K. Kurabayashi and E. Meyhofer, "Protein Pattern Assembly by Active Control of a Triblock Copolymer Monolayer," *Nano Letters*, vol. 6, no. 12, pp. 2763-2767, 2006.

[63] D. Burgos-Ojeda, B. Rueda and R. Buckanovich, "Ovarian cancer stem cell markers: Prognostic and therapeutic implications," *Cancer Letters*, vol. 322, no. 1, pp. 1-7, 2012.

[64] I. Silva, S. Bai, K. McLean, K. Yang, K. Grifffith, D. Thomas, C. Ginestier, C. Johnston, A. Kueck, R. Reynolds, M. Wicha and R. Buckanovich, "Aldehyde Dehydrogenase in Combination with CD133 Defines Angiogenic Ovarian Cancer Stem Cells That Portend Poor Patient Survival," *Cancer Research*, vol. 71, p. 3991, 2011.

[65] M. Alison and E. al, " Finding Cancer Stem Cells: Are Aldehyde," *Journal of Pathology*, vol. 22, no. 4, pp. 335-344, 2010.

[66] I. Ma and A. Allan, "The Role of Human Aldehyde Dehydrogenase," *Stem Cell Rev and Rep,* vol. 7, no. 2, pp. 292-306, 2011.

[67] I. Kryczek, S. Liu, M. Roh, L. Vatan, W. Szeliga, S. Wei, M. Banerjee, Y. Mao, J. Kotarski, M. Wicha, R. Liu and W. Zou, "Expression of aldehyde dehydrogenase and CD133 defines ovarian cancer stem cells.," *Int Journal of Cancer,* vol. 130, no. 1, pp. 29-39, 2012.

[68] C. Landedn, B. Goodman, A. Katre, A. Steg, A. S. R. S. A. Nick and e. al, "Targeting Aldehyde Dehydrogenase Cancer Stem Cells in Ovarian Cancer," *Mol Cancer Ther,* vol. 9, p. 3186, 2010.

[69] S. AG, H. Snippert, D. Stange, M. van den Born, J. van Es, M. van de Wetering and H. Clevers, "Lineage tracing reveals Lgr5+ stem cell activity in mouse intestinal adenomas.," *Science,* vol. 6095, pp. 730-735, 2012.

[70] G. Driessens, B. Beck, A. Caauwe, B. Simons and C. Blanpain, "Defining the mode of tumour growth by clonal analysis," *Nature,* vol. 488, pp. 527-530, 2012.

[71] S. Charati and S. Stern, "Diffusion of Gases in Silicone Polymers: Molecular Dynamics Simulations," *Macromolecules,* vol. 31, no. 16, pp. 5529-5535, 1998.

[72] E. Leclerc, Y. Sakai and T. Fujii, "Cell Culture in 3-Dimensional Microfluidic Structure of PDMS (polydimethylsiloxane)," *Biomedical Microdevices,* vol. 5, no. 2, pp. 109-114, 2003.

[73] A. Paguirigan and D. Beebe, "From the cellular perspective: exploring differences in the cellular baseline in macroscale and microfluidic cultures," *Integrative Biology,* vol. 1, pp. 182-195, 2009.

[74] C. Rogers, J. Pagaduan, G. Nordin and A. Woolley, "Single-Monomer Formulation of Polymerized Polyethylene Glycol Diacrylate as a Nonadsorptive Material for Microfluidics," *Analytical Chemistry,* vol. 83, pp. 6418-6425, 2011.

[75] A. Butterswoth, M. del Garcia and D. Beebe, "Photopolymerizable poly (ethylene) glycol diacrylate (PEGDA) microfluidic devices," *International Conference on Miniaturized Systems for Chemistry and Life Sciences,* 2004.

[76] T. Yu, S. Yang, C. Fu, M. Liu, L. Hsu and H. Chang, "Integration of organic opto-electrowetting and poly (ethylene) glycol diacrylate (PEGDA) microfluidics for droplets manipulation," *Sensors and Actuators B: Chemical,* 2011.

[77] D. Castro, D. Conchouso, Y. Fan and I. Foulds, "Surface Treatments of Soft Molds for High Aspect Ratio Molding of Poly-PEGDA," *International Conference on Miniaturized Systems for Chemistry and Life Sciences (MicroTas),* pp. 1231-1233, 2012.

[78] Y. Yan, M. Chan-Park, J. Gao and C. Yue, ""Electroless nickel-plated UV-embossed microstructured surface with very high aspect ratio channels.," *Langmuir,* vol. 20, pp. 1031-1035, 2004.

[79] A. Sawhney, C. Pathak and J. Hubbell, "Bioerodible hydrogels based on photopolymerized poly (ethylene glycol)-co-poly (. alpha.-hydroxy acid) diacrylate macromers," *Macromolecules,* vol. 26, pp. 581-587, 1993.

[80] K. W. L. T. E. H. B. L. C. M. J. Y. a. L. L. J. Kim, "Synthesis and evaluation of novel biodegradable hydrogels based on poly(ethylene glycol) and sebacic acid as tissue engineering scaffolds," *Biomacromolecules,* vol. 9, pp. 149-157, 2007.

[81] S. Bryant, C. Nuttelman and K. Anseth, "Cytocompatibility of UV and visible light photoinitiating systems on cultured NIH/3T3 fibroblasts in vitro," *Journal of Biomaterials Science, Polymer Edition,* vol. 11, pp. 439-457, 2000.

[82] P. Patel and C. Patrick Jr, "Cytocompatibility of preadipocytes in diacrylated polyethylene glycol crosslinked with various UV light photoinitiating systems," *Engineering in Medicine and Biology, Fall Meeting of the Biomedical Engineering Society EMBS/BMES Conference,* pp. 757-758, 2002.

[83] K. Studer, C. Decker, E. Beck and R. Schwalm, "Overcoming oxygen inhibition in UV-curing of acrylate coatings by carbon dioxide inerting," *Progress in Organic Coatings,* vol. 48, pp. 92-100, 2003.

[84] R. Kodzius, K. Xiao, J. Wu, X. Yi, X. Gong and I. Foulds, "Inhibitory effect of common microfluidic materials on PCR outcome," *Sensors and Actuators B: Chemical,* 2011.

[85] D. Eddington, J. Puccinelli and D. Beebe, "Thermal aging and reduced hydrophobic recovery of polydimethylsiloxane," *Sensors and Actuators B: Chemical,* vol. 114, no. 1, pp. 170-172, 2006.

[86] K. Mclean, Y. Gon, Y. Choi, D. Deng, K. B. S. Yang, L. Cabrerea, E. Keller, L. McCauley, K. Cho and R. Buckanovich, "Human ovarian carcinoma–associated mesenchymal stem cells regulate cancer stem cells and tumorigenesis via altered BMP production," *J Clin Invest.,* vol. 121, no. 8, pp. 3206-3219, 2011.

[87] A. Tada, T. Nishihara and H. Kato, "Bone morphogenetic protein 2 suppresses the transformed phenotype and restores actin microfilaments of human lung carcinoma A549 cells.," *Oncol Rep,* vol. 5, no. 5, pp. 1137-1140, 1998.

[88] M. W, J. Ma, J. Xu, C. Qiao, A. Branscum, A. Cardenas, A. Baron, P. Schwartz, N. Maihle and Y. Huang, "Lin28 regulates BMP4 and functions with Oct4 to affect ovarian tumor microenvironment.," *Cell Cycle,* vol. 12, no. 1, pp. 88-97, 2013.

[89] S. Schwitalla, F. AA, P. Cammareri, T. Nebelsiek, M. Arkan, F. Greten and e. al, "Intestinal tumorigenesis initiated by dedifferentiation and acquisition of stem-cell-like properties," *Cell,* vol. 152, no. 1-2, pp. 25-38, 2012.

[90] E. Carragee, E. Hurwitz and B. Weiner, "A critical review of recombinant human bone morphogenetic protein-2 trials in spinal surgery: emerging safety concerns and lessons learned," *Spine J,* vol. 11, no. 6, pp. 471-491, 2011.

[91] C. Calabrese, H. Poppleton, M. Kocak, T. Hogg, C. Fuller, B. Hamner, E. Oh, M. Gaber, D. Finklestein, M. Allen and e. al, "A perivascular niche for brain tumor stem cells.," *Cancer Cell,* vol. 11, pp. 69-82, 2007.

[92] R. Gilbertson and J. Rich, "Making a tumour's bed: glioblastoma stem cells and the vascular niche.," *Nat Rev Cancer,* vol. 7, no. 10, pp. 733-736, 2007.

[93] J. Butler, H. Kobayashi and S. Rafii, "Instructive role of the vascular niche in promoting tumour growth and tissue repair by angiocrine factors.," *Nat Rev Cancer,* vol. 10, no. 2, pp. 138-146, 2010.

[94] R. Buckanovich, D. Sasaroli, A. O'Brien-Jenkins, J. Botbyl, R. Hammond, D. Katsaros, R. Sandaltzopoulos, L. Liotta, P. Gimotty and G. Coukos, "Tumor vascular proteins as biomarkers in ovarian cancer.," *J Clin Oncology,* vol. 25, pp. 852-861, 2007.

[95] D. Rhodes, S. Kalyana-Sundaram, V. V. R. Mahavisno, J. Yu, B. Briggs, T. Barrette, M. Anstet, C. Kincead-Beal, P. Kulkarni, S. Varambally, D. Ghosh and A. Chinnaiyan,

"Oncomine 3.0: genes, pathways, and networks in a collection of 18,000 cancer gene expression profiles.," *Neoplasia,* vol. 9, no. 2, pp. 166-180, 2007.

[96] E. Boscolo and J. Bischoff, "Vasculogenesis in infantile hemangioma.," *Angiogenesis,* vol. 12, pp. 197-207, 2009.

[97] P. Mehlen and A. Puisieux, "Metastasis: a question of life or death," *Nat Rev Cancer,* vol. 6, no. 6, pp. 449-458, 2006.

[98] J. Friedrich, C. Seidel, R. Ebner and L. Kunz-Schughart, "Spheroid-based drug screen: considerations and practical approach.," *Nature Protocols,* vol. 4, no. 3, pp. 309-324, 2009.

[99] J. Lee, S. Kotliarova, Y. Kotliarov, A. Li, Q. Su, N. Donin, S. Pastorino, B. Purow, N. Christopher, W. Zhang, J. Park and H. Fine, "Tumor stem cells derived from glioblastomas cultured in bFGF and EGF more closely mirror the phenotype and genotype of primary tumors than do serum-cultured cell lines.," *Cancer Cell,* vol. 9, no. 5, pp. 391-403, 2006.

[100] G. Dontu and M. Wicha, "Survival of Mammary Stem Cells in Suspension Culture: Implications for Stem Cell Biology and Neoplasia.," *J Mammary Gland Biol Neoplasia,* vol. 10, no. 1, pp. 75-86, 2005.

[101] G. Dontu, W. Abdallah, J. Foley, J. Jackson, F. Clarke, M. Kawamura and M. Wicha, "In vitro propagation and transcriptional profiling of human mammary stem/progenitor cells.," *Genes Dev,* vol. 17, pp. 1253-1270, 2003.

[102] S. Wang and L. Jiang, "Definition of superhydrophobic states," *Advanced Materials,* vol. 19, no. 21, p. 3423–3424, 2007.

[103] R. Wenzel, "Resistance of Solid Surfaces to Wetting by Water," *Ind. Eng. Chem.*, vol. 28, no. 8, p. 988–994, 1936.

[104] Y. Park and e. al, *International Conference on Miniaturized Systems for Chemisry and Life Sciences* , vol. 14, pp. 1175-1177, 2010.

[105] H. Im and e. al., *International Conference on Miniaturized Systems for Chemisry and Life Sciences* , vol. 14, pp. 1940-1942, 2010.

[106] J. F. Schumacher, M. L. Carman, T. G. Estes, A. W. Feinberg, L. H. Wilson, M. E. Callow, J. A. Callow, J. A. Finlay and A. B. Brennana, "Engineered antifouling microtopographies – effect of feature size, geometry, and roughness on settlement of zoospores of the green alga Ulva," *Biofouling,* vol. 23, no. 1, pp. 55-62, 2007.

[107] U. Horzum, B. Ozdil and D. Pesen-Okvur, "Step-by-step quantitative analysis of focal adhesions," *MethodsX* , vol. 1, pp. 56-59, 2014.

[108] Y.-B. Park, M. Im, H. Im and Y.-K. Choi, "Superhydrophobic Cylindrical Nanoshell Array," *Langmui,* vol. 26, no. 11, p. 7661–7664, 2010 .

[109] A. Baxter and S. Cassie, "Wettability of Porous Surfaces," *Trans. Faraday Soc.*, vol. 40, p. 546–551, 1944.

[110] C. Extrand, "Modeling of ultralyophobicity: Suspension of liquid drops by a single asperity," *Langmuir,* vol. 21, no. 23, p. 10370–10374, 2005.

[111] V. Bahadur and S. Garimella, "Preventing the Cassie−Wenzel Transition Using Surfaces with Noncommunicating Roughness Elements," *Langmuir,* vol. 25, no. 8, pp. 4815-4820, 2009.

[112] F. Re, A. Zanetti, M. Sironi, N. Polentarutti, L. Lanfrancone, E. Dejana and F. Colotta, "Inhibition of anchorage-dependent cell spreading triggers apoptosis in cultured human endothelial cell," *J Cell Biol.,* vol. 127, no. 2, pp. 537-546, 1994.

[113] B. D. Ratner, A. S. Hoffman, F. J. Schoen and J. E. Lemons, Biomaterials Science: An Introduction to materials in Medicine, Elsevier Academic Press, 2004.

[114] J. Glowacki, E. Trepman and J. Folkman, "Cell shape and phenotypic expression in chondrocytes," *Proc Soc Exp Biol Med.,* vol. 172, no. 1, pp. 93-98, 1983.

[115] M. J. Lydon, T. W. Minett and B. J. Tighe, "Cellular interactions with synthetic polymer surfaces in culture," *Biomaterials,* vol. 6, no. 6, pp. 396-402, 1985.

[116] T. Minett, B. Tighe, M. Lydon and D. Rees, "Requirements for cell spreading on polyHEMA coated culture substrates," *Cell Biol Int Rep.,* vol. 8, no. 2, pp. 151-159 , 1984.

[117] K. Yamada and B. Geiger, "Molecular interactions in cell adhesion complexes.," *Curr Opin Cell Biol.,* vol. 9, no. 1, pp. 76-85, 1997.

[118] P. Gupta, C. Chaffer and R. Weinberg, "Cancer stem cells: mirage or reality?," *Nat. Methods,* vol. 15, no. 9, pp. 1010-1012 , 2009.

[119] M. Mei Zhang, F. Behbod, R. Atkinson, M. Landis, F. Kittrell, D. Edwards, D. Medina, A. Tsimelzon, S. Hilsenbeck, J. Green, A. Michalowska and J. Rosen, "Identification of Tumor-Initiating Cells in a p53-Null Mouse Model of Breast Cancer.," *Cancer Research,* vol. 68, p. 46, 2008.

[120] L. Prestegarden, A. Svendsen, J. Wang, L. Sleire, K. Skaftnesmo, R. Bjerkvig, T. Yan, L. Askland, A. Persson, P. Sakariassen and P. Enger, "Glioma Cell Populations Grouped by Different Cell Type Markers Drive Brain Tumor Growth," *Cancer Research,* vol. 70, p. 4274, 2010.

[121] C. R, N. MC, B. SM, K. S, F. WF, K. IM, G. JM, S. RH, G. LL, R. CS, M. Z, N. S, G. S, E. KA, W. JJ, L. K, W. M, H. S, J. CD, V. SR, C. JF and e. al, "A hierarchy of self-renewing tumor-initiating cell types in glioblastoma.," *Cancer Cell,* vol. 17, no. 4, pp. 362-375, 2010.

[122] A. Croker, D. Goodale, J. Chu, C. Postenka, B. Hedley, D. Hess and A. Allan, " High aldehyde dehydrogenase and expression of CSC markers selects for breast cancer cells with enhanced malignant and metastatic ability.," *J Cell Mol Med,* vol. 13, no. 8, pp. 2236-2252, 2009.

[123] M. Guadamillas and A. d. P. M. Cerezo, "Overcoming anoikis – pathways to anchorage independent growth in cancer," *J Cell Science,* vol. 124, pp. 3189-3197, 2011.

[124] J. Stingl, "Detection and analysis of mammary gland stem cells.," *J Pathology,* vol. 217, no. 2, pp. 229-241, 2009.

[125] B. Booth, C. Boulanger and G. Smith, "Alveolar progenitor cells develop in mouse mammary glands independent of pregnancy and lactation.," *J Cell Physiol* , vol. 212, p. 729–736, 2007.

[126] M. Liao, C. Zhang, B. Zhou, D. Zimonjic, S. Mani and M. Kaba, "Enrichment of a population of mammary gland cells that form mammospheres and have in vivo repopulating activity.," *Cancer Res* , vol. 67, p. 8131–8138 , 2007.

[127] A. Singh, K. Sugimoto and C. Harris, " Juxtacrine Activation of Epidermal Growth Factor (EGF) Receptor by Membrane-anchored Heparin-binding EGF-like Growth Factor Protects Epithelial Cells from Anoikis While Maintaining an Epithelial Phenotype.," *Journal of Biological Chemistry,* vol. 282, pp. 32890-32901, 2007.

[128] B. Reynolds and R. Rietze, "Neural stem cells and neurospheres — re-evaluating the relationship.," *Nat Methods,* vol. 2, pp. 333-336, 2005.

[129] S. Louis, R. Rietze, L. Deleyrolle, R. Wagey, T. Thomas and A. Eaves, "Enumeration of neural stem and progenitor cells in the neural colony-forming cell assay.," *Stem Cells ,* vol. 26, pp. 988-996, 2008.

[130] A. Hsiao, Y. Tung, C. Kuo, B. Mosadegh, R. Bedenis, K. Pienta and S. Takayama, "Micro-ring structures stabilize microdroplets to enable long term spheroid culture in 384 hanging drop array plates.," *Biomed Microdevices,* vol. 14, no. 2, pp. 313-323, 2012.

[131] J. Friedrich, C. Seidel, R. Ebner and L. Kunz-Schughart, "Spheroid-based drug screen: considerations and practical approach.," *Nat Protoc. ,* vol. 4, no. 3, pp. 309-324, 2009.

[132] W. Lee, D. Ortmann, M. Hancock, H. Bae and A. Khademhosseini, "A hollow sphere soft lithography approach for long-term hanging drop methods.," *Tissue Eng Part C Methods,* vol. 16, no. 2, pp. 249-259, 2010.

[133] H. Ota, T. Kodama and N. Miki, "Rapid formation of size-controlled three dimensional hetero-cell aggregates using micro-rotation flow for spheroid study.," *Biomicrofluidics,* vol. 3, pp. 34105-34115 , 2011.

[134] A. Huebner, D. Bratton, G. Whyte, M. Yang, A. Demello, C. Abell and F. Hollfelder, "Static microdroplet arrays: a microfluidic device for droplet trapping, incubation and release for enzymatic and cell-based assays.," *Lab Chip,* vol. 9, no. 5, pp. 692-698, 2009.

[135] D. Siolas and G. Hannon, "Patient Derived Tumor Xenografts: transforming clinical samples into mouse models.," *Cancer Research ,* vol. 73, no. 17, pp. 1-5, 2013.

[136] S. Liu, Y. Cong, D. Wang, Y. Sun, L. Deng, Y. Liu, R. Martin-Trevino, L. Shang, S. McDermott, M. Landis, S. Hong, A. Adams, R. D'Angelo, C. Ginestier, E. Charafe-Jauffret and e. al, "Breast Cancer Stem Cells Transition between Epithelial and Mesenchymal States Reflective of their Normal Counterparts," *Stem Cell Reports,* vol. 2, no. 1, pp. 78-91, 2014.

[137] R. D'Angelo, M. Ouzounova, A. Davis, D. Choi, S. Tchuenkam, G. Kim, T. Luther, A. Quraishi, Y. Senbabaoglu, S. Conley, S. Clouthier, K. Hassan, M. Wicha and H. Korkaya, "Notch reporter activity in breast cancer cell lines identifies a subset of cells with stem cell activity.," *Mol Cancer Therapy,* p. Epub, 2015.

[138] J. Wang, B. Sullenger and J. Rich, "Notch signaling in cancer stem cells," *Adv Exp Med Biol,* vol. 727, pp. 174-185, 2012.

[139] G. Wong, G. Knowles, T. Mak, F. AA and J. Zúñiga-Pflücker, "HES1 opposes a PTEN-dependent check on survival, differentiation, and proliferation of TCRβ-selected mouse thymocytes.," *Blood ,* vol. 120, no. 7, pp. 1439-1448, 2012.

[140] F. Camargo, S. Gokhale, J. Johnnidis, D. Fu, G. Bell, R. Jaenisch and T. Brummelkamp, "YAP1 increases organ size and expands undifferentiated progenitor cells.," *Curr Biol.,* vol. 17, no. 23, pp. 2054-2060, 2007.

[141] M. Liu, K. Zhou and Y. Cao, "MCRS1 overexpression, which is specifically inhibited by miR-129*, promotes the epithelial-mesenchymal transition and metastasis in non-small cell lung cancer.," *Molecular Cancer* , vol. 13, p. 245, 2014.

[142] S. Krishnamurthy, K. Warner, Z. Dong, A. Imai, C. Nör, B. Ward, J. Helman, R. Taichman, E. Bellile, K. McCauley L, P. PJ, M. Prince, M. Wicha and J. Nör, "Endothelial interleukin-6 defines the tumorigenic potential of primary human cancer stem cells," *Stem Cells,* vol. 32, no. 11, pp. 2845-2857, 2014.

[143] S. Mosser, J. Alattia, M. Dimitrov, A. Matz, J. Pascual, B. Schneider and P. Fraering, "The adipocyte differentiation protein APMAP is an endogenous suppressor of Aβ production in the brain.," *Hum Mol Genetic,* vol. 24, no. 2, pp. 371-382, 2015.

[144] C. Ginestier, S. Liu, M. Diebel, H. Korkaya, M. Luo, M. Brown, J. Wicinski, O. Cabaud, E. Charafe-Jauffret, D. Birnbaum, J. Guan, G. Dontu and M. Wicha, "CXCR1 blockade selectively targets human breast cancer stem cells in vitro and in xenografts.," *J Clin Invest,* vol. 120, no. 2, pp. 485-497, 2010.

[145] P. Marcato, C. Dean, C. Giacomantonio and P. Lee, "Aldehyde dehydrogenase: its role as a cancer stem cell marker comes down to the specific isoform.," *Cell Cycle* , vol. 10, no. 9, pp. 1378-1384, 2011.

[146] T. Borovski, F. Melo, L. Vermeulen and J. Medema, "Cancer Stem Cell Niche: The Place to Be," *Cancer Research,* vol. 71, p. 634, 2011.

[147] J. Sleeman and N. Cremers, "New concepts in breast cancer metastasis: tumor initiating cells and the microenvironment," *Clin Exp Metastasis,* vol. 24, pp. 707-715, 2007.

[148] S. Liu, C. Ginestier, S. Ou, S. CLouthier, S. Patel, F. Monville, H. Korkaya, A. Heath, J. Dutcher, C. Kleer, Y. Jung, G. Dontu, R. Taichman and M. Wicha, "Breast Cancer Stem Cells Are Regulated by Mesenchymal Stem Cells through Cytokine Networks," *Cancer Research,* vol. 71, p. 614, 2011.

[149] C. Naujokat and R. Steinhart, "Salinomycin as a Drug for Targeting Human Cancer Stem Cells," *Journal of Biomed and Biotech,* vol. 2012, p. 17, 2012.

[150] A. Huczynski, "Salinomycin – A New Cancer Drug Candidate," *Chemical Biology and Drug Design,* vol. 79, no. 3, pp. 235-238, 2013.

[151] S. Kim, H. Kim and N. Jeon, "Biological applications of microfluidic gradient devices," *Integrative Biol,* vol. 2, pp. 584-603, 2010.

[152] E. Ronowicz and A. Coutinho, "Functional Analysis of B Cell Heterogeneity," *Immunological Reviews,* vol. 24, no. 1, pp. 3-40, 1975.

[153] W. Aird, "Mechanisms of Endothelial Cell Heterogeneity in Health and Disease," *Circulation Research,* vol. 98, pp. 159-162, 2006.

[154] T. Schroeder, "Hematopoietic Stem Cell Heterogeneity: Subtypes, Not Unpredictable Behavior," *Cell Stem Cell,* vol. 6, no. 3, pp. 203-207, 2010.

[155] N. Moore and S. Lyle, "Quiescent, Slow-Cycling Stem Cell Populations in Cancer: A Review of the Evidence and Discussion of Significance," *Journal of Oncology,* vol. 2011, p. 11, 2011.

[156] J. Lee, H. Jun and J. Kim, "Polydiacetylene–Liposome Microarrays for Selective and Sensitive Mercury(II) Detection," *Advanced Materials,* vol. 21, pp. 3674-3677, 2009.

[157] J. Lee, H. Kim and J. Kim, "Polydiacetylene Liposome Arrays for Selective Potassium Detection," *J Am Chem Soc,* vol. 120, no. 15, pp. 5010-5011, 2008.

[158] B. Gumbiner, "Cell adhesion: the molecular basis of tissue," *Cell,* vol. 84, p. 345, 1996.

[159] G. Cama, T. Jacobs, M. Dimaki, W. Svendsen and P. Hauptmann, "Disposable micro-fluidic biosensor," *Measurement Sci Technol,* vol. 21, p. 085801, 2010.

[160] D. Di Carlo, N. Aghdam and L. Lee, "Single-Cell Enzyme Concentrations, Kinetics, and Inhibition Analysis Using High-Density Hydrodynamic Cell Isolation Arrays," *Analytical Chem,* vol. 78, no. 14, pp. 4925-4930, 2006.

[161] D. Di Carlo and L. Lee, "Dynamic Single-Cell Analysis for Quantitative Biology," *Analytical Chem,* vol. 78, no. 23, pp. 7913-7925, 2006.

[162] B. Taff, S. Desai and J. Voldman, "Electroactive hydrodynamic weirs for microparticle manipulation and patterning," *Applied Physics Letters,* vol. 94, p. 084102, 2009.

[163] C. Ginestier, M. Hur, E. Charafe-Jauffret, F. Monville, J. Dutcher, M. Brown, J. Jacquemier, P. Viens, C. Kleer, S. Liu, A. Schott, D. Hayes, W. M. Daniel Birnbaum3 and D. Dontu, "ALDH1 Is a Marker of Normal and Malignant Human Mammary Stem Cells and a Predictor of Poor Clinical Outcome," *Cell Stem Cell,* vol. 1, no. 5, pp. 555-567, 2007.

[164] G. Whitesides, "Overview The origins and the future of microfluidics," *Nature,* vol. 442, pp. 368-373 , 2006.